From the: Institute of Anatomy, Rostock University Medical Center
Director: Univ. Prof. Dr.med. Dr.rer.nat. Markus Kipp


Dissertation
zum Erwerb des Doctor of Philosophy (Ph.D.)
an der Medizinischen Fakultät der
Ludwig-Maximilians-Universität zu München

# Oligodendrocyte Degeneration and Demyelination: Pathways Involved and Functional Consequences

vorgelegt von:

Jiangshan Zhan

aus:

Shandong

Jahr:

2021

Mit Genehmigung der Medizinischen Fakultät der
Ludwig-Maximilians-Universität zu München

**First supervisor:** *Univ. Prof. Dr.med. Dr.rer.nat. Markus Kipp*

**Second supervisor*:*** *Univ. Prof. Dr. med. Jens Waschke*

**Dean:** **Univ. Prof. Dr. med. dent. Reinhard Hickel**

Datum der Verteidigung:

28.04.2021

# Affidavit

Zhan, Jiangshan

Surname, first name

I hereby declare, that the submitted thesis entitled

**Oligodendrocyte Degeneration and Demyelination: Pathways Involved and Functional Consequences**

is my own work. I have only used the sources indicated and have not made unauthorised use of services of a third party. Where the work of others has been quoted or reproduced, the source is always given.

I further declare that the submitted thesis or parts thereof have not been presented as part of an examination degree to any other university.

Rostock, 28.04.2021

Place, Date

Jiangshan Zhan

Signature doctoral candidate

# Table of Contents

# 1. Abstract

Multiple sclerosis (MS) is a chronic inflammatory disease of the central nervous system (CNS) that involves demyelination and axonal degeneration. It remains controversial regarding the pathophysiology of MS whether brain-intrinsic degenerative cascades or recruited inflammatory processes drive the disease. In this thesis, I investigated the long-term consequences of an acute demyelinating white matter CNS lesion with the hypothesis that focal white matter lesions can induce long-lasting neuropathologies in MS. For this purpose, acute demyelination was induced by 5-week-Cuprizone intoxication in male C57BL/6J mice, followed by 7-month remyelination with normal chow. I show that ongoing gliosis (i.e., astrogliosis and microgliosis) and axonal damage persist after 7-month remyelination using immunohistochemistry/immunofluorescence, accompanied with gait abnormalities quantified using the DigiGait$^{TM}$ high speed ventral plane videography. Moreover, microglia presented a reactive phenotype with hyper-ramified morphology after 7-month remyelination, determined by complex morphological analyses using 3D reconstruction of serial image sequences acquired for microglia. I further verified the ongoing pathology after 7-month remyelination using Affymetrix GeneChip microarrays and found that protein kinase C delta (PRKCD) expression is up-regulated and predominately expressed in microglia/macrophages using immunohistochemistry/immunofluorescence. Induction of PRKCD in microglia/macrophages was also found in chronic (active) lesions and the normal appearing white matter of progressive MS patients compared to non-MS controls. In summary, my findings suggest that an initial brain pathology (i.e., acute demyelination) *per se* could induce prolonged gliosis, axonal damage as well as gait abnormalities even after complete remyelination. A better understanding of factors regulating these persistent pathologies would pave the way for novel MS therapies.

# 2. Abbreviations

$_a$: Research Resource Identifier

#: Number

ABC-HRP: Avidin–Biotin Complex coupled with Peroxidase

AGCC: Affymetrix GeneChip Command Console

ANXA2: annexin a2

APP: Amyloid Precursor Protein

*Arc*: Activity regulated cytoskeleton associated protein

Bp: Base pairs

CA3: Cornu Ammonis 3

*Cadps2*: Calcium dependent secretion activator 2

cc: corpus callosum

cing: cingulum bundle

CPG: Central Pattern-Generating Networks

CTX: Cerebral Cortex;

EAE: Experimental Autoimmune Encephalomyelitis

EDSS: Expanded Disability Status Scale

FDR: False Discovery Rate

*Gapdh*: Glyceraldehyde 3-phosphate dehydrogenase

GFAP: Glial Fibrillary Acidic Protein

GO: Gene Ontology

GWAS: Genome-Wide Association Study

*Hprt*: Hypoxanthine Phosphoribosyltransferase

Human Leukocyte Antigen:  LN3/HLA-DR

IBA1: Ionized Calcium-Binding Adapter Molecule 1

IFN-ß: Interferon-Beta

IHC/IF: immunohistochemistry/immunofluorescence

*Lcn2*: Lipocalin 2

LF: Left Fore limb

LH: Left Hind limb

MBP: Myelin Basic Protein

MOG: Myelin Oligodendrocyte Protein

MOSS: Motor Skill Sequence

MRI: Magnetic Resonance Imaging

mRNA: Messenger RNA

MS: Multiple Sclerosis

NAWM: Normal Appearing White Matter

*Ndst4*: N-Deacetylase and N-Sulfotransferase 4

NG2: Neural/Glial Antigen 2

NHPT: Nine Hole Peg Test

OLIG2: Oligodendrocyte Transcription Factor 2

OPCs: Oligodendrocyte Progenitor Cells

PBS: Phosphate-Buffered Saline

PKC: Protein Kinase C

PLP: Proteolipid Protein

*Pln*: Phospholamban

PRKCD: Protein Kinase C Delta

RF: Right Fore limb

RH: Right Hind limb

RI: Ramification Index

$RI_v$: Volume Ramification Index

RMA: Robust Multi-Array average

ROI: Region of Interest

RRMS: Relapsing-Remitting MS

RT-PCR: Reverse Transcription Polymerase Chain Reaction

SEM: Standard Error of the Mean

*Sgk1*: serum/glucocorticoid regulated kinase 1

*Slitrk6*: SLIT and NTRK like family member 6

SPMS: Secondary Progressive MS

T25-FW: 25-Foot Walk Test

$T_a$: Annealing Temperature

$T_H1$, $T_H17$: T Helper Type 1, 17

$V_c$: Cell Volume

VL: Lateral Ventricle

$V_p$: Maximum Projection Volume

# 3. Introduction

## 3.1 Multiple sclerosis

Multiple sclerosis (MS), as an autoimmune, demyelinating disease of the central nervous system (CNS), is histopathologically characterized by demyelination, peripheral immune cell infiltration, gliosis and axonal damage (Popescu, Pirko, & Lucchinetti, 2013; Rohr et al., 2020). MS is found to be more common in women than men and cause motor, sensory and cognitive disabilities in the patients (Kipp, Nyamoya, Hochstrasser, & Amor, 2017).

Initially, most patients present with a relapsing-remitting MS (RRMS) disease course. In RRMS, the patients suffer from acute clinical attacks (i.e., relapse) and recover afterwards (i.e., remit) (Kipp, 2020). At the histopathological level, RRMS is characterized by focal, inflammatory white matter lesions. Around 85% patients with RRMS eventually develop secondary progressive MS (SPMS) in their 40s or 50s. Clinically, SPMS patients show a continuous worsening of the neurological function (Kipp, 2020; Thompson et al., 2018). Although various therapies are available nowadays for RRMS, options for delaying the progression of the disability during progressive MS are extremely limited (Faissner, Plemel, Gold, & Yong, 2019), which reflects the elusive mechanisms underlying the MS progression. Most clinical trials of progressive MS failed in phase II/III and currently only two drugs (i.e., siponimod and ocrelizumab) have been approved for the treatment of progressive MS (Correale, Gaitan, Ysrraelit, & Fiol, 2017; Faissner et al., 2019; Kappos et al., 2018; Kipp, 2020; Montalban et al., 2017). Histopathologically, SPMS is characterized by diffuse microglia activation and axonal injury, cortical demyelination and the expansion of existing white matter lesions (i.e., smoldering lesions) (Frischer et al., 2015).

Focally demyelinated lesions have the potential to regenerate myelin by an endogenous reparative process termed remyelination. To remyelinate, oligodendrocyte progenitor cells (OPCs) need to proliferate firstly and migrate to the demyelinated lesion. After the OPCs find the demyelinated axons, they will differentiate into premature oligodendrocytes and thereafter wrap the axons (Kipp & Amor, 2012). Remyelination, together with neuronal

plasticity (i.e., functional reorganization of neuronal connectivity) appear to be key mechanisms to allow for complete clinical recovery after an episode of focal inflammatory demyelination (Flachenecker, 2015; Irvine & Blakemore, 2008; Kerschensteiner et al., 2004; Smith, Blakemore, & McDonald, 1979, 1981; Tomassini et al., 2012).

There is ample evidence that despite complete recovery from clinical symptoms, there is ongoing neuronal damage in progressive MS patients. For example, it has been demonstrated that after complete remyelination, axonal degeneration progresses at a low level, and is thus accumulating over time (Manrique-Hoyos et al., 2012). In experimental autoimmune encephalomyelitis (EAE), the most commonly applied autoimmune model of MS, neurodegeneration continues despite arresting clinical relapses (D. W. Hampton et al., 2013). In humans, advanced imaging modalities revealed metabolite abnormalities suggestive of ongoing glia cell activation and neurodegeneration despite a stable clinical disease course (Kirov et al., 2009; Wattjes et al., 2007). These results suggest that although at the clinical level, patients can completely recover from symptoms induced by such focally demyelinated lesions, these lesions eventually trigger an ongoing chronic pathology within the CNS.

## 3.2 Detection of motor deficits in mice

Rhythmic motor behaviors (e.g.; walking or running) are under delicate control of the CNS (Grillner & Wallen, 1985; Grillner, Wallen, Saitoh, Kozlov, & Robertson, 2008; Rossignol, Dubuc, & Gossard, 2006). In general, the basic locomotion pattern is known to be largely controlled by spinal central pattern-generating networks (CPG). During walking, the CPG *per se* receives afferent cutaneous and proprioceptive feedbacks from skin, muscles and special senses (i.e., vision, vestibular sense, audition) (Grillner & Wallen, 1985; Rossignol et al., 2006). Besides the basic locomotion pattern regulated by the CPG, various descending pathways from the brain dynamically coordinate adaptions of locomotion pattern in response to the changeable environment (Grillner et al., 2008).

Motor performances in small laboratory animals can be evaluated by various methods. Different categories of the most frequently used motor tests in mice are summarized in ***table 1*** (Brooks & Dunnett, 2009). Motor abnormalities could be simply evaluated by observational tests such as the cylinder test (Emerich, Dean III, & Sanberg, 1999). In the

cylinder test, mice are put in a transparent cylinder allowing for observing the surrounding environment. Meanwhile, the number and time of paw contacts with the cylinder wall are recorded for evaluating the motor deficits especially during exploring the environment. This method was firstly developed and widely used for detecting unilateral motor deficits in Parkinson's disease models of rats. However, the cylinder test is suboptimal for detecting bilaterally symmetric dysfunctions such as disorders in the coordination and balance (Brooks & Dunnett, 2009).

| **Categories** | **Representative Tests** | **Descriptions** | **Ref** |
|---|---|---|---|
| Observational test | Cylinder test | -mice are put in a transparent cylinder<br>-useful for detecting unilateral but not bilateral motor deficits | (Emerich et al., 1999) |
| Motor coordination and balance | Rotarod test | -mice are put on a rotating rod<br>-most frequently used for detecting coordination deficits. | (Dunham & Miya, 1957) |
| | Beam walking test | -mice are put on a balance beam. | (Gentile, Green, Nieburgs, Schmelzer, & Stein, 1978) |
| Locomotion activity | Open-field test | -mice are put in the center of an open arena.<br>-useful for detecting exploration activity but confounded with the anxiety level. | (Hall, 1934) |
| | Wheel running test | -mice are put on a running wheel with regular intervals.<br>-improved test on a running wheel with irregular intervals (i.e., the motor skill sequence, MOSS test) | (Liebetanz & Merkler, 2006; Sherwin, 1998) |
| Gait analysis | Footprint test | -mice walk over the paper in a narrow corridor after painting the paws with different dyes.<br>-cheap and sensitive method but time-consuming during manual analyses | (Klapdor, Dulfer, Hammann, & Van der Staay, 1997) |

| | | | |
|---|---|---|---|
| | Commercial platforms (DigiGait™, CatWalk™ and TreadScan™) | -mice are recorded using a high-speed camera while running on a treadmill.<br>-sensitive and objective but expensive | (Amende et al., 2005; Dorman, Krug, Frizelle, Funkenbusch, & Mahowald, 2014; Hamers, Lankhorst, van Laar, Veldhuis, & Gispen, 2001) |

**Table 1: Commonly used motor behavior tests in mice**

For analyzing the motor coordination and balance, Dunham and Miya developed a rapid and simple method (i.e., rotarod) for assessing drugs on animal behaviors (Dunham & Miya, 1957). The rotarod apparatus is composed of a rod rotating at a constant or increasing speed, assessing the motor coordination of mice walking on it. The time duration, the maximum speed and the total distance travelled of mice walking on the rod are commonly used for the quantification of the motor coordination. Due to its ease to use, the rotarod test remains one of the most frequently used motor function tests in rodents (Brooks & Dunnett, 2009). The motor coordination and balance could as well be evaluated by another method (i.e., the beam walking test), which was developed for measuring sensorimotor coordination and balance in rodents especially following cortical injury (Gentile et al., 1978). The beam walking test, also called the balance beam test, assesses the mice's ability to maintain balance while crossing a horizontal or elevated beam to reach the escape platform. The time taken by the mice to transverse the beam and the number of paw slips are recorded to evaluate the motor performance of balance.

Besides assessing the motor coordination and balance, the motor performance could be as well evaluated at the level of locomotion activity. Two tests which allow the quantification of locomotion activity are the open-field test and the wheel running test (Brooks & Dunnett, 2009). In the open-field test, mice are placed in the center of an open arena. Typically, the

mice will immediately run to the edge of the arena and continue exploring the arena while remaining close to the edge. After habituating to the environment, the mice will increasingly explore the center parts of the arena. Based on this distinct behavioral profile, the open-field test is a powerful tool for assessing the locomotion activity of mice during exploring a novel environment (Hall, 1934). With the development of automated recording using video tracking, the distance traveled as well as the number of arena center entrances can be automatically measured (Drai, Kafkafi, Benjamini, Elmer, & Golani, 2001). As mentioned above, the motor performance of mice in the open-field test is largely confounded by the anxiety level in mice. It is almost impossible to distinguish the anxiety-related activity from the motor-related activity in the open-field test (Brooks & Dunnett, 2009). Another method for assessing the locomotion activity is the wheel running test. The wheel running test is widely used to study the effect of the voluntary exercise in inactivity-related diseases such as obesity and type II diabetes (de Carvalho, Benfato, Moretto, Barthichoto, & de Oliveira, 2016; Hicks et al., 2016). As the test name implicates, the mice are provided with a running wheel in the home cage with regular intervals (around 10-15 cm). The distance traveled, the speed of running and the number of breaks during running on the wheel are commonly used for the evaluation of voluntary locomotion activity (Sherwin, 1998). The sensitivity of the wheel running test is largely improved by replacing the regular intervals of the wheel with irregularly spaced crossbars, which require high coordination skills for mice walking on them. The improved version of the wheel running test is called the motor skill sequence (MOSS) test, which allows for detecting latent deficits in motor performance (Liebetanz & Merkler, 2006; Manrique-Hoyos et al., 2012).

Although the abovementioned methods provide important insights into the abnormalities of motor coordination and locomotion activity, subtle abnormalities in the gait, for example alternations in individual limbs or missteps of fore and hind limbs, may not be detected using those methods. In 1997, Klapdor and colleagues developed a cheap and more precise method (i.e., footprint test/inked-paw test) for detecting subtle abnormalities in gait patterns (Klapdor et al., 1997). In the foot print test, the mice paws are painted with different dyes and the animals are put in a narrow corridor, which allows the mice to walk straightly over paper. The gait pattern of individual limbs is thus recorded manually. With the burgeoning development of computer science in the 21$^{st}$ century, the footprint of animals during

walking can be captured using high-speed cameras and further digitalized and evaluated by computer programming. In our days, there are several commercial platforms for fine-tuned gait analysis, such as the CatWalk™ (Noldus Inc., Wageningen, The Netherlands), DigiGait™ (Mouse Specifics Inc., Framingham, MA), and TreadScan™ (CleverSys Inc., Reston, VA) (Amende et al., 2005; Dorman et al., 2014; Hamers et al., 2001). Worth to mention, the gait analysis is one of the few tests which can be directly translated from animal studies into clinical studies (Brooks & Dunnett, 2009). In this study, I used the DigiGait™ platform for fine-tuned gait analyses in MS animal models (schematic drawing for DigiGait™ imaging system see ***figure 1***).

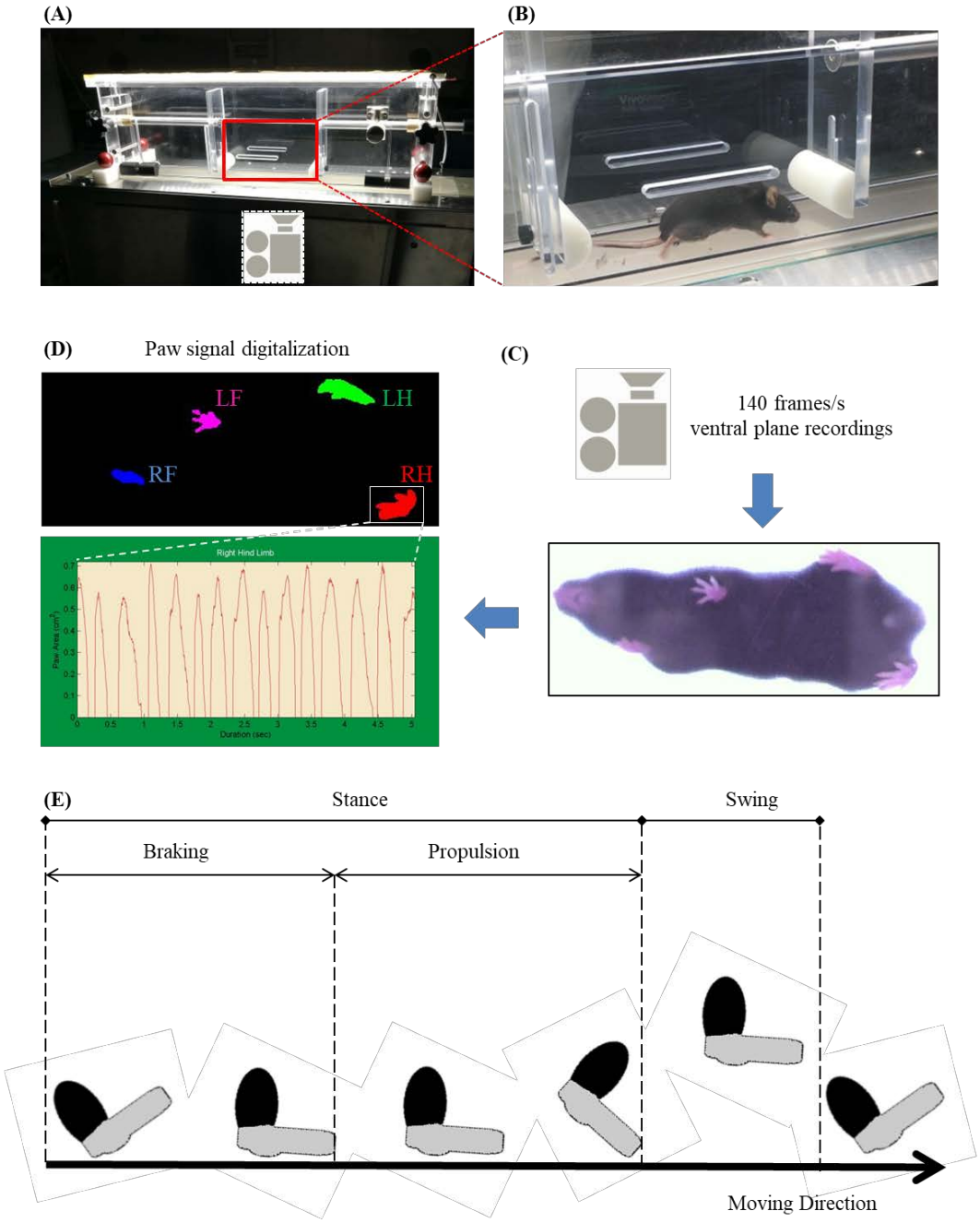


**Figure 1: DigiGait™ gait analysis platform**

„ **(A)** DigiGait™ apparatus composed of a running chamber and a high-speed camera. **(B)** A mouse in the running chamber during recordings. **(C)** Representative picture of ventral plane video recordings. **(D)** Digitalization of individual paw signal using the provided analysis tool and representative time-course paw signal graph of right hind limb. **(E)** Schematic depiction of a single mouse stride. Each stride composes of a stance and swing part. The stance part can be further subdivided into a braking and propulsion phase. LF: Left Fore; LH: Left Hind; RF: Right Fore; RH: Right Hind.“ Figure 1 is revised from my previously published work (Zhan et al., 2019).

## 3.3 Detection of motor deficits in multiple sclerosis and associated animal models

Motor deficits are major symptoms affecting the life quality of MS patients (Benecke & Conrad, 1980). Therefore, measurements of motor abnormalities are largely used to represent the functional deficits in MS patients. The extent of motor deficits in MS, such as impairments in gait and balance, can be estimated using different methods. The expanded disability status scale (EDSS), the most frequently used method to evaluate the disability of MS patients, is conducted by individual and subjective examination by a neurologist. Gait deficits are an important criterion for the EDSS. The EDSS score, ranging from 0 to 10 in 0.5 increments, represents increasing levels of disability in walking (Kurtzke & Berlin, 1954). Besides the EDSS, the timed 25-foot walk (T25-FW) and the nine hole peg test (NHPT) are also used to evaluate ambulatory function and manual dexterity respectively (Feys et al., 2017; Motl et al., 2017).

Experimental autoimmune encephalomyelitis (EAE), the most frequently used animal model in MS, sheds light on the disease-modifying therapies for RRMS (Nutma, Willison, Martino, & Amor, 2019; Olitsky & Yager, 1949). In brief, the EAE model can be actively induced by immunizing rodents (C57BL/6, SJL/J mice or Lewis, Dark Agouti rats) with a CNS-related antigen e.g.; CNS homogenate, proteins/ peptides of myelin basic protein (MBP), proteolipid protein (PLP) or myelin oligodendrocyte protein (MOG), together with (in)complete Freud's adjuvant and pertussis toxin (Stromnes & Goverman, 2006). „ Following immunization, antigens are phagocytized and presented by local professional antigen-presenting cells which travel to the spleen or local lymph nodes to trigger encephalitogenic $Th_1$- and $Th_{17}$-cell mediated autoimmune responses. This finally leads to multifocal inflammation in specific CNS regions such as the spinal cord and the cerebellum. At the behavioral level, EAE-induced mice develop a typical caudal-to-rostral paralysis, beginning at the tail, spreading to the hind limbs and, finally, fore limbs (Zhan et al., 2019)." (This paragraph is revised from my previously published work). According to this, a standardized scoring system is commonly used to evaluate the severity of the motor deficits in EAE-induced mice (Constantinescu, Farooqi, O'Brien, & Gran, 2011). However, there is already severe spinal cord inflammation at the time point when the first motor abnormalities

by conventional EAE scoring can be detected (i.e., tail limpness). Therefore, more sophisticated motor behavioral analyses, such as the gait analysis, are required to study the early phase of inflammation development or beneficial drug effects during the preclinical phase (Zhan et al., 2019).

Each single MS animal model only reflects distinct features of the disease instead of its entire complexity (Kipp et al., 2017). While the EAE model provides significant insights into the autoimmune aspect of MS, other animal models, such as the cuprizone model, are available to study the non-immune mediated demyelination in MS. Several studies have demonstrated the functional deficits in the cuprizone model. The methods used for detecting functional deficits and their main findings are summarized chronologically in ***table 2***. In 2006, Liebetanz and Merkler developed a sensitive motor test (i.e., MOSS test), which is composed of wheels with irregularly spaced crossbars. It demands high-level motor coordination of mice walking on it, thus it can reveal subtle abnormalities in the gait. Using this method, they found obvious gait abnormalities in 6-week 0.2% cuprizone intoxicated mice (Liebetanz & Merkler, 2006), which could not be detected by visual observations (Morell et al., 1998). Moreover, latent gait abnormalities were observed using the MOSS test during remyelination (i.e., 4 weeks after cuprizone removal) (Liebetanz & Merkler, 2006). They concluded that the extent of motor deficits seemed to be positively correlated to the extent of corpus callosum demyelination. Similarly, the genetic absence or surgical transection of the corpus callosum is associated with subtle behavior deficits in mice and humans (Bonzano et al., 2008; Kennerley, Diedrichsen, Hazeltine, Semjen, & Ivry, 2002; Schalomon & Wahlsten, 2002; Wahlsten, Crabbe, & Dudek, 2001). In 2007, Franco-Pons *et al.* found that 6-week 0.2% cuprizone-intoxication in mice results in an impaired motor coordination, quantified *via* the rotarod test. Moreover, the motor deficits did not recover during remyelination (i.e., 6 weeks after cuprizone removal) (Franco-Pons, Torrente, Colomina, & Vilella, 2007). Motor deficits in the cuprizone model were further confirmed by other studies (Hibbits, Pannu, Wu, & Armstrong, 2009; Manrique-Hoyos et al., 2012). Besides the motor deficits, other functional deficits, such as cognitive impairments and spatial working memory deficits were also found in cuprizone-intoxicated mice (Hibbits et al., 2009; Makinodan et al., 2009; Xu, Yang, McConomy, Browning, & Li, 2010; Xu et al., 2009).

| Year | Methods | Main findings | Ref |
|---|---|---|---|
| 1998 | Visual observation | **During cuprizone exposure:** Cuprizone-intoxicated mice were less active<br>**After cuprizone withdrawal:** Cuprizone-intoxicated mice were normal | (Morell et al., 1998) |
| 2006 | Wheel running<br>MOSS | **During cuprizone exposure:** Cuprizone-intoxicated mice showed reduced running performance in both wheel running and MOSS tests<br>**After cuprizone withdrawal:** Cuprizone-intoxicated mice appeared normal in the wheel running but exhibited motor impairments on the MOSS test | (Liebetanz & Merkler, 2006) |
| 2007 | Observation battery<br>Open field<br>Rotarod | **During cuprizone exposure:** Cuprizone-intoxicated mice were hyperactive and showed motor disorders<br>**After cuprizone withdrawal:** Cuprizone-intoxicated mice showed impairments in the open field and the rotarod tests | (Franco-Pons et al., 2007) |
| 2009 | Open field<br>Climbing test<br>Y-Maze test<br>Social interaction test | **During cuprizone exposure:** Cuprizone-intoxicated mice showed hyperactivity in the climbing test but appeared normal in the open field test<br>Cuprizone-intoxicated mice presented damaged spatial working memory and social activity in the Y-maze test and the social interaction test | (Xu et al., 2009) |
| 2009 | Wheel running<br>MOSS<br>Social interaction test | **During cuprizone exposure:** Cuprizone-intoxicated mice showed impaired sensorimotor coordination in the MOSS test and increased interactive behaviors in the social interaction test<br>**After cuprizone withdrawal:** Cuprizone-intoxicated mice showed persistent motor impairments in the MOSS test | (Hibbits et al., 2009) |
| 2009 | Y-maze test<br>Social interaction test | **During cuprizone exposure:** Cuprizone-intoxicated mice presented damaged spatial working memory and social activity in the Y-maze test and the social interaction test<br>**After cuprizone withdrawal:** Cuprizone-intoxicated young mice (P27) but not adult mice (P56) showed irreversible impairments in the spatial working memory and social activity | (Makinodan et al., 2009) |
| 2012 | MOSS | **After cuprizone withdrawal:** Cuprizone-intoxicated mice showed initial recovery and later on decline of locomotor performance in the MOSS test | (Manrique-Hoyos et al., 2012) |

**Table 2 Functional deficits in the cuprizone model**

## 3.4 Hypothesis

The hypothesis of this work is that focal white matter lesions induce long-lasting neuropathologies in MS. In order to test this hypothesis, I first induced focal white matter lesions followed by long-term (7 months) remyelination in mice using the cuprizone model. After 7-month remyelination, axonal degeneration and neuroinflammation were evaluated at both mRNA and protein levels using gene array/real-time reverse transcription polymerase chain reaction (RT-PCR) and immunohistochemistry/immunofluorescence (IHC/IF) respectively. Functional deficits (i.e., motor behavioral deficits) were evaluated using high speed ventral plane videography, namely DigiGait$^{TM}$. Finally, tissue pathologies in the applied animal model were compared to progressive MS post-mortem tissues. A schematic picture of the methods used in this study to test the hypothesis is shown in ***figure 2***

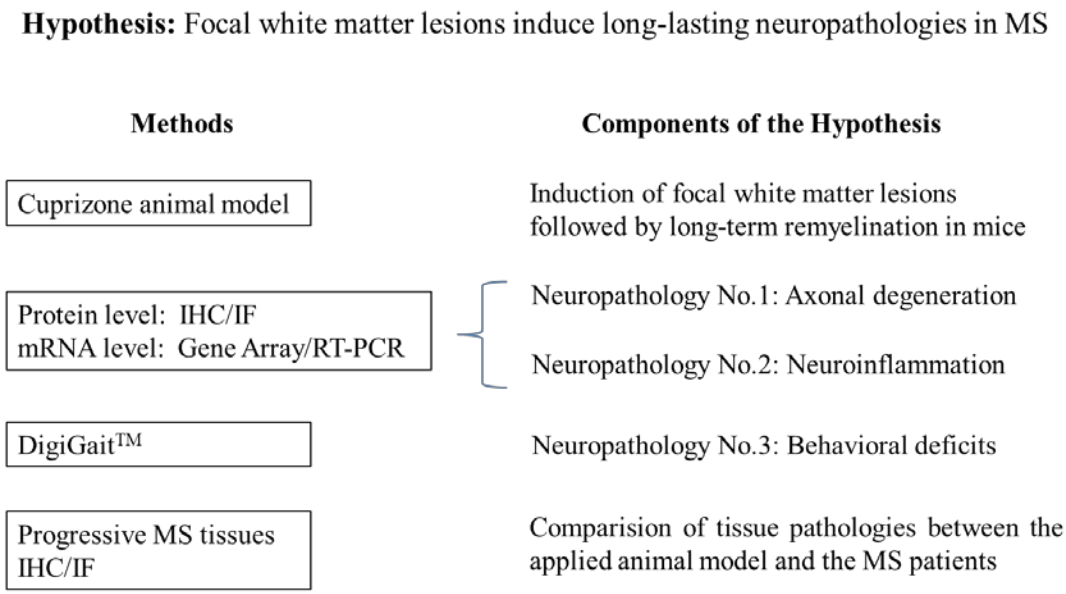


**Figure 2 A schematic drawing of the methods used in this study to test the hypothesis**

# 4. Materials and Methods

## 4.1 Animals

C57BL/6J male mice at 8 weeks of age were purchased from Janvier Labs, Le Genest-Saint-Isle, France. A maximum of five animals were housed per cage (500 $cm^2$). The animals were kept under standard laboratory conditions (12 h light/dark cycle, controlled temperature 23 °C ± 2 °C and 50% ± 5% humidity) with access to food and water *ad libitum*. The mice were allowed to accommodate to the environment for at least 1 week prior to the beginning of the experiments and were provided with nestlets for environmental enrichment. Body weights of mice were controlled once per week. The mice were randomly assigned to the experimental groups as illustrated in ***table 3***. **Control** group: mice were fed with standard pelleted rodent chow for the entire duration of the study (i.e., age-matched controls). **Cup-Recov** group: age- matched mice were intoxicated with a diet containing cuprizone (bis(cyclohexanone)oxaldihydrazone, C9012, Sigma-Aldrich, USA) mixed into ground standard rodent chow (V1530-0; Ssniff, Soest, Germany) for 5 weeks (first 2 weeks 0.2% following by 3 weeks 0.25%) to induce acute demyelination, followed by 28 weeks standard pelleted rodent chow allowing for long-term recovery. Mice intoxicated with cuprizone for 5 weeks (**5w Cup**) and in-parallel controls (**5w Control**) from an independent experiment were included to demonstrate acute demyelination in the corpus callosum (Chrzanowski, Schmitz, Horn-Bochtler, Nack, & Kipp, 2019). All experimental procedures were approved by the Review Board for the Care of Animal Subjects of the district government (Regierung Oberbayern; reference number 55.2-154-2532-73-15; Germany).

| | **Groups** | **Number of Animals** |
|---|---|---|
| IHC/IF | Cup-Recov | 4 |
| | Control | 4 |
| Gene Array | Cup-Recov | 4 |
| | Control | 4 |
| RT-PCR | Cup-Recov | 4 |
| | Control | 4 |
| DigiGait™ | $Cup\text{-}Recov^{DigiGait}$ | 19 |
| | $Control^{DigiGait}$ | 19 |

**Table 3 Experimental groups and number of animals**

## 4.2 Tissue preparation

For immunohistochemical studies, mice (n = 5 per group) were deeply anaesthetized with ketamine (100 mg/kg i.p., 9089.01.00, Bela-Pharm, Vechta, Germany) and xylazine (Rompun®, 10 mg/kg i.p., Bayer, Leverkusen, Germany) and transcardially perfused with 20 ml ice-cold phosphate-buffered saline (PBS), followed by 100 ml of a 3.7% formaldehyde fixative solution (pH 7.4) (see ***supplementary table 4***). After overnight post-fixation in the same fixative solution, the brains were transferred to tissue cassettes and rinsed under running tap water for 6-12 hours and then incubated overnight at 4 °C in 50% ethanol (WAL642 6025, Walter CMP, Kiel, Germany). This was followed by the manual dehydration (***table 4***) and embedding in paraffin (1.07158.9025, Merck, Darmstadt, Germany).

| Steps | Time |
|---|---|
| 70% ethanol | 40 minutes |
| 70% ethanol | 40 minutes |
| 96% ethanol | 40 minutes |
| 96% ethanol | 40 minutes |
| 100% ethanol | 40 minutes |
| 100% ethanol | 40 minutes |
| 100% ethanol | 60 minutes |
| xylene | 40 minutes |
| xylene | 40 minutes |
| xylene | 40 minutes |
| paraffin (65 °C) | 60 minutes |
| paraffin (65 °C) | 60 minutes |
| paraffin (65 °C) | 2 days |

**Table 4 Dehydration and embedding in paraffin of brain tissues**

The paraffin blocks were then cut into 5-µm-thick coronal sections using a rotary microtome (RM2255, Leica Microsystems, Wetzlar, Germany) at the level 265 (shown in ***figure 3***) according to the mouse brain atlas published by Sidman et al. („ Source: http://

www.hms.harvard.edu/research/brain/atlas.html"). This level is defined as the first appearance of pyramidal cells in the hippocampal cornu ammonis region. The paraffin sections were stretched in a water bath at 42-45 °C, two sections each were drawn onto a Superfrost Plus (J1800AMNZ, Thermo Scientific, Germany) slide and dried overnight at 37 °C in a heating cabinet. For gene expression studies, the corpus callosum (n = 8 per group) was manually dissected after PBS perfusion, immediately frozen and kept in liquid nitrogen until further processing (Krauspe et al., 2015).

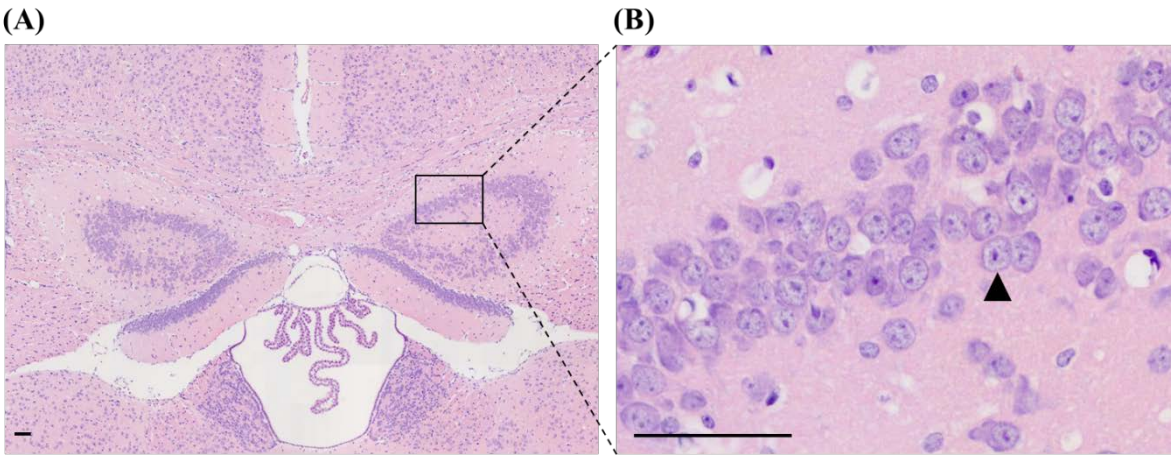


**Figure 3 The anatomical hallmark of R265**

(**A**) Hematoxylin and eosin (H&E) stained section at the level R265, defined as the first appearance of pyramidal cells in the hippocampal cornu ammonis region. (**B**) Arrowhead indicates the nucleus of a pyramidal neuron. Scale bar = 50 µm.

## 4.3 Immunohistochemistry and immunofluorescence analyses

For immunohistochemistry, sections were deparaffinized and rehydrated manually (***table 5***) and, if necessary, antigens were unmasked with heat in Tris/EDTA (pH 9.0) or citrate (pH 6.0) buffer (***supplementary table 4***). After washing in PBS, sections were blocked in the blocking solution (serum of the species in which the secondary antibody was produced, ***supplementary table 4***) for 1 h. Then, the sections were incubated overnight (4 °C) in primary antibodies diluted in the blocking solution (***supplementary table 4***). On the next day, the sections were washed in PBS and then incubated in 0.35% hydrogen peroxide buffer (***supplementary table 4***) for 30 minutes in the dark in order to reduce endogenous peroxidase activity. After the peroxidase blocking, sections were incubated in biotinylated

secondary antibody solution at room temperature for 1 h and then incubated in a peroxidase-coupled avidin–biotin complex solution (ABC-HRP kit, PK-6100, Vector Laboratories, USA) (***supplementary table 4***). Alternatively, to better visualize the fine morphology of microglia cells, a peroxidase labelled polymer conjugate was used to visualize antigen-antibody complexes (EnVision+System-HRP labelled polymer anti-rabbit, K4003, Dako, Hamburg, Germany). Next, sections were incubated in 3,3′-diaminobenzidine (DAB) solution (***supplementary table 4***) for 10 mintutes (K3468, Dako, Hamburg, Germany) (Chrzanowski, Bhattarai, et al., 2019; Hoflich et al., 2016). Sections were counterstained with hematoxylin solution to visualize cell nuclei if appropriate and covered with DePeX (18243.02, Serva, Heidelberg Germany). Negative control sections without primary antibodies were processed in parallel to ensure the specificity of the staining.

| Steps | Time |
|---|---|
| xylene | 10 minutes |
| xylene | 10 minutes |
| xylene | 10 minutes |
| xylene/ethanol 1:1 | 5 minutes |
| 100% ethanol | 3 minutes |
| 100% ethanol | 3 minutes |
| 96% ethanol | 3 minutes |
| 96% ethanol | 3 minutes |
| 70% ethanol | 3 minutes |
| 50% ethanol | 3 minutes |
| distilled water | 3 minutes |

**Table 5 Deparaffinization and rehydration of paraffin slides**

For immunofluorescence double labeling experiments, sections were rehydrated, unmasked by heating in Tris/EDTA buffer (pH 9.0), blocked with PBS containing 5% normal donkey serum (D9663, Sigma-Aldrich, USA) (***supplementary table 4***) and incubated overnight (4 $^{\circ}$C) in the appropriate combination of primary antibodies diluted in blocking solution. For mouse slides, anti-protein kinase c delta (PRKCD) antibodies were either combined with anti-oligodendrocyte transcription factor 2 (OLIG2) antibodies to visualize oligodendrocytes, with anti-glial fibrillary acidic protein (GFAP) antibodies to visualize astrocytes, or with anti-ionized calcium-binding adapter molecule 1 (IBA1)

antibodies to visualize microglia/macrophages. Anti-PRKCD antibodies were combined with anti-LN3 (HLA-DR) antibodies to visualize activated microglia/macrophages in human tissues. After washing, sections were incubated for 2 hours at room temperature in appropriate fluorescent secondary antibodies diluted in blocking solution. To quench autofluorescence in human tissues, sections were incubated 10 minutes in 0.1% Sudan Black B (S0395, Sigma-Aldrich, USA) diluted in 70% ethanol (Schnell, Staines, & Wessendorf, 1999). Subsequently, sections were mounted with Fluoroshield™ DAPI solution (F6057, Sigma-Aldrich, USA) for the staining of cell nuclei. Appropriate negative controls (i.e., omission of primary antibodies and/or incubation with the "wrong" secondary antibody) were performed in parallel (Fischbach et al., 2019; Nyamoya et al., 2019). Detailed lists of applied primary and secondary antibodies are provided in the supplementary material section (***supplementary table 1, supplementary table 2***).

Sections were digitalized using a Nikon ECLIPSE E200 microscope (Nikon Instruments, Düsseldorf, Germany) equipped with a camera (Basler acA1920-40uc) or a Leica DM6 B automated microscope (Leica Microsystems CMS GmbH, Wetzlar, Germany) equipped with a DMC6200 camera. To analyze cell densities, the region of interest (ROI; midline of the corpus callosum or deep layer cortex) was manually outlined using the open source program ViewPoint Online (version 1.0.0.9628, PreciPoint, Freising, Germany) (***figure 4A***), positive cells within the ROI were counted by at least two evaluators blinded to the treatment groups and results were transformed into cells/mm$^2$. ImageJ (version 1.52d, NIH, Bethesda, USA) was further used to evaluate the staining intensities using semi-automated densitometrical evaluation using a threshold algorithm. Relative staining intensities were semi-quantified in binary converted images, and the results were transformed into percentage of areas (***figure 4B***).

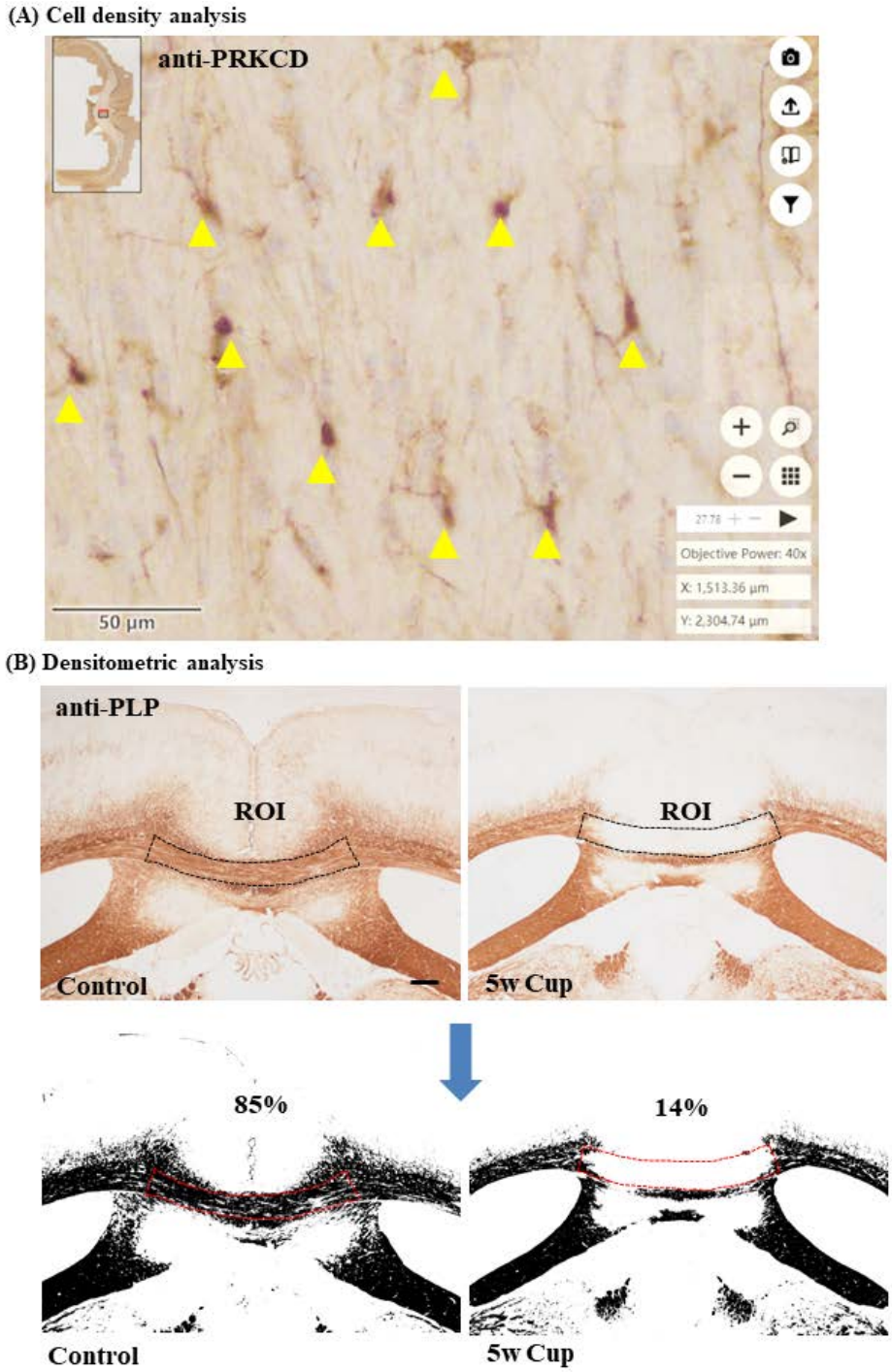


**Figure 4 Histological evaluation of IHC stained slides**

(**A**) Evaluation of cell densities in anti-PRKCD stained slides using the open source program ViewPoint Online. Arrowheads indicate the PRKCD$^{+}$ cells. (**B**) Principal of densitometric analysis in anti-PLP stained slides to quantify the demyelination in the corpus callosum. PRKCD: protein kinase c delta; ROI: region of interest. Scale bar = 50 µm.

To visualize acute axonal injury, we performed anti-amyloid precursor protein (APP) IHC in paraffin-embedded brain slides. „APP is an integral glycoprotein type 1, synthetized in the neuronal soma and then transported to the axonal terminal *via* the anterograde axonal transport machinery“ This paragraph is from my previously published work (Zhan et al., 2020), the original idea originates from (Koo et al., 1990). In case of a disturbed axonal transport caused by acute injury, APP accumulates at the sites of axonal injury as spheroids and can be visualized by IHC (Sherriff, Bridges, Gentleman, Sivaloganathan, & Wilson, 1994; Stone, Singleton, & Povlishock, 2000). A schematic picture demonstrating the principle of anti-APP immunohistochemistry for analyzing acute axonal injuries is shown in ***figure 5***.

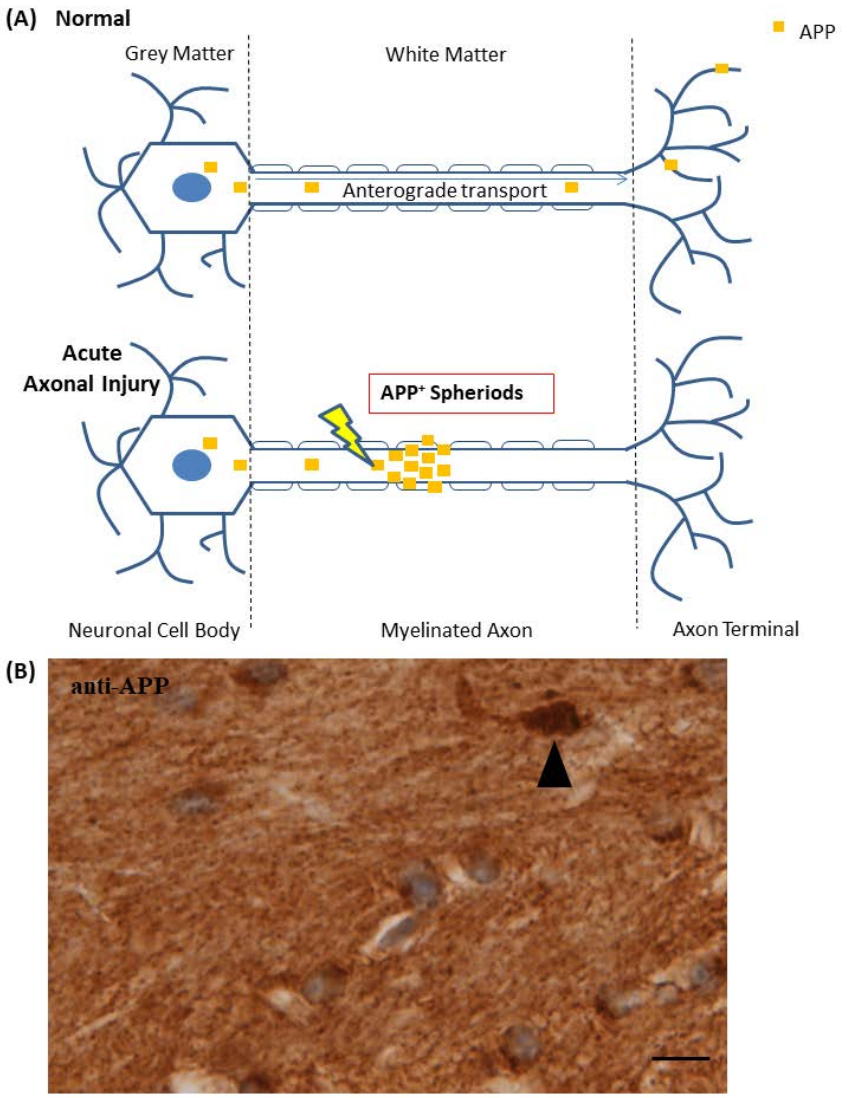

**Figure 5 Evaluation of acute axonal injury using anti-APP staining**

„ (**A**) Principle of anti-APP staining in visualizing acute axonal injury. Under physiological conditions, amyloid precursor protein (APP) is synthetized in the neuronal soma and transported to the axonal terminal *via* the anterograde axonal transport machinery. During acute axonal injury, APP accumulates at the sites of axonal injury as spheroids and thus can be visualized as spheroids using (**B**) anti-APP immunohistochemistry. The arrowhead indicates an $APP^+$ spheroid. Scale bar = 10 μm. " This paragraph is revised from my previously published work (Zhan et al., 2020).

# 4.4 Analysis of microglial morphology

Analysis of microglial morphology was done by a medical doctoral student, Florian Nepomuk Fegg under my supervision. Evaluation of the Sholl analyses data (see above) was performed by myself. The method is described as following for the sake of clarity. To analyze microglial morphology, anti-IBA1-stained sections were digitalized using an Olympus BX51-Wi microscope (Olympus, Munich, Germany). Serial z-stack images (n=40) were generated with a 0.5 μm step size. Randomly selected microglial cells (4-6 cells per animal, in total 25 cells per group) within the ROI were then traced and reconstructed (***figure 9B***) using Neurolucida360 (version 2017.01.2, MBF Bioscience, Williston, VT, USA). In this study, we consistently focused on cortical layer 5-6 (***supplementary figure 1A***) where microglial morphology is not biased by the dense network of axonal bundles in the corpus callosum. The structural complexity of microglial cells was quantified by Sholl analysis using NeuroLucida Explorer (version 11, MBF Bioscience). As shown in ***figure 9C***, concentric circles (radii) of 1 μm increment were expanded from the center of the microglial soma to the ending point of the longest microglial process. The area between the 6 μm and 31 μm radii were included for further analyses as previously described (H. W. Morrison & Filosa, 2013). For a schematic illustration of the morphological parameters see ***figure 9C***. The following parameters were evaluated: "***Intersection***" which is defined as the number of intersections of the process within the shell (i.e., area between two concentric circles) at the given radius; "***Area***" which is defined as the surface area ($\mu m^2$) of the occupied structure within the shell at the given radius; "***Volume***" which is defined as the volume ($\mu m^3$) of the occupied structure within the shell at the given radius; "***Avg.Diameter***" which is defined as the average diameter (μm) of the occupied structure within the shell at the given radius; "***Node***" which is defined as the number of branch points within the shell at the given radius;

"***Ending***" which is defined as the number of process endings within the shell at the given radius. In addition, the morphology of microglia cells was quantified by determining a volume ramification index ($RI_v$) using the following formula: $RI_v$ = maximum projection volume ($V_p$)/cell volume ($V_c$) (Becker et al., 2018; York, LeDue, Bernier, & MacVicar, 2018). $V_p$, calculated by Convex Hull 3D analysis, represents the territorial volume of a polygonal object defined by the cell's most prominent projections. $V_c$ represents the total cell volume (***supplementary figure 1C***). When ramified or resting microglial cells are fully activated, they will adopt an amoeboid morphology by retracting their processes, which results in a decrease of the $V_p$ and $RI_v$ values (***supplementary figure 1D***).

## 4.5 Gene array analysis

Gene array analyses were performed by Dr. rer. nat. Bernd Denecke from the Gene-Chip Facility of RWTH, Aachen University as part of a scientific collaboration. Data evaluation and interpretation of the gene array was performed by myself. The method is described as following for the sake of clarity. Cup-Recov and control mice were included (n = 4 per group). Regulation of gene expression was analyzed using Affymetrix GeneChip microarrays (Affymetrix Santa Clara, CA, USA) as previously described (Kipp et al., 2011; Kipp et al., 2008). Total RNA was isolated, and the quality was assessed using RNA NanoChips with the Agilent 2100 Bioanalyzer (Agilent Technologies, Santa Clara, California, USA). Probes for GeneChip Mouse Gene 1.0 ST Arrays were prepared and hybridized to the arrays according to the Affymetrix GeneChip whole transcript sense target labeling assay manual. Raw image data was analyzed with Affymetrix GeneChip command console (AGCC) software, and gene expression intensities were normalized and summarized with robust multi-array average (RMA) algorithm (Irizarry et al., 2003). Genes up-regulated in the Cup-Recov group *vs* age-matched control group were identified according to the following criteria: expression of genes in Cup-Recov sample was at least 1.5-fold higher compared to control samples, and the false discovery rate (FDR) adjusted p-value for changes in expression was $<0.05$.

Gene enrichment analyses were performed using a Gene Ontology (GO) enrichment analysis online tool (Ashburner et al., 2000; Mi, Muruganujan, Ebert, Huang, & Thomas, 2019; The Gene Ontology, 2019). Names of genes which were differentially expressed were

copied into the GO enrichment analysis online tool (Released version 20200323), where I selected the species (Mus musculus) and specific ontologies (biological process and molecular function) for the enrichment analyses. Fischer's exact test with FDR correction was used for testing statistic power. Results are presented from highest to lowest fold enrichment.

## 4.6 Gene expression analysis

Total RNA was isolated using the phenol-chloroform extraction method (Total RNA kit peqGOLD, 30-2010, Germany). RNA concentration and purity were assessed by using OD260 and OD260/OD280 ratio, determined by the spectrophotometer NanoDrop 2000 (Thermo Scientific, Germany). 1 µg RNA was subsequently reverse-transcribed using the M-MLV RT-kit (28025-021, Invitrogen, Germany) and random hexanucleotide primers (48190-011, Invitrogen, Germany). Potential contamination with the genomic DNA was further checked by a conventional PCR using a hypoxanthine guanine phosphoribosyl transferase 1 (*Hprt*) primer pair (***supplementary table 3***), which was designed as an intron/exon spanning oligonucleotide. If the isolated RNA is contaminated with the genomic DNA, one will get two bands with one from the cDNA and the other from genomic DNA. The "contaminated" genomic DNA band is longer, thus migrating slower during electrophoresis. In this study, no genomic DNA contamination was observed for all included samples. After the reverse transcription, cDNA samples were diluted 1:10 in RNase/DNase free water (10977-035, Invitrogen, Germany). Before diluting the cDNA, a certain amount of each cDNA sample from all experimental samples was pooled and designated as '100% standard'. This 100% standard was 7-times diluted 1:1 to create an internal standard curve (i.e., 100%, 50%, 25%, 12.5%, 6.25%, 3.125%, 1.5626%). This standard is called "internal" standard because the DNA is obtained from cDNA which was generated within the experiment, so "internally". The diluted cDNA samples and pooled internal standards were stored in -20°C until further usage.

To verify the obtained gene array results, I chose appropriate primer pairs of four up-regulated genes (i.e., *Prkcd, Slitrk6, Pln, Ndst4*) and four down-regulated genes (i.e., *Lcn2, Cadps2, Arc, Sgk1*) (***supplementary table 3***) from the online *primerbank* database („ Source: http://pga.mgh.harvard.edu/primerbank/"). The specificity of the primer pairs was

further checked using the Basic Local Alignment Search Tool (BLAST, „ Source: http://blast.ncbi.nlm.nih.gov/Blast.cgi“). Thereafter, the primer pairs of the abovementioned genes were then synthesized by the company Invitrogen, Germany. The annealing temperature of each primer pair was optimized by increasing the temperature in 1.5 °C steps using the Mastercycler® gradient thermal cycler (Eppendorf, Germany). After the PCR reaction, the products were applied on a 2% agarose gel containing Midori Green Advance (MG03, Biozym, Vienna, Austria) and separated by electrophoresis (Bio-Rad, Germany). The annealing temperature giving rise to the brightest and single band of the expected size is determined as the most optimized annealing temperature for the primer pair.

I performed real-time RT-PCR (Bio-Rad, Germany) using SensiMix Plus SYBR Fluorescein (QT615-05, Quantace, Germany) (Slowik et al., 2015) under the following conditions: 10min enzyme activation at 95°C, 40 cycles of 15 seconds denaturation at 95°C, 30sec annealing at the optimized temperature, 30sec amplification at 72°C and 5sec fluorescence measurement at 80°C. Glyceraldehyde 3-phosphate dehydrogenase (*Gapdh*) was used as the reference gene for normalization of *Prkcd* and *Lcn2*. *Hprt* was used as the reference gene for normalization of *Slitrk6, Pln, Ndst4, Cadps2, Arc, Sgk1*. Relative quantification was performed by the delta Ct method, which results in ratios between the expression of target genes and a housekeeping reference gene (i.e., *Hprt* or *Gapdh*). The concentration of the target genes was calculated by comparing Ct values in each sample with Ct values of the internal standard curve. Finally, data was expressed as the ratio of the amount of each transcript *vs* the concentration of *Hprt*/*Gapdh*. Melting curves and gel electrophoresis of the PCR products were routinely performed to determine the specificity of the PCR reaction. For each experiment, negative controls were performed in which 2 µl of RNase/DNase free water was added to the PCR reaction instead of cDNA. Positive controls using cDNA samples, which were affirmed to contain the template to be amplified, were performed as well.

## 4.7 High speed ventral plane videography DigiGait™ and evaluation

Gait parameters were assessed in the Cup-Recov and control mice between week 33 and

week 34 using the DigiGait™ imaging system along with the DigiGait™ analysis software (version 15.0, Mouse Specifics, Inc.; Quincy MA) as previously published (Zhan et al., 2019). ***Figure 8A*** illustrates the timeline of the performed gait analyses. The DigiGait™ apparatus consists of a clear plastic treadmill with an under-mounted high-speed digital camera (140 frames/s, Basler Technologies Inc.) used for imaging paw prints (***figure 1***). Animals were habituated to the machine 1 day prior to testing. During the testing procedure, I alternately processed mice from the Cup-Recov and Control group to avoid potential confounding variables. The minimal duration of each video sequence required for subsequent foot-print analyses was 5 s, which has been shown to be sufficient for reliable gait analyses in mice (Kale, Amende, Meyer, Crabbe, & Hampton, 2004). Runs in which mice could not run at a speed of 15 cm/s for a minimum of 5 s were excluded from subsequent analyses (red boxes in ***figure 6***). Data obtained from the training day were not included in the final data evaluation.

As shown in ***figure 6***, the gait of the mice was recorded daily for 4 subsequent days (i.e., d1-d4). Four animals could not run on the machine at the given speed and thus, these runs were excluded for further data analyses (i.e., #13, #23, #28 and #36; red boxes). Runs included for further data analyses are indicated by yellow crosses. Following this strategy and pooling the data from two independent experiments, 95 gait analyses were performed in the $Control^{DigiGait}$ group for different time points with a success rate of 87% (equals 83 completed gait analyses). 96 gait analyses were performed in the $Cup\text{-}Recov^{DigiGait}$ group with a success rate of 88% (equals 84 completed gait analyses). To analyze gait abnormalities in Cup-Recov mice, Evaluator#1 (J.Z.) quantified fore limb and hind limb gait patterns in 9 Cup-Recov and 10 control mice. This first group is referred to as Cohort#1. To verify results of this first experiment, fore limb and hind limb gait patterns were analyzed by Evaluator#1 in another cohort of 10 Cup-Recov and 9 control mice referred to as Cohort#2. Both cohorts were finally re-evaluated by a second evaluator blinded to the treatment groups (i.e., Evaluator#2, Julia Frenz).

| | | | Digigait Training | Digigait Recording | | | |
|---|---|---|---|---|---|---|---|
| Mouse Number | | Treatment | d0 | d1 | d2 | d3 | d4 |
| #1 | Cohort#1 (n=10) | Control$^{DigiGait}$ | | × | × | × | × |
| #2 | | | | × | × | × | × |
| #3 | | | | × | × | × | × |
| #4 | | | | × | × | × | × |
| #5 | | | | × | × | × | × |
| #6 | | | | × | × | × | × |
| #7 | | | | × | × | × | × |
| #8 | | | | × | × | × | × |
| #9 | | | | × | × | × | × |
| #10 | | | | × | × | × | × |
| #11 | Cohort#2 (n=9) | | | × | × | × | × |
| #12 | | | | × | × | × | |
| #13 | | | | | | | |
| #14 | | | | × | | | |
| #15 | | | | × | × | × | × |
| #16 | | | | × | × | × | × |
| #17 | | | | × | | × | × |
| #18 | | | | × | × | × | × |
| #19 | | | | × | × | × | |
| #20 | Cohort#1 (n=9) | Cup-Recov$^{DigiGait}$ | | × | × | × | × |
| #21 | | | | × | × | × | × |
| #22 | | | | × | × | × | × |
| #23 | | | | | | | |
| #24 | | | | × | × | × | × |
| #25 | | | | × | × | × | × |
| #26 | | | | × | × | × | × |
| #27 | | | | × | × | × | × |
| #28 | | | | | | | |
| #29 | Cohort#2 (n=10) | | | × | × | × | × |
| #30 | | | | | × | × | × |
| #31 | | | | × | × | × | × |
| #32 | | | | × | × | × | × |
| #33 | | | | × | × | × | × |
| #34 | | | | × | × | × | × |
| #35 | | | | × | × | × | × |
| #36 | | | | | | | |
| #37 | | | | × | × | × | × |
| #38 | | | | × | × | × | × |

| Pattern | Illustration | Control$^{DigiGait}$ (n=19) | Cup-Recov$^{DigiGait}$ (n=19) |
|---|---|---|---|
| × | Time points included for data analyses | 66 | 63 |
| | Completed DigiGait assessments at 15cm/s | 83 | 83 |
| | Failed DigiGait assessments at 15cm/s | 12 | 12 |
| Completed Ratio | | 87.4% | 87.4% |

**Figure 6 DigiGait™ assessments of individual mice**

Days with successfully conducted DigiGait™ recordings are highlighted in green, whereas days on which mice could not perform DigiGait™ recordings at 15 cm/s are highlighted in red. Days when no DigiGait™ recordings performed are shown in blank. Yellow crosses indicate time points included for data analyses. Cup-Recov and control mice showed no difference in completed ratio on DigiGait™ recordings.

## 4.8 Multiple sclerosis tissues

Paraffin-embedded post-mortem brain tissues were obtained by a medical doctoral student, Hannes Kaddatz, through a rapid autopsy protocol from subjects with progressive MS (in collaboration with the Netherlands Brain Bank, Amsterdam). The study was approved by the institutional ethics review board and all donors or their relatives provided written consent for the use of brain tissues and clinical information for research purposes. In brief, chronic active lesions were defined as lesions with a hypocellular center and a hypercellular rim. Staging of lesions was performed as previously described using anti-PLP and anti-LN3 stained sections (shown in ***figure 7B***) (Grosse-Veldmann et al., 2016; Kipp, van der Valk, & Amor, 2012; Trepanier et al., 2018; van der Valk & De Groot, 2000). For this study, 7 lesions from 5 progressive MS patients and 4 non-MS control patients were included. The average age of control patients in years was 76.50 ± 12.71 (mean ± SD). The average age of MS patients in years was 59.00 ± 7.483. The average disease duration of MS patients in years was 21.60 ± 8.905. Detailed clinical information is given in ***figure 7A***. Normal appearing white matter (NAWM) of MS patients is often used as control reference tissue. However, accumulative evidence shows that various pathologies are present in those areas as well (Chard et al., 2002; Zeis, Graumann, Reynolds, & Schaeren-Wiemers, 2008). For the analyses, normal appearing white matter (NAWM) was defined as a white matter area where myelin appeared normal in anti-PLP stained sections and was distant to the rim of the lesions (illustrated in ***figure 7B***) (Allen, McQuaid, Mirakhur, & Nevin, 2001; van Horssen et al., 2012).

(A)

| Gender | Age at death (y) | Diagnosis | MS Disease duration (y) | Cause of death |
|---|---|---|---|---|
| F | 73 | Control | N/A | Lung fibrosis with rhabdomyolysis and progressive renal insufficiency |
| M | 87 | Control | N/A | Pneumonia, heart failure |
| F | 86 | Control | N/A | Sequelae of end-stage multiple myeloma |
| F | 60 | Control | N/A | Infection |
| M | 49 | SPMS | 25 | Pneumonia |
| M | 66 | PPMS | 26 | Ileus |
| F | 60 | SPMS | 10 | Euthanasia |
| M | 54 | PPMS | 15 | Euthanasia |
| F | 66 | PPMS | 32 | Euthanasia |

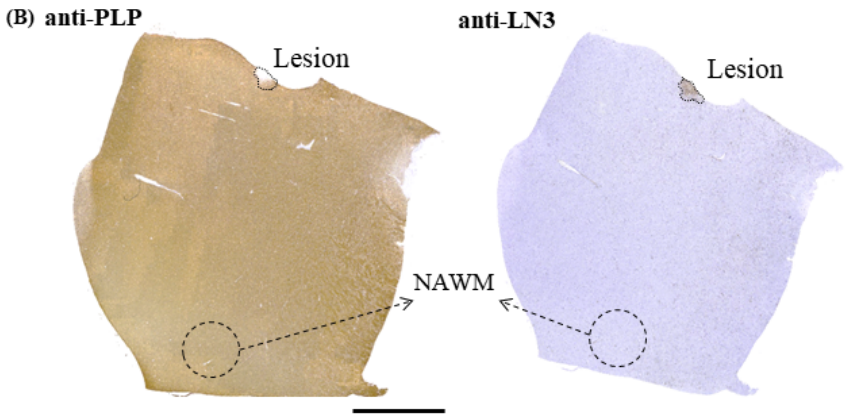


**Figure 7 Summary of progressive MS tissues used in this study**

(**A**) Patient demographics of the progressive MS tissues used in this study. (**B**) Representative pictures demonstrating criteria for NAWM applied in this study. ROIs of NAWM were defined as the white matter area where myelin appeared normal in anti-PLP stained sections and was distant to the rim of the lesions. F: female; M: male; ROI: region of interest; SPMS: secondary progressive multiple sclerosis; PPMS: primary progressive multiple sclerosis; N/A: not applicable; NAWM: normal appearing white matter; PLP: proteolipid protein; LN3: anti-HLA-DR. Scale bar = 5 mm

## 4.9 Statistical analysis

The statistical analyses were performed using GraphPad Prism 5 (GraphPad Software Inc., San Diego, CA, USA). The data is presented as arithmetic means ± standard error of the mean (SEM). D'Agostino and Pearson test was applied to test for Gaussian distribution of the data. Pearson's correlation analysis was used to test the correlation between the density of $PRKCD^+$ and $LN3^+$ cells in MS lesions. The definite statistical procedures applied for the different analyses are provided in the respective figure legends. The following symbols were used to indicate the level of significance: * $p \leq 0.05$, ** $p \leq 0.01$, *** $p \leq 0.001$ and ns = not significant.

# 5. Results

## 5.1 Ongoing glial activation and axonal damage after long-term remyelination

It is well known that after 5 weeks of cuprizone-intoxication several white and grey matter areas are demyelinated, among the medial part of the corpus callosum at the level R265 of the rostral hippocampus (refer to the material and methods section). Spontaneous remyelination occurs when animals are provided with normal chow following acute cuprizone-induced demyelination (Goldberg, Clarner, Beyer, & Kipp, 2015; Kipp, Clarner, Dang, Copray, & Beyer, 2009; Nyamoya et al., 2019). To examine the long-term consequence of an acutely demyelinated white matter lesion, a first group of mice was subjected to a 5-week cuprizone intoxication period followed by 7-month normal chow for recovery (i.e., 28 weeks; Cup-Recov). A second group of mice was sacrificed after 5 weeks of cuprizone intoxication to verify the presence of acutely demyelinated lesions. Age-matched controls were fed with a normal diet throughout the entire experiment. To verify demyelination at week 5, coronal sections were processed for anti-PLP staining intensity analyses. As shown in ***figure 8B,*** profound demyelination of the medial part of the corpus

callosum was observed after 5 weeks cuprizone, paralleled by cortical demyelination. After 28 weeks of recovery, anti-PLP staining intensities (Cup-Recov, 96.33 ± 0.9803% *vs* control, 96.88 ± 0.5042%, p = 0.6320) as well as the densities of anti-$OLIG2^+$ cells (Cup-Recov, 1672 ± 117.9 cells/$mm^2$ *vs* control, 1702 ± 67.44 cells/$mm^2$, p = 0.8334) recovered, thus were comparable in Cup-Recov and age-matched controls mice (shown in ***figure 8C***), suggesting a complete remyelination of the previously demyelinated white matter tract corpus callosum. To address ongoing glial reactivity despite completed remyelination, brain sections from Cup-Recov mice and age-matched controls were processed for anti-IBA1 and anti-GFAP immunohistochemistry to label microglia and activated astrocytes, respectively. As shown in ***figure 8D***, both stains, anti-IBA1 (Cup-Recov, 7.207 ± 1.316% *vs* control, 3.289 ± 0.3240%, p = 0.0317) and anti-GFAP (Cup-Recov, 13.87 ± 4.282 *vs* control, 2.713 ± 0.7328%, p = 0.0317), revealed persistent activation of microglia and astrocytes in the corpus callosum of Cup-Recov mice. Consistent with a previous report (Manrique-Hoyos et al., 2012), the density of amyloid precursor protein-positive ($APP^+$) axonal spheroids was significantly increased in Cup-Recov animals as compared to age-matched controls (Cup-Recov, 7.262 ± 0.9408 $APP^+$ spheroids/$mm^2$ *vs* control, 4.077 ± 0.5502 $APP^+$ spheroids/$mm^2$; p = 0.0065; see ***figure 8E***), indicating ongoing acute axonal injury.

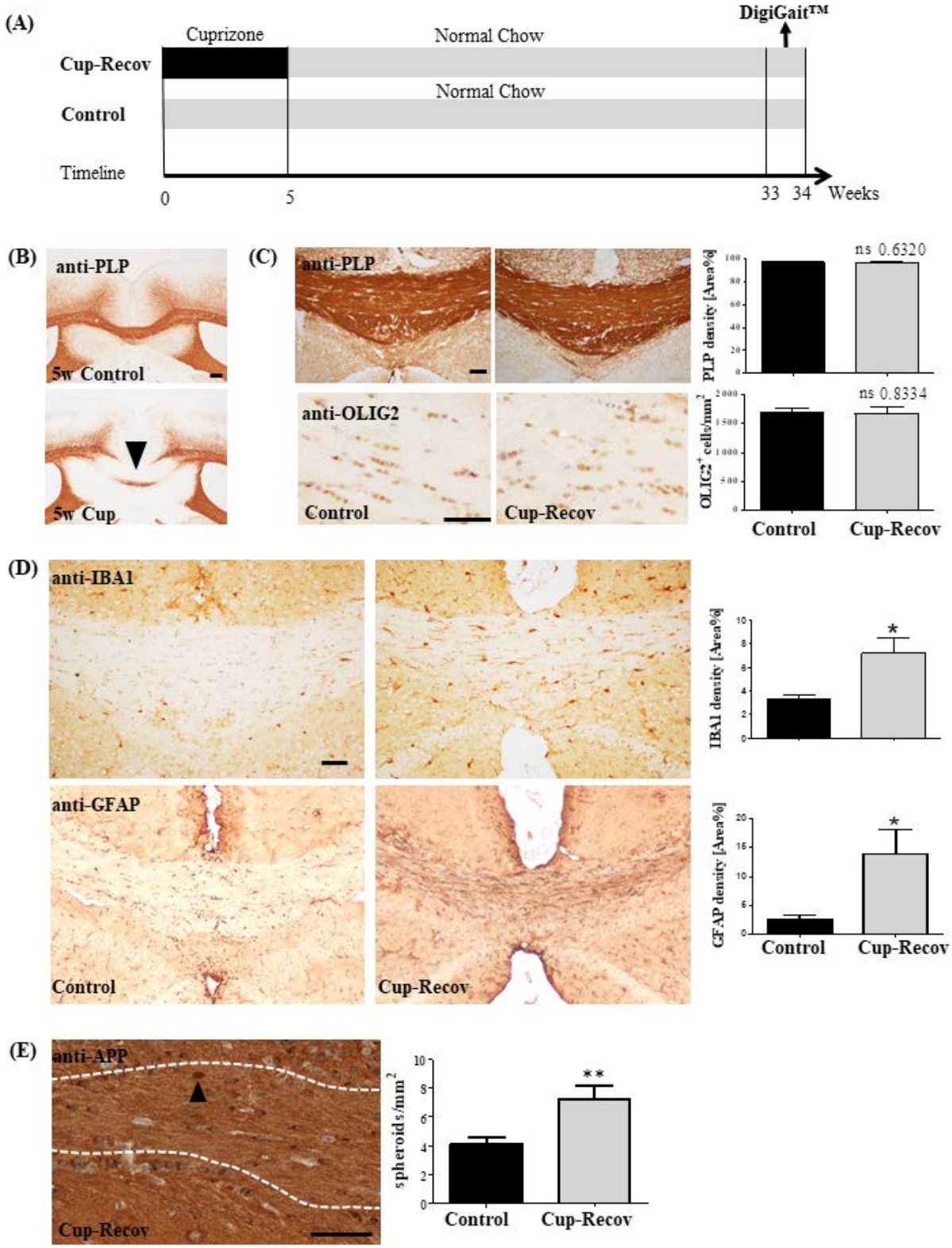


**Figure 8 Ongoing glial activation and axonal damage after long-term remyelination**

(**A**) Schematic drawing illustrating the experimental setup. 8-week-old mice were intoxicated with cuprizone

for 5 weeks followed by 28 weeks normal chow (Cup-Recov). Age-matched controls were fed with normal chow throughout the experiment (Control). DigiGait™ analyses were conducted during the last week of the experiment and mice were sacrificed after DigiGait™ measurements for subsequent IHC/IF or molecular biological studies. (**B**) Histopathological characteristics of acute demyelination (arrowhead) after 5 weeks of cuprizone intoxication. (**C**) Representative anti-PLP and anti-OLIG2 stains of Cup-Recov and control mice. Densitometric analyses were used to evaluate staining intensity of anti-PLP stains. $OLIG2^+$ cell numbers were manually counted by two independent evaluators (J.Z. and H.K.) blinded to the treatment groups (n = 5 per group, *ns*: not significant; unpaired t-test). (**D**) Representative anti-IBA1 and anti-GFAP stains of Cup-Recov and control mice. Densitometric analyses were used to evaluate staining intensity of anti-IBA1and anti-GFAP stains (n = 5 per group, * $p < 0.05$; Mann–Whitney test). (**E**) Representative $APP^+$ spheroid (arrowhead) of Cup-Recov mice. Dashed line demarcates the corpus callosum region. Quantification of $APP^+$ spheroids numbers was done manually by two independent evaluators (J.Z. and H.K.) blinded to the treatment groups (n = 5 per group, ** $p < 0.01$; unpaired t-test). OLIG2: oligodendrocyte transcription factor 2; PLP: proteolipid protein. IBA1: ionized calcium-binding adapter molecule 1; GFAP: glial fibrillary acidic protein; APP: amyloid precursor protein. Scale bar = 50 μm (B) (C) (D) (E).

## 5.2 Reactive microglial phenotype after long-term remyelination

So far I was able to demonstrate ongoing glial activation after long-term remyelination. Besides cell numbers, cell morphology is critical to distinguishing resting and activated microglia (Crews & Vetreno, 2016; H. W. Morrison & Filosa, 2013). To address this aspect, anti-IBA1 stained sections were digitalized, and the morphology of deep layer cortex microglia (25 cells per group) was analyzed using the software environment Neurolucida360. The following parameters were evaluated: ***Intersection***, ***Node***, ***Ending***, ***Area***, ***Volume*** and ***Avg.Diameter***. For a schematic illustration of the morphological parameters see ***figure 9C*** and the material and methods section. As shown in ***figure 9D,E***, in general all of the evaluated morphological parameters were by trend increased in Cup-Recov compared to control mice. The increases applies to both, microglia processes near (i.e., 6-15μm) and distant (i.e., >15μm) to the cell somata (***figure 9F, supplementary figure 1B***). The volume ramification index ($RI_v$) determined by Convex Hull 3D analysis was comparable in Cup-Recov and age-matched controls mice (***supplementary figure 1E***). These results suggests that the microglia cells in Cup-Recov mice show an intermediate morphology between the resting microglia cells and the fully activated phagocytes.

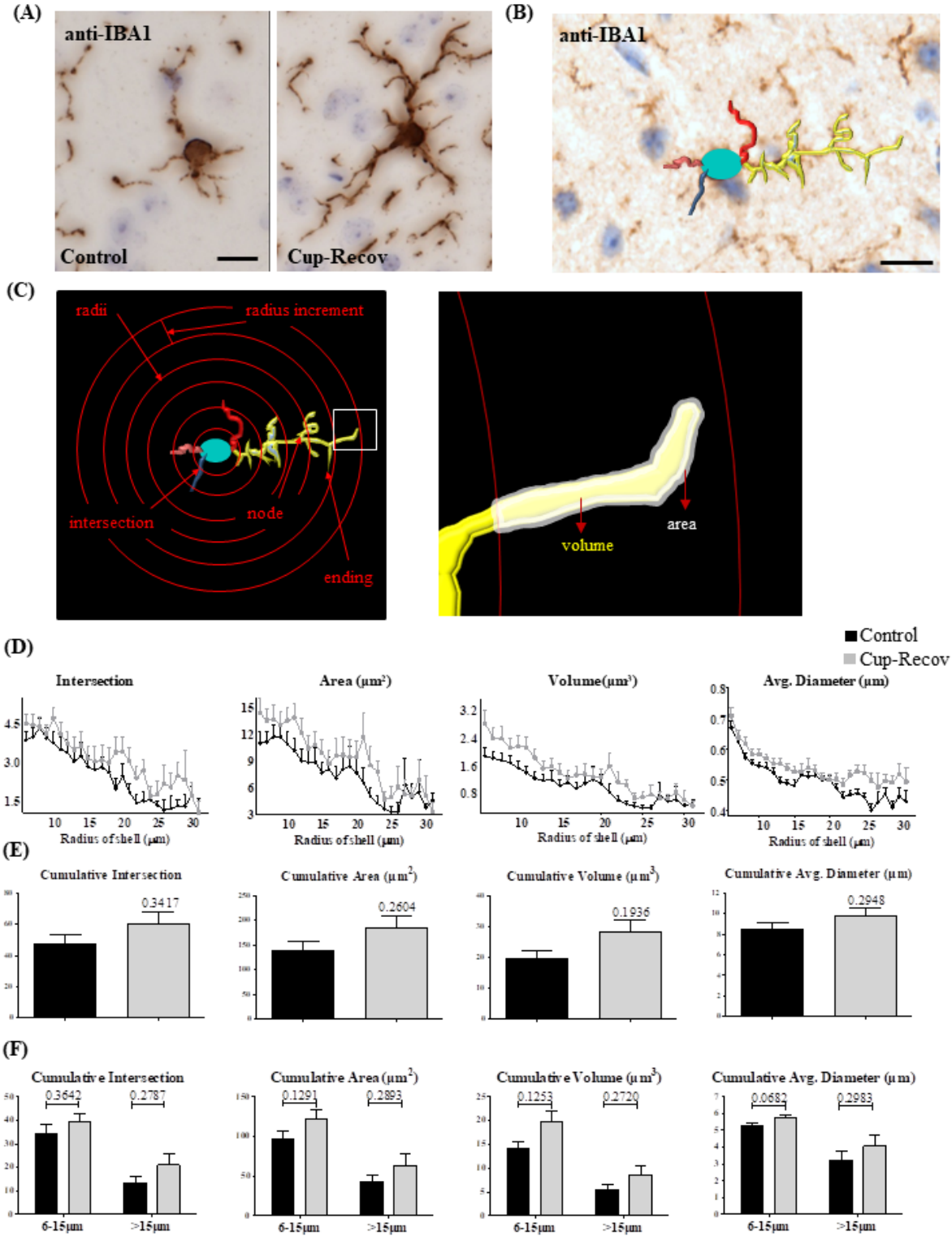


**Figure 9 Reactive microglial phenotype after long-term remyelination**

**(A)** Representative anti-IBA1 stains of Cup-Recov and control mice. **(B)**. Reconstruction of microglial

morphology using Neurolucida360 with z-stack images (n=40), generated with a 0.5 μm step size. **(C)** Representative images illustrating evaluation of microglial morphology using Sholl analysis. **(D)** Sholl analysis plots of morphological parameters in microglia (i.e., ***Intersection***, ***Area, Volume*** and ***Avg. Diameter***. n = 25 cells per group). **(E)** Overall and **(F)** subgroup differences between Cup-Recov and control mice were determined from the area under each Sholl curve (n = 25 cells per group, respective *p*-values were shown on the graph). *IBA1*: ionized calcium-binding adapter molecule 1; *Avg.*: Average. Scale bar = 10 μm.

## 5.3 Verification of ongoing pathology after long-term remyelination at the transcriptional level by gene array analyses

Our histological results suggest a minor yet distinct ongoing pathology 7 months after an acute demyelinating event. To verify this observation at the transcriptome level, mRNA samples from the corpus callosum and cortex of Cup-Recov and age-matched control mice were analyzed using gene arrays. In the corpus callosum, the expression of 115 probe sets was found to be significantly up-regulatedand the expression of 103 probe sets was significantly reduced (***figure 10A***). In the cortex, the expression of 148 probe sets was found to be significantly up-regulatedand the expression of 112 probe sets was significantly reduced (***supplementary table 5***). To understand which pathways are involved, I performed gene enrichment analyses with the up- and down-regulated genes in the corpus callosum. Up-regulated genes are highly related to the biological processes ‘positive regulation of transcription by RNA polymerase II’ (3.17-fold enrichment), ‘positive regulation of cell population proliferation’ (3.22-fold enrichment) or ‘regulation of cell adhesion’ (3.27-fold enrichment). Down-regulated genes are highly related to the molecular function term ‘hormone binding’ (14.86-fold enrichment). Taken together, the gene array data verifies the ongoing pathology in long-term remyelinating mice.

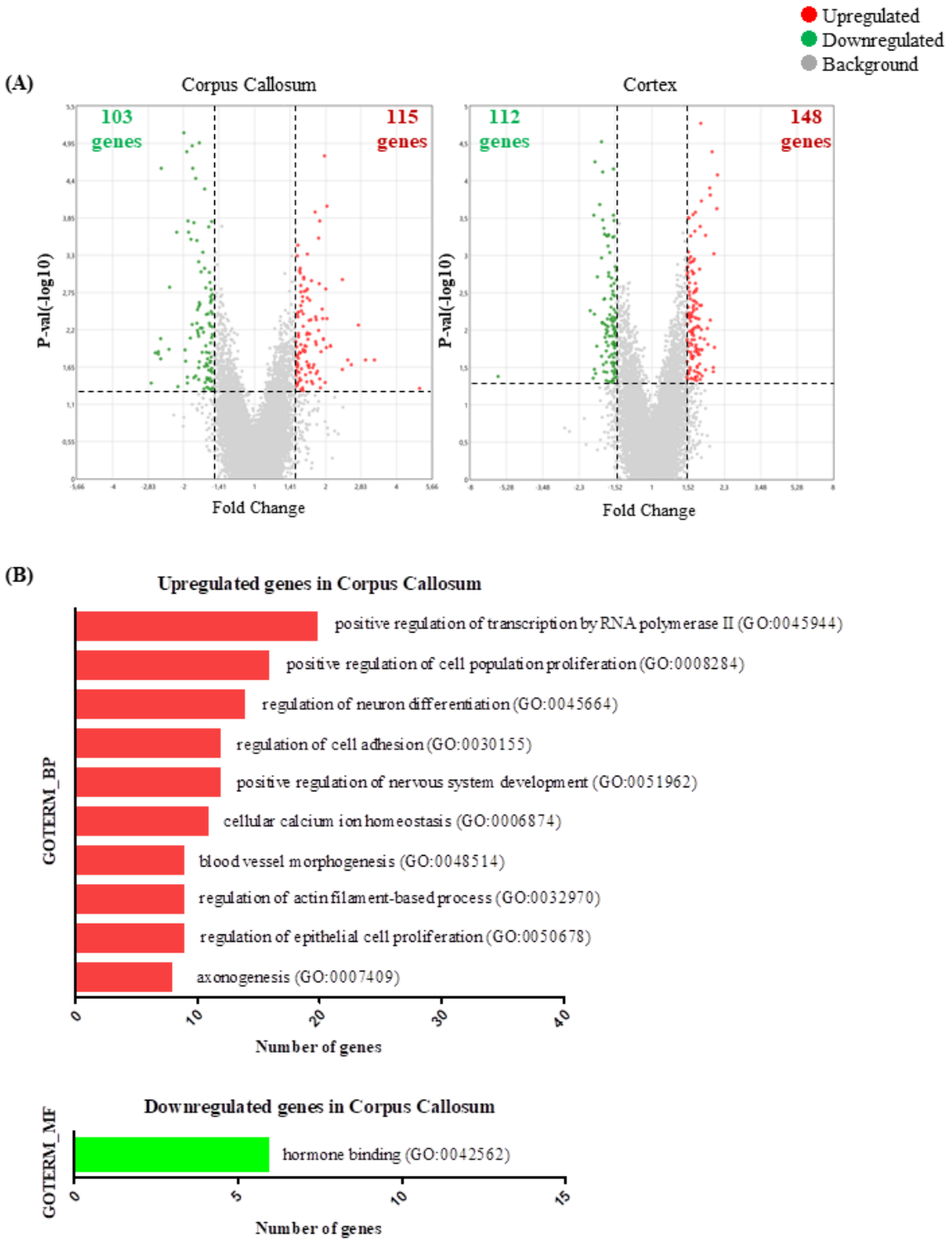


**Figure 10 Transcriptome changes after long-term recovery**

Differentially expressed genes determined by gene array analysis of mRNA isolated from corpus callosum and cortex. (**A**) Volcano plot of differentially expressed genes in corpus callosum and cortex samples of Cup-

Recov compared to control mice. Genes differentially expressed in corpus callosum showed more prominent fold change than those in the cortex. Red dots indicate the genes that were significantly up-regulated in Cup-Recov compared to control mice. Green dots represent the genes that were significantly down-regulated in Cup-Recov compared to control mice. Grey dots represent non-regulated genes. The dash lines indicate the applied threshold of a 1.5-fold change in the gene expression. **(B)** Gene enrichment analyses of biological process (GOTERM_BP) and molecular function (GOTERM_MF) were performed using GO online tool (http://geneontology.org/). Top10 terms of GOTERM_BP were shown on the graph based on gene numbers.

Among the differentially expressed genes in the corpus callosum, the most up−regulated gene was protein kinase c delta (*Prkcd*, 5.01-fold up-regulated vs control, p = 0.046). The online RNA-seq Database („Source: http://brainrnaseq.org/“) indicates that PRKCD is highest expressed in microglia among all other cell types in the brain under physiological conditions (Y. Zhang et al., 2014). Gene array results were further tested at both mRNA and protein levels using independent biological samples. At mRNA level, I systematically detected mRNA expression of up-regulated genes (i.e., *Prkcd, Slitrk6, Pln, Ndst4*) and down-regulated genes (i.e., *Lcn2, Cadps2, Arc, Sgk1*) using real-time RT-PCR (***figure 11C***). Five out of eight re-investigated genes showed the same expression pattern in gene array and real-time RT-PCR. Beyond, at the protein level, I verified the induction of ANXA2 by immunohistochemistry (***figure 11A, B***).

(A)

| Gene Symbol | FC (Cup-Recov/Control) | $Control_{Average}$ (log2) | $Cup\text{-}Recov_{Average}$ (log2) |
|---|---|---|---|
| *Anxa2* | 1.94 | 6.19 | 7.15 |

(B)

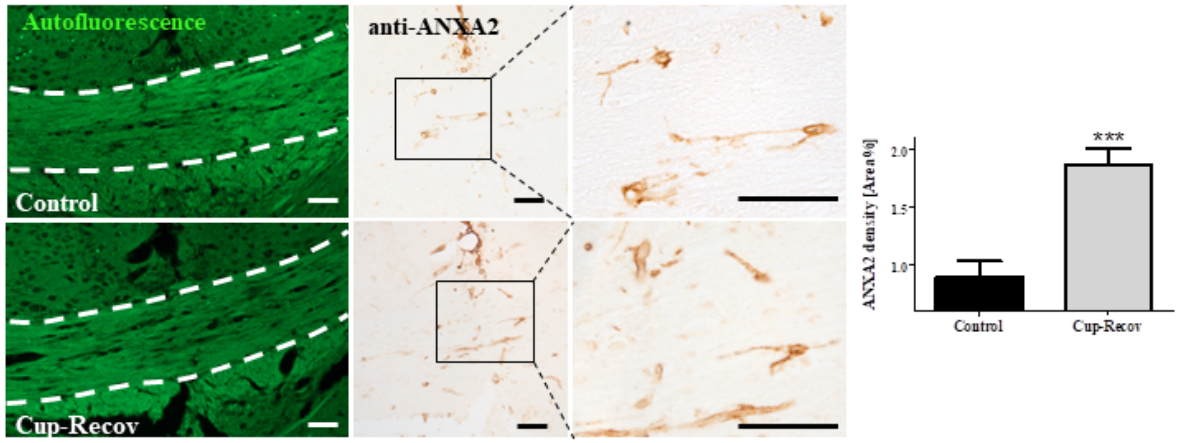


(C)

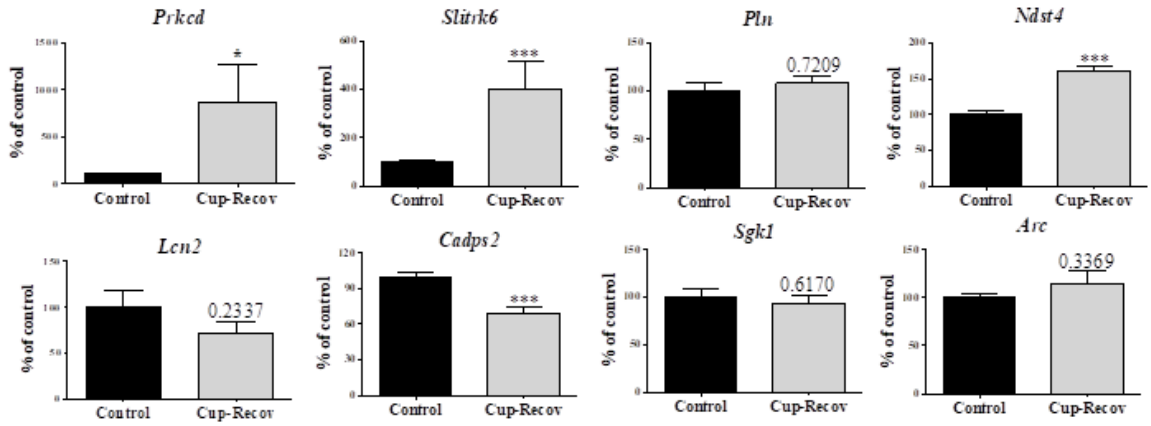


**Figure 11: Verification of the gene array results**

(**A**) Fold change of *Anxa2* expression levels in the corpus callosum of Cup-Recov mice compared to age-matched controls identified by gene array analyses (n = 4 per group). (**B**) Cup-Recov showed increased intensity of anti-ANXA stains compared to age-matched controls (center). Autofluorescence of paraffin embedded slides was used to distinguish anatomical borders (left). Densitometric analysis was used to evaluate staining intensity of anti-ANXA2 stains (n = 5 per group, ***p < 0.001; Mann–Whitney test). (**C**) Gene array results were further verified by real-time RT-PCR for selected up-regulated genes (*Prkcd, Slitrk6, Pln, Ndst4)* and down-regulated genes (*Lcn2, Cadps2, Sgk1, Arc)* (n = 4 per group, ***p < 0.001; unpaired t-test or Mann–Whitney test according to data distribution). ANXA2: annexin a2; *Prkcd*: protein kinase c delta; *Slitrk6*: SLIT and NTRK like family member 6; *Pln*: Phospholamban; *Ndst4*: N-Deacetylase and N-Sulfotransferase 4; *Lcn2*: lipocalin 2; *Cadps2*: calcium dependent secretion activator 2; *Sgk1*: serum/glucocorticoid regulated kinase 1; *Arc*: activity regulated cytoskeleton associated protein. Scale bar = 50 µm.

## 5.4 Ongoing functional deficits after long-term remyelination

So far, I was able to demonstrate by means of histological and transcriptome techniques that 7 month after a demyelinating insult, ongoing neuropathologies such as glia cell activation, axonal injury paralleled by transcriptome activity can be detected in the previously injury white matter. In a next step, I asked whether the persistent pathology, observed on the cellular and transcriptome level, is paralleled by motor behavioral deficits. To address this point, I systematically compared a set of different gait parameters in Cup-Recov (referred to as Cup-Recov$^{DigiGait}$, n = 19) and age-matched control mice (referred to as Control$^{DigiGait}$, n = 19) using the DigiGait$^{TM}$ apparatus as previously published by our group (Zhan et al., 2019). „High speed ventral plane videography recordings were performed in two independent cohorts of animals, referred to as Cohort#1 (9 Cup-Recov$^{DigiGait}$ and 10 Control$^{DigiGait}$ animals) and Cohort#2 (10 Cup-Recov$^{DigiGait}$ and 9 Control$^{DigiGait}$ animals). In a first step, 39 fore limb and 43 hind limb gait parameters were systematically evaluated by the first evaluator (i.e., Evaluator#1) in the Cohort#1 mice and statistically compared. As demonstrated in ***figure 12A***, 5 distinct fore or hind limb gait metrics were found to be significantly increased or decreased in Cup-Recov$^{DigiGait}$ compared to Control$^{DigiGait}$. To verify these findings, the 5 gait parameters which were found to be significantly altered in the Cohort#1 mice were re-evaluated in Cohort#2 mice. 5 out of the 5 gait parameters were verified in the second cohort. These were the gait metrics *Propel* in fore limbs and *Swing Time, %Swing Stride, %Stance Stride, Stance Width* in hind limbs (***figure 12B***). Detailed illustration of those gait metrics is provided in the discussion section.

Since the gait signals provided by the software require some manual, thus subjective, adjustments (T. G. Hampton, Stasko, Kale, Amende, & Costa, 2004), another independent evaluator (Evaluator#2) performed analyses of both Cohort#1 and Cohort#2 video sequences blinded to the treatment to validate the results. As shown in ***figure 12A***, all 5 gait parameters which were found to be different in Cup-Recov$^{DigiGait}$ mice were verified by the second evaluator (Evaluator#2). “ The description of DigiGait$^{TM}$ results is adopted from my previously published work to keep consistent (Zhan et al., 2019).

**(A)**

| | Number | Parameters | Evaluator#1 Cohort#1 (Change, Significance, *p*-Value) | Evaluator#1 Cohort#2 (Change, Significance, *p*-Value) | Evaluator#2 Cohort#1 and Cohort#2 (Change, Significance, *p*-Value) |
|---|---|---|---|---|---|
| **Fore Limbs** | #1 | Propel (Average) | ↑, **, 0.0070 | ↑, *, 0.0367 | ↑, **, 0.0018 |
| **Hind Limbs** | #2 | Swing Time (Average) | ↑, *, 0.0413 | ↑, **, 0.0016 | ↑, *, 0.0486 |
| | #3 | %Swing Stride (Average) | ↑, *, 0.0202 | ↑, ***, 0.0003 | ↑, *, 0.0249 |
| | #4 | %Stance Stride (Average) | ↓, *, 0.0202 | ↓, ***, 0.0003 | ↓, *, 0.0249 |
| | #5 | Stance Width | ↓, *, 0.0137 | ↓, ***, < 0.0001 | ↓, *, 0.0203 |

**(B)**

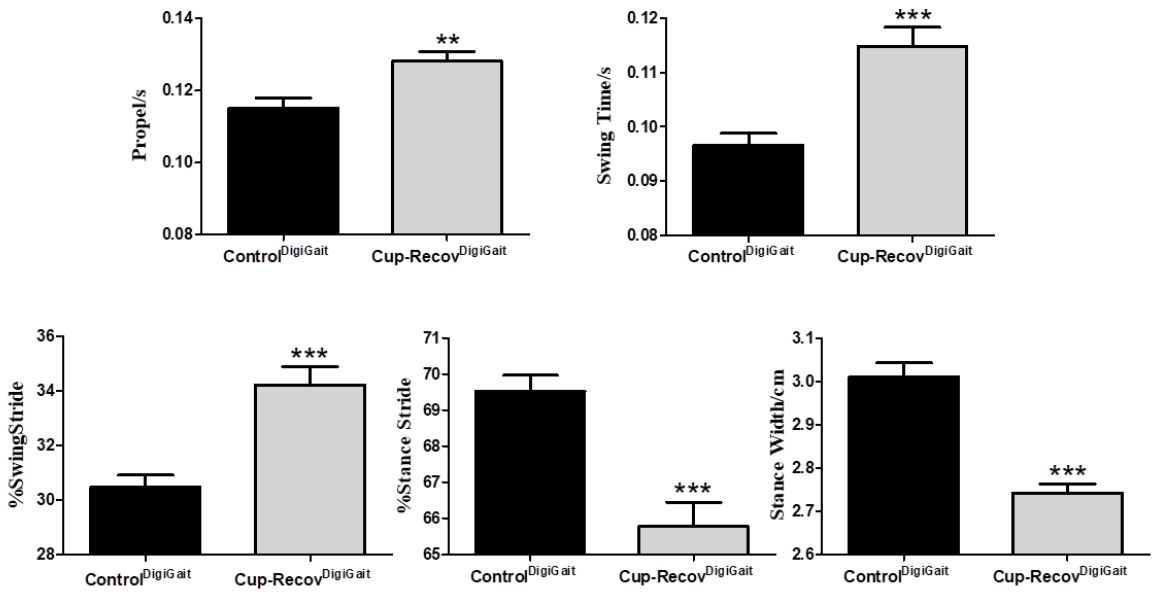


**Figure 12 Gait abnormalities after long-term remyelination**

„(**A**) Summary of the 5 gait parameters found to be altered in Cup-Recov compared to control mice. Two independent experiments were performed, referred to as Cohort#1 (9 Cup-Recov and 10 control mice) and Cohort#2 (10 Cup-Recov and 9 control mice). Gait parameters were evaluated by two independent evaluators, referred to as Evaluator#1 (J.Z.) and Evaluator#2 (J.F.) blinded for the experimental groups. Arrows indicate whether gait parameters were increased ( ↑ ) or decreased ( ↓ ) in Cup-Recov compared to control mice. In fore limbs, time required for accelerating the motion and continuing forward (i.e., ***Propel***) was found significantly increased in both Cohort#1 and Cohort#2. In hind limbs, time duration/percentage of the swing phase (i.e.,

***Swing Time***, ***%Swing Stride***) were found significantly increased, meanwhile percentage of the stance phase (i.e., ***%Stance Stride***) and the width of step (i.e., ***Stance Width***) significantly decreased in both Cohort#1 and Cohort#2 (indicated by respective *p*-values). All of these 5 parameters were verified by Evaluator#2 (last column). (**B**) Shown are the mean values of significantly changed parameters in Cup-Recov with the respective SEM. The D'Agostino and Pearson test was applied to test for normal distribution of the data. *p*-values were calculated using unpaired t-test or Mann-Whitney test according to data distribution. * $p < 0.05$, ** $p < 0.01$, *** $p < 0.001$." The description of DigiGait™ results is adopted from my previously published work (Zhan et al., 2019).

## 5.5 PRKCD is predominately expressed by microglia/macrophages

Among the differentially expressed genes in the corpus callosum, the most up-regulated gene was protein kinase c delta (*Prkcd*, 5.01-fold up-regulated vs control, p = 0.046). The online RNA-seq Database („Source: http://brainrnaseq.org/") indicates that PRKCD is highest expressed in microglia among all other cell types in the brain under physiological conditions (Y. Zhang et al., 2014). Induced *Prkcd* expression was further confirmed by real-time RT-PCR (Cup-Recov, 865.5 ± 409.8% vs control, 100 ± 9.412%, p = 0.0207; ***figure 14C***). Next, I wanted to verify this finding on the protein level by processing slides for anti-PRKCD immunohistochemistry. In line with the *in situ* hybridization data retrieved from the Allen Brain atlas (Lein et al., 2007), in control mice *Prkcd* was found to be highly expressed in the cornu ammonis 3 (CA3) field of the hippocampus, thalamic nuclei and lateral septal nuclei (see representative thalamic $PRKCD^+$ neuron in ***figure 13***), whereas in the corpus callosum of healthy mice, low numbers of $PRKCD^+$ cells were found. In line with the mRNA results, the numbers of $PRKCD^+$ cells were found to be increased after long-term remyelination compared to controls (Cup-Recov, 118.4 ± 7.667 cells/$mm^2$ *vs* control, 73.00 ± 6.239 cells/$mm^2$, p = 0.0002; ***figure 14A***). It has been reported that in the injured CNS, PRKCD is expressed by microglia cells (Gordon et al., 2016; Y. Zhang et al., 2014). To determine the cellular source of PRKCD expression in Cup-Recov and control mice, we performed immune-fluorescence double labelling experiments and examined 178 representative $PRKCD^+$ profiles among 34 ROIs derived from 3 Cup-Recov and 3 control mice, analyzed by 2 independent evaluators (J.Z. and H.K.). This analysis showed that ~64%

and ~82% of PRKCD$^{+}$ cells co-labeled with the microglia/macrophages marker protein IBA1$^{+}$ in Cup-Recov and control mice, respectively. Beyond, densities of PRKCD$^{+}$/IBA1$^{+}$ cells (yellow) were low (23.24 ± 3.11 cells/mm$^{2}$; ***figure 14B***) in control mice, but increased in Cup-Recov mice (83.01 ± 7.18 cells/mm$^{2}$; ***figure 14B***).

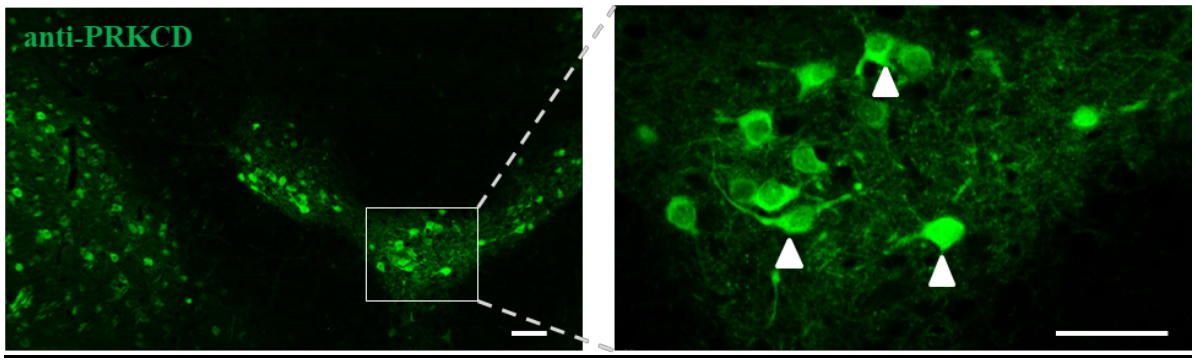


**Figure 13 Validation of anti-PRKCD IHC stains**
PRKCD$^{+}$ thalamic neuron (arrowheads) as previously reported. PRKCD: protein kinase c delta; Scale bar = 50 µm.

To further verify our finding that PRKCD is predominantly expressed by microglia in the injured corpus callosum, we performed anti-IBA1 and anti-PRKCD immunohistochemistry with brain sections from 5 weeks cuprizone-intoxicated and control mice, where profound microgliosis can be found (Gudi, Gingele, Skripuletz, & Stangel, 2014; Nack et al., 2019). As demonstrated in ***figure 14D, E***, the densities of IBA1$^{+}$ and PRKCD$^{+}$ cells were profoundly increased after acute cuprizone-induced demyelination. Furthermore, we found that PRKCD is predominately expressed by IBA1$^{+}$ microglia/macrophages (***figure 14F***) rather than GFAP$^{+}$ astrocytes or OLIG2$^{+}$ oligodendrocytes (data not shown) in the corpus callosum of 5 weeks cuprizone-intoxicated mice.

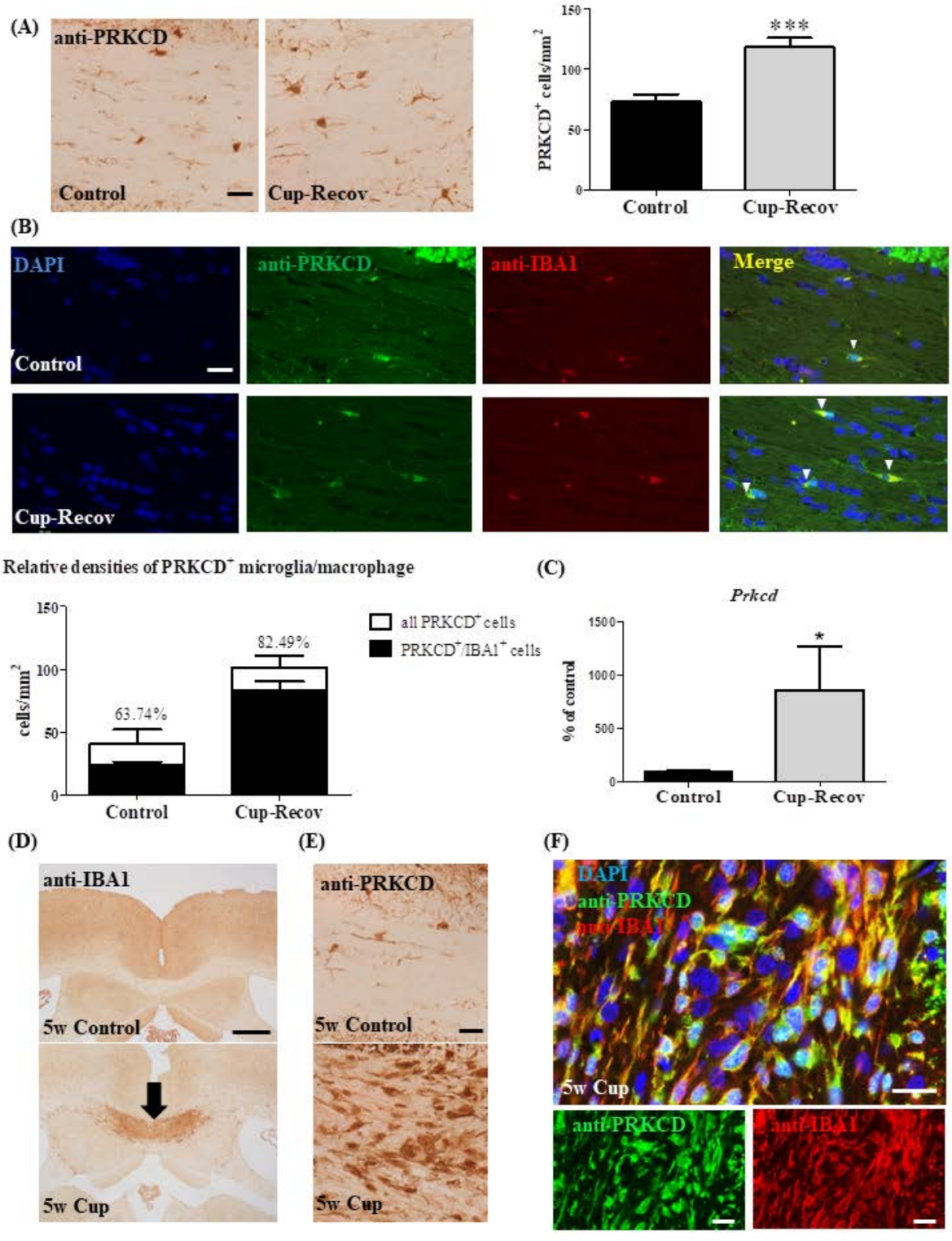


**Figure 14: Expression of PRKCD in microglia/macrophages of mice**

**(A)** Expression of PRKCD was significantly induced in the corpus callosum of long-term remyelination mice (Cup-Recov) compared to age-matched control mice. Quantification of $PRKCD^+$ cell numbers was done

manually by two independent evaluators blinded to the treatment groups (n = 5 per group, ***p < 0.001; unpaired t-test). **(B)** The relative numbers of PRKCD$^{+}$ microglia/macrophages in Cup-Recov and age-matched control mice were determined by PRKCD/IBA1 immunofluorescence double staining. Arrowheads highlight PRKCD$^{+}$ microglia/macrophages. Note that most (82.49%) of the PRKCD$^{+}$ cells were microglia/macrophages in Cup-Recov. **(C)** Induced expression of *Prkcd* was further verified by real-time RT-PCR compared to age-matched controls (n = 4 per group, *p < 0.05; Mann–Whitney test). **(D)** Representative anti-IBA1 and **(E)** anti-PRKCD stains of mice intoxicated with cuprizone for 5 weeks (5w Cup) and control mice. **(F)** Representative images illustrating that PRKCD co-localizes with IBA1$^{+}$ microglia/macrophages in the corpus callosum of 5 weeks cuprizone-intoxicated mice. PRKCD: protein kinase c delta; IBA1: ionized calcium-binding adapter molecule 1. Scale bar =20 µm (A) (B) (E) (F); 500 µm (D).

## 5.6 Induced expression of PRKCD in progressive MS patients

As previously reported, there are several similarities between histopathological alterations described in *post-mortem* MS brain lesions and cuprizone-induced pathologies, which include profound demyelination, microgliosis, astrocytosis and axonal damage (Kipp et al., 2017). Therefore, I next aimed to investigate whether the induction of PRKCD expression observed in cuprizone-intoxicated mice can as well be found in chronic (active) lesions of progressive MS patients. To this end, brain sections from 5 progressive MS patients together with 4 non-MS control patients were processed for anti-PRKCD immunohistochemistry. PRKCD$^{+}$ cells, resembling microglia-like morphology with slender process (see arrowheads in ***figure 15C, left***), were found to be evenly distributed throughout the white matter of the non-MS control patients. Moreover, high density of PRKCD$^{+}$ cells were also observed in the periventricular areas of the non-MS control patients.

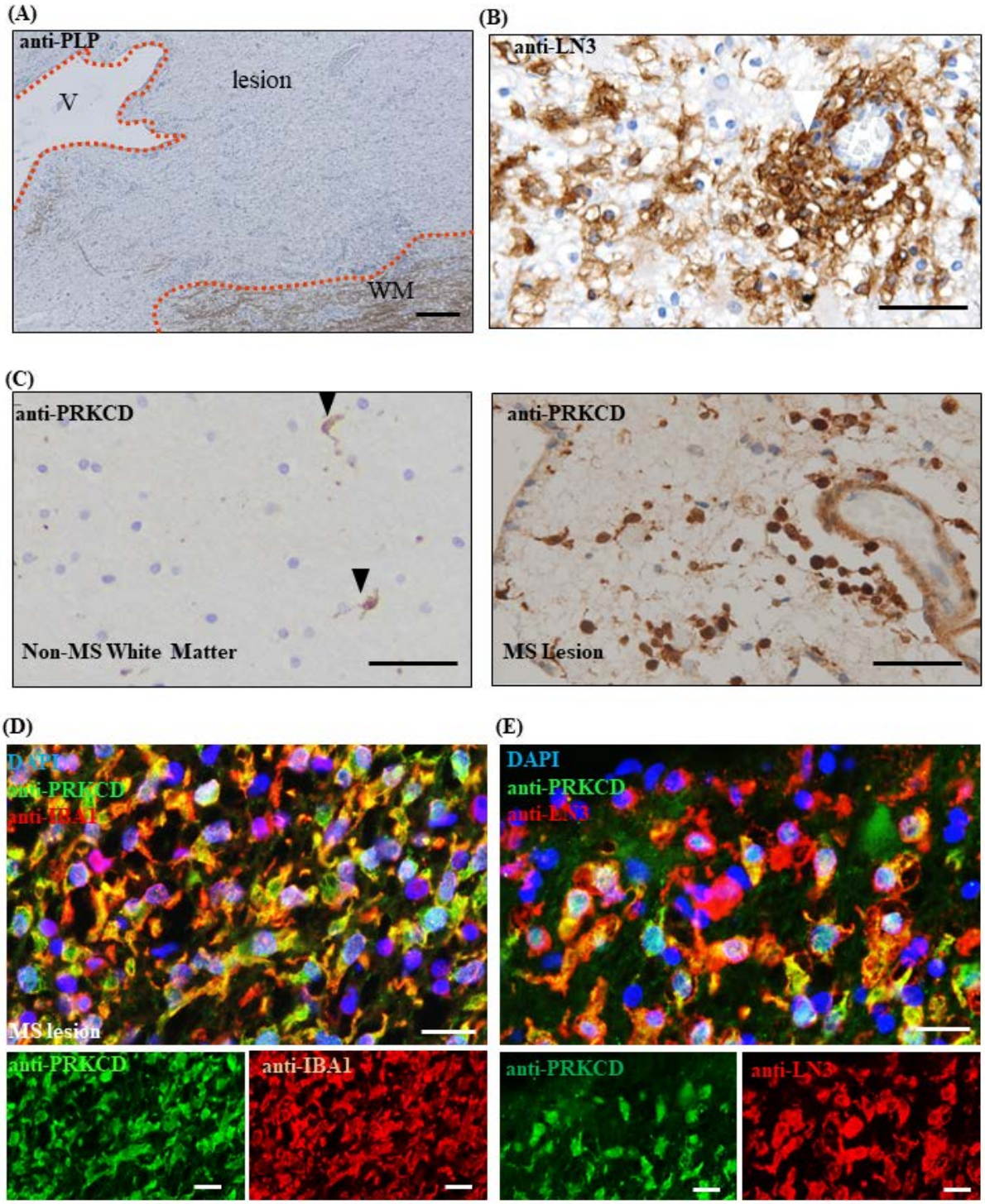


**Figure 15 Induced expression of PRKCD in chronic (active) lesions of progressive MS patients**

Representative chronic (active) MS lesion illustrated by **(A)** anti-PLP and **(B)** anti-LN3 immunohistochemistry. **(C)** Representative anti-PRKCD stains of a non-MS white matter control section (n = 4) and a chronic (active) MS lesion (n = 5). Black arrowheads highlight PRKCD$^{+}$ cells resembling resting microglia in non-MS white matter control. Representative images illustrating that PRKCD co-localizes with **(D)** IBA1$^{+}$

microglia/macrophages or **(E)** $LN3^+$ activated microglia/macrophages in chronic (active) MS lesions. MS: multiple sclerosis; PLP: proteolipid protein; PRKCD: protein kinase c delta; LN3: HLA-DR; V: Ventricle; Scale bar = 200 µm (A); 50µm (B) (C); 20µm (D) (E).

Increased numbers of $PRKCD^+$ cells were observed in the active lesions and at the rim of the chronic active lesions when compared to the non-MS control patients. A representative periventricular chronic active lesion is shown in ***figure 15A***, where the red-dotted line demarcates the lesion border in an anti-PLP processed section. Within the lesion high numbers of MHC-II/LN3-expressing cells can be found (***figure 15B)***. In such lesions, numbers of $PRKCD^+$ cells were highly increased with particular high numbers around the perivascular spaces (***figure 15C, right***), where clusters of $LN3^+$ cells were found (***figure 15B***). Double immunofluorescence stains showed almost complete co-localization of PRKCD with IBA1 (***figure 15D***) and partial co-localization of PRKCD with LN3 (***figure 15E***). Next, I was interested whether the number of $PRKCD^+$ cells is as well increased in areas of normal myelin densities (i.e., NAWM) (Evangelou, Esiri, Smith, Palace, & Matthews, 2000; Kipp et al., 2017; Kutzelnigg et al., 2005). As demonstrated in ***figure 16A, B***, I found increased numbers of $PRKCD^+$ cells in NAWM compared to non-MS white matter (Non-MS white matter, 26.56 ± 9.325 cells/$mm^2$ *vs* NAWM, 78.22 ± 16.16 cells/$mm^2$, $p = 0.0368$). Pearson's correlation analysis revealed a significant correlation between density of $PRKCD^+$ and $LN3^+$ cells in the lesion sites ($r = 0.7333$; 95% confidence interval = 0.1346 to 0.9398; $p = 0.0246$; ***figure 16C***). Furthermore, double immunofluorescence stains showed almost complete co-localization of PRKCD with IBA1 (***figure 16D***) and partial co-localization of PRKCD with LN3 (***figure 16E***) in the NAWM of MS patients.

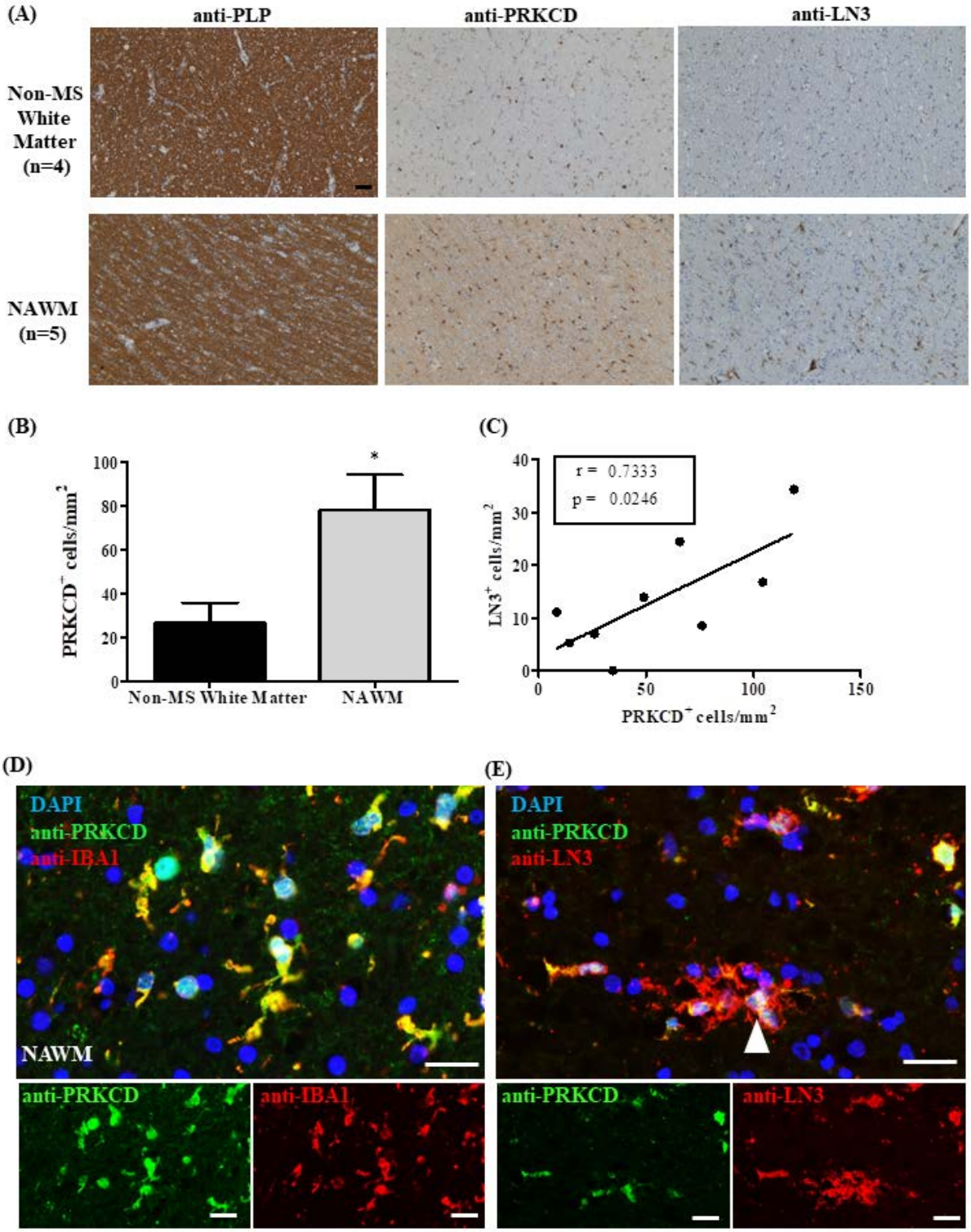


**Figure 16 PRKCD expression in activated microglia/macrophages of the NAWM**

**(A)** Representative pictures demonstrating induced expression of PRKCD in NAWM compared to non-MS white matter controls. See material and methods section for further detail regarding NAWM criteria. **(B)** Quantification of $PRKCD^+$ cell numbers were done manually by two independent evaluators (J.Z. and H.K.)

blinded to the lesion type (n = 5 in NAWM and n = 4 in non-MS white matter controls, *p < 0.05; unpaired t-test). **(C)** Correlation analysis for $PRKCD^+$ and $LN3^+$ cell densities (n = 9, *p < 0.05; Pearson's test). Representative images illustrating that PRKCD co-localizes with **(D)** $IBA1^+$ microglia/macrophages or **(E)** $LN3^+$ activated microglia/macrophages in NAWM. Arrowhead highlights a $PRKCD^+/LN3^+$ cell. MS: multiple sclerosis; NAWM: normal appearing white matter; PLP: proteolipid protein; PRKCD: protein kinase c delta; LN3: anti-HLA-DR. Scale bar = 50µm (A); 20µm (D) (E).

# 6. Discussion

Within my thesis, I was able to demonstrate by various techniques that (i) there are ongoing cuprizone-induced pathologies (i.e., glial activation and axonal damage) and functional deficits (i.e., gait abnormalities) after long-term remyelination, (ii) that microglial cells present a hyper-ramified morphology and overexpress PRKCD during this chronic process, and (iii) that PRKCD expression in microglia/macrophages is characteristic for progressive, post-mortem MS lesions and NAWM areas.

## 6.1 Ongoing long-term axonal injury and glial activation in the CNS

It is a fascinating question whether the CNS 'remembers' focal pathologies which impact neuronal integrity in the long-term. To investigate this, I first induced a clearly defined pathology (i.e., acute demyelination) in the mouse brain by cuprizone intoxication, and let the mice recover for a period of 7 months. Although the myelin density and the numbers of oligodendrocytes were at the physiological, age-matched range analyzed by routine stains (see ***figure 8C***), slow-burning pathologies, such as glial activation and axonal damage remained detectable even after this long period of remyelination (see ***figure 8D, E***). These results are in line with a previous study using comparable methods (Manrique-Hoyos et al., 2012). In MS patients, ongoing pathology also persists after long-term remyelination (Lubetzki, Zalc, Williams, Stadelmann, & Stankoff, 2020). As a consequence of the initial myelin damage, OPCs might repopulate and form remyelinated areas, so-called shadow plaques, which are prone to second attacks (Bramow et al., 2010). However, the mechanism

underlying this selective vulnerability remains still unknown. Ongoing axonal injury and glia activation persist in many CNS disorders. Axonal injury following traumatic brain injury was found to be a progressive, long-term neurodegenerative process (Chen, Johnson, Uryu, Trojanowski, & Smith, 2009) and might contribute to the development of Alzheimer-like pathologies (Johnson, Stewart, & Smith, 2010). A previous study indicated that the microglia-mediated immune memory (i.e., training and tolerance) could last for at least 6 months after stimulation and modify neuropathology in animal models of Alzheimer's disease and stroke (Wendeln et al., 2018). The glial scar, formed by reactive astrocytes, NG2 glia and microglia is prominent in many CNS disorders and limits the damage expansion in short term but plays divergent roles in long-term CNS regeneration (Adams & Gallo, 2018).

In a next step, I further verified the ongoing pathology after long-term remyelination at the transcriptional level by gene array analyses. Interestingly, grey matter *per se* shows less severe damage than white matter in the cuprizone model (Clarner et al., 2012; Grosse-Veldmann et al., 2016). This might partly explain why I found slow-burning abnormalities in the corpus callosum rather than in the cortex by gene enrichment analyses (see ***figure 10B***). Another interesting finding based on the gene array data is that the mRNA levels of genes related to axonogenesis, which should be expressed in the perikaryon of neurons under normal conditions, were increased in the corpus callosum of Cup-Recov mice (GO:0007409). This might indicate impaired axonal mRNA transport and accumulation of RNA transport granules (i.e., ribonucleoprotein complexes ) along the axon (Sahoo, Smith, Perrone-Bizzozero, & Twiss, 2018).

As previously well established, microglial cells present different morphologies at different stages of their activation (Beynon & Walker, 2012). Upon activation, microglia can transform from a resting phenotype, characterized by ramified processes and a small cell body, into an activated amoeboid-like phenotype with no or only a few processes but a hypertrophic cell body. Therefore, one can distinguish resting and fully activated microglia by calculating a so called ramification index (RI) (i.e., microglial process territory area / cell body area) (Zhan et al., 2020). Additionally, microglia can also appear hyper-ramified or bushy at an intermediate stage transforming from rest to activation, characterized by increased secondary but not primary branching of microglial processes (Crews & Vetreno,

2016). To investigate microglial activation using a more fine-graded method, we reconstructed the microglia using Neurolucida360 and systematically analyzed different morphological parameters. I found that microglia showed a hyper-ramified morphology in Cup-Recov mice (see ***figure 9A***), indicating that ongoing stress still persisted in the CNS even after long-term remyelination (H. Morrison, Young, Qureshi, Rowe, & Lifshitz, 2017).

## 6.2 Function and expression of PRKCD in the CNS and MS

Protein kinase C delta (PRKCD), a subtype of the Protein kinase C (PKC) family, regulates various inflammatory responses and signalling pathways in peripheral immune cells including neutrophils, B cells and macrophages (Bey et al., 2004; Carpenter & Alexander, 2008; Mecklenbräuker, Kalled, Leitges, Mackay, & Tarakhovsky, 2004). In the brain, PRKCD is highly expressed in microglia, subtypes of neurons and neural fibers (Irani et al., 2010; D. Zhang, Anantharam, Kanthasamy, & Kanthasamy, 2007). Moreover, previous studies have shown that PRKCD is also expressed by subpopulations of neurons in the thalamus, hippocampus, amygdala and cerebellum (Barmack, Qian, & Yoshimura, 2000; Cai, Haubensak, Anthony, & Anderson, 2014; Irani et al., 2010) and participates in the regulation of learning paradigms (Yu et al., 2017). Functional studies indicated that the pharmacological inhibition of PRKCD by the inhibitor rottlerin could alleviate neuronal apoptosis in a Parkinson's disease model (Anantharam, Kitazawa, Wagner, Kaul, & Kanthasamy, 2002; Hanrott et al., 2008; Kaul, Kanthasamy, Kitazawa, Anantharam, & Kanthasamy, 2003). Moreover, pharmacological or genetic inhibition of PRKCD could ameliorate methamphetamine-induced dopaminergic toxicity and reduce serotonergic behaviors in different mouse models (Dang et al., 2018; Shin et al., 2019; Tran et al., 2019). However, the role of PRKCD in glial activation during MS is not well characterized and warrants further studies.

Of note, I found that the expression of PRKCD was induced in $IBA1^{+}$ microglia/macrophages after cuprizone intoxication and remained up-regulated even after long-term remyelination (see ***figure 14***). In line with these findings, a previous study has shown in an Alzheimer's disease mouse model that peripheral inflammation could stimulate microglia and lead to epigenetic reprogramming of microglia, which persists for at least 6 months (Wendeln et al., 2018). Moreover, PRKCD was previously shown to be expressed in

monocytes and macrophages/microglia in a neurodegenerative disease model (Gordon et al., 2016). Worth to mention, it is difficult to further elucidate the function of PRKCD without conditional knockout in microglia (Gordon et al., 2016). From a translational viewpoint, our findings are of great significance because more and more evidence accumulates that progressive MS shares many similarities with neurodegenerative diseases such as Parkinson's and Alzheimer's disease, regarding neurodegeneration and axonal dysfunction. Therefore, our study might provide a potential insight into the interplay between microglia dysfunction and neurodegeneration in progressive MS.

One of the most important findings in the present study is that PRKCD, which was found up-regulated in our long-term remyelination animal model, showed an induction of expression in chronic (active) lesions from progressive MS patients (see ***figure 15***). Moreover, I was able to demonstrate that PRKCD expression positively correlates with the activation of microglia/macrophages in the lesions. In line with this study, a genome-wide association study (GWAS) showed that *PRKCD*, among other genes, is associated with MS susceptibility, disease severity and responsiveness to interferon-beta (IFN-ß) treatment (Mahurkar, Moldovan, Suppiah, & O'Doherty, 2013). Bergman and colleagues found, using next-generation sequencing (NGS), that *Prkcd*, *Cxcr3* and *Stat1* are direct targets of differentially expressed microRNAs in EAE-susceptible and EAE-resistant rat models (Bergman et al., 2013). Analyses using the Gene Expression Omnibus (GEO) ( „ Source: http://www.ncbi.nlm.nih.gov/geo/“) database indicated that *PRKCD*/*Prkcd* was up-regulated in peripheral blood cells and brain lesions of MS patients and spinal cord of EAE mice (Han et al., 2012; Nakatsuji et al., 2012; Spach et al., 2004). Taken together, all those studies indicate the potential role of PRKCD in MS pathology.

The normal-appearing myelin after the long-term remyelination in the cuprizone model shares, on the histological level, intriguing similarities with the NAWM in the CNS of MS patients. Surprisingly, I found PRKCD correlating with activated microglia/macrophages in the NAWM of MS patients (see ***figure 16***). In MS patients, the NAWM refers to white matter areas that do not show classically demyelinated lesions by routine myelin stains and imaging techniques. More and more studies revealed that those 'normal-appearing' areas do have subtle abnormalities at both radiological and histopathological levels (Kipp et al., 2012; Loevner et al., 1995; Moll et al., 2011). It is now believed that NAWM injury is resistant to

currently available anti-inflammatory and immunomodulatory drugs for progressive MS patients and is as well associated with Wallerian-like degeneration within MS lesions (Evangelou, Konz, et al., 2000; Evangelou et al., 2001; Inglese et al., 2003; Moll et al., 2011; Richert et al., 1998). This study might provide a translational insight into the mechanism underlying pathology of NAWM and thus be useful for the research of new protective treatments for MS patients.

## 6.3 Correlation between functional deficits and neurodegeneration in MS

Functional deficits (e.g.; motor and cognitive deficits) are positively correlated with neurodegeneration in MS patients, especially in SPMS (Musella et al., 2018). Motor deficits are one of the hallmarks in MS which significantly influences the life quality of individuals (Heesen et al., 2008). Several measuring tools, such as the expanded disability status scale (EDSS), the timed 25-foot walk test and the 9-hole peg test, are currently used to evaluate the motor disability of MS patients. A follow-up study showed that early neurodegenerative signs, such as faster whole-brain atrophy rate, are valuable for predicting the motor disability during disease progression (Dekker et al., 2019). Besides motor deficits, approximately 40% - 65% of MS patients suffer from cognitive impairments such as episodic memory, sustained attention and reduced verbal fluency (McIntosh-Michaelis et al., 1991). Longitudinal studies indicated that neurodegenerative markers, such as atrophy determined by magnetic resonance imaging (MRI), might predict cognitive impairments during disease progression (Dekker et al., 2019; Filippi et al., 2013; Zivadinov et al., 2001). Other studies indicated that the observed cortical pathology might be associated with meningeal inflammation and finally contributes to cognitive impairments (Dendrou, Fugger, & Friese, 2015; Howell et al., 2011). Therefore, more objective and quantitative gait approaches would be of great benefit to reveal slow-burning processes before irreversible progression occurs (Manrique-Hoyos et al., 2012; Silva et al., 2014; Zhan et al., 2019).

In this study, I found minor motor deficits, accompanying the slow-burning pathology, persistent after the long-term remyelination using the fine-graded behavior analyses DigiGait$^{TM}$ (see ***figure 12***). The gait parameters ***Propel***, ***Swing Time***, ***%Swing***

***Stride***, ***%Stance Stride***, ***Stance Width***, were altered in Cup-Recov mice compared to age-matched control mice. „ The definitions of these parameters, as provided by the manufacturer of the DigiGait™ system are as follows: ***Propel***—Time duration of the propulsion phase (maximum paw contact to just before the swing phase) given in seconds; ***Swing Time***—Time duration of the swing phase (no paw contact with the belt) given in seconds; ***%Swing Stride***—Percentage of the total stride duration that the paw is in the air (swing phase); ***%Stance Stride***—Percentage of the total stride duration that the paw is in contact with the belt. ***Stance Width***—The perpendicular distance between the centroids of either set of axial paws during peak stance given in centimeters (see ***figure 17***) “. This is the direct citation from the guidelines of DigiGait™ website: mousespecifics.com/digigait/. „ Having these definitions in mind, it is not surprising to find the parameters ***Swing Time*** and ***%Swing Stride*** to be increased while the gait parameter ***%Stance Stride*** is decreased, which verified the reliability of the method *per se*. “ This is revised from my previously published work (Zhan et al., 2019). In line with my findings, late-onset gait abnormalities of long-term remyelination mice were verified by other groups using an elegantly designed complex wheel test, namely MOSS test (Manrique-Hoyos et al., 2012). Previous studies also indicated that impaired gait abnormalities after cuprizone intoxication might be linked with the demyelination of the corpus callosum (Hibbits et al., 2009; Liebetanz & Merkler, 2006; Xu et al., 2010). With an almost complete recovery at the myelin level, these prolonged gait abnormalities might not be detected through a ‘routine’ gait analysis method such as the rotarod test.

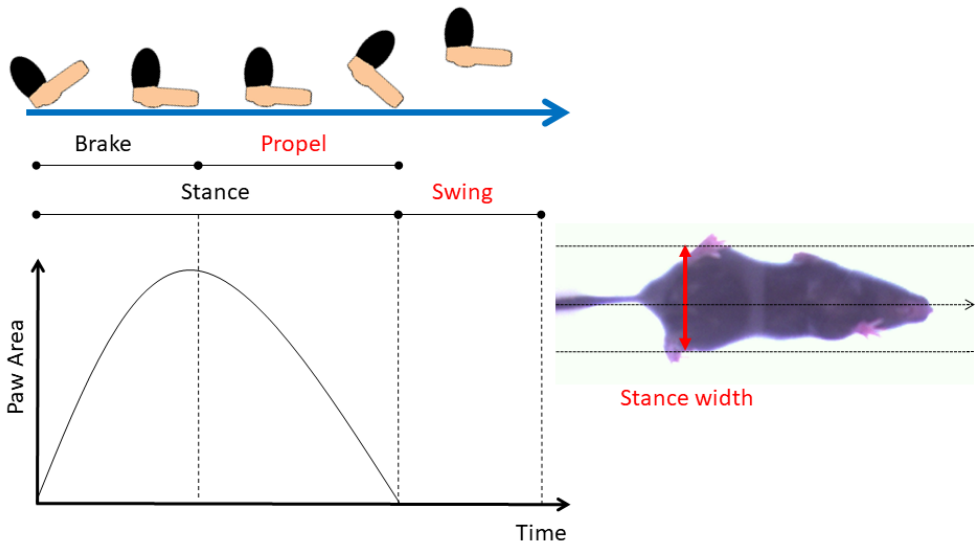

**Figure 17 Motor deficits found in Cup-Recov$^{DigiGait}$ mice**

Schematic drawing illustrating the minor motor deficits found in Cup-Recov$^{DigiGait}$ mice.

# 7. Conclusion Remarks

Taken together, my work indicates that initial, cytodegenerative processes in the CNS *per se* could have prolonged effects. Ongoing axonal damage, gliosis as well as neurodegeneration might finally lead to functional deficits. This resembles the disease progression in MS. The patients might first suffer from vision loss or motor deficit at early age and recover from these deficits without any obvious clinical symptoms. However, ominous, neurodegenerative processes might still persist in the CNS and lead to the irreversible outcome which progressive MS patients inevitably face.

# 8. Supplementary Materials

## 8.1 Supplementary Figure 1: Analysis of microglial morphology

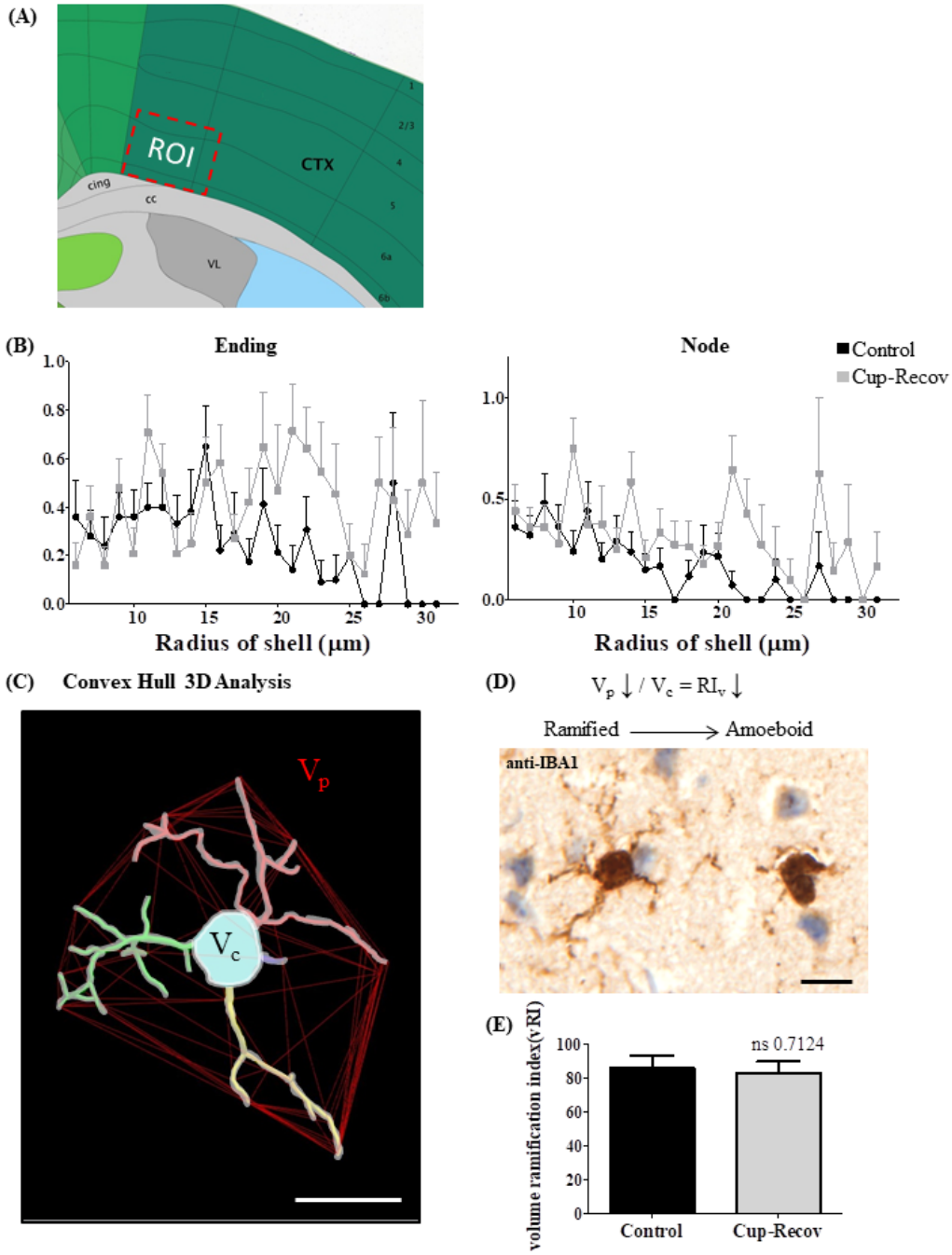


(**A**) Schematic drawing illustrating the ROI selected for morphological analyses of microglial cells. **(B)** Sholl

analysis plots of morphological parameters evaluated in microglia (i.e., ***Endings*** and ***Nodes***. n = 25 cells per group). (**C**) Microglial morphology was further evaluated by $RI_v$ ($V_p/V_c$) determined by Convex Hull 3D analysis. (**D**) The principle of quantifying microglia morphology by calculating $RI_v$. (**E**) Comparison of microglial $RI_v$ between Cup-Recov and control mice. *ROI*: region of interest; *CTX*: cerebral cortex; *1, 2/3, 4, 5, 6a, 6b*: cortex layer; *cing*: cingulum bundle; *cc*: corpus callosum; *VL*: lateral ventricle; $RI_v$: volume ramification index; $V_p$: maximum projection volume; $V_c$: cell volume; *IBA1*: ionized calcium-binding adapter molecule 1; Scale bar = 10 µm.

# 8.2 Supplementary Table 1: Primary antibodies

| **Antigen** | **Species** | **Application** | **HIER method** | **Purchase number** | **RRID$_a$** | **Supplier** | **Info** |
|---|---|---|---|---|---|---|---|
| **PLP** | mouse | 1:5000 IHC | None | MCA839G | AB_2237198 | Bio-Rad/Serotec | Myelin |
| **ANXA2** | rabbit | 1:4000 IHC | Citrate | ab41803 | AB_940267 | Abcam, UK | Extracellular matrix |
| **OLIG2** | rabbit | 1:4000 IHC | Tris/EDTA | ab9610 | AB_570666 | Millipore, Germany | Oligodendrocyte |
| **OLIG2** | mouse | 1:250 IF | Tris/EDTA | MABN50 | AB_10807410 | Millipore, Germany | Oligodendrocyte |
| **IBA1** | rabbit | 1:5000 IHC<br>1:4000 IHC$^{EnVision}$ | Tris/EDTA | 019-19741 | AB_ 839504 | Wako, Japan | Microglia/Macrophage |
| **IBA1** | goat | 1:500 IF | Tris/EDTA | SAB2500041 | AB_10600296 | Sigma-Aldrich, USA | Microglia/Macrophage |
| **GFAP** | chicken | 1:8000 IHC | Tris/EDTA | ab4674 | AB_304558 | Abcam, UK | Astrocyte |
| **PRKCD** | rabbit | 1:2000 IHC<br>1:4000$^h$ IHC<br>1:200 IF<br>1:1500$^h$ IF | Tris/EDTA | ab182126 | Not found | Abcam, UK | Kinase |
| **HLA-DRI/LN3** | mouse | 1:1500$^h$ IHC<br>1:1000$^h$ IF | Citrate | MA5-11966 | AB_10979984 | Thermo Fisher Scientific, USA | Activated microglia/macrophage |

List of primary antibodies used for IHC and IF in this study. $_a$: Research resource identifier; $^h$: Application on

human paraffin slides. PLP: proteolipid protein; LN3: anti-HLA-DR; ANXA2: annexin a2; PRKCD: protein kinase c delta; IBA1: ionized calcium-binding adapter molecule 1; GFAP: glial fibrillary acidic protein; APP: amyloid precursor protein; OLIG2: oligodendrocyte transcription factor 2.

# 8.3 Supplementary Table 2: Secondary antibodies

| **Secondary antibodies** | **Dilution** | **Purchase number** | **RRID$_a$** | **Supplier** |
|---|---|---|---|---|
| Biotinylated Goat anti-chicken IgG | 1:200 | BA-9010 | AB_2336114 | Vector laboratories, USA |
| Biotinylated Goat anti-mouse IgG | 1:200 | BA-9200 | AB_2336171 | Vector laboratories, USA |
| Biotinylated Goat anti-rabbit IgG | 1:200 | BA-1000 | AB_2313606 | Vector laboratories, USA |
| Biotinylated Goat anti-rat IgG | 1:200 | BA-9400 | AB_2336202 | Vector laboratories, USA |
| Biotinylated Rabbit anti-goat IgG | 1:200 | BA-5000 | AB_2336126 | Vector laboratories, USA |
| Alexa Fluor 488-coupled Donkey anti-rabbit IgG | 1:250 | ab150065 | Not found | Abcam, UK |
| Alexa Fluor 594-coupled Donkey anti-mouse IgG | 1:250 | A21203 | AB_2535789 | Invitrogen, USA |
| Cy3-coupled Donkey anti-goat IgG | 1:300 | 705-165-147 | AB_2307351 | Jackson ImmunoResearch, USA |
| EnVision System- HRP Labeled Polymer goat anti-rabbit | 1:1 | K4003 | AB_2630375 | DAKO, Germany |

List of secondary antibodies used for IHC and IF in this study. $_a$: Research resource identifier; IgG: immunoglobin G.

# 8.4 Supplementary Table 3: Real-time RT-PCR primers

| **Gene Symbol** | **Sense** | **Antisense** | **$T_a$ /°C** | **Bp** |
|---|---|---|---|---|
| *Gapdh* | AGG TCG GTG TGA ACG GAT TTG | GTA GAC CAT GTA GTT GAG GTC A | 60 | 123 |
| *Hprt* | TCA GTC AAC GGG GGA CAT AAA | GGG GCT GTA CTG CTT AAC CAG | 62 | 142 |
| *Prkcd* | CCT CCT GTA CGA AAT GCT CAT C | GTT TCC TGT TAC TCC CAG CCT | 64.5 | 181 |
| *Slitrk6* | AGG CTC TTG CGA CAC TCT TTG | GTG GCA CAC TGA TTT GGG ATA AT | 64 | 104 |
| *Pln* | AAA GTG CAA TAC CTC ACT CGC | GGC ATT TCA ATA GTG GAG GCT C | 64 | 56 |
| *Ndst4* | ACT TTT TGC TTG GTG AGC ATC C | CCG ATA AGG GAG GTC TTT GAT GT | 64 | 126 |
| *Lcn2* | GCA GGT GGT ACG TTG TGG G | CTC TTG TAG CTC ATA GAT GGT GC | 58 | 95 |
| *Cadps2* | AAT ATC GCC AAC AGT CTT CCC A | TCC ACG GAG GAG TAG AAA AGC | 64 | 97 |
| *Sgk1* | CTG CTC GAA GCA CCC TTA CC | TCC TGA GGA TGG GAC ATT TTC A | 64 | 175 |
| *Arc* | GTT AGC CCC TAT GCC ATC ACC | CTG GCC CAT TCA TGT GGT TCT | 64 | 244 |

List of real-time RT-PCR primers used in this study. *Gapdh*: Glyceraldehyde 3-phosphate dehydrogenase; *Hprt*: Hypoxanthine Phosphoribosyltransferase; *Prkcd*: protein kinase c delta; *Lcn2*: lipocalin 2; *Slitrk6*: SLIT and NTRK like family member 6; *Pln*: Phospholamban; *Ndst4*: N-Deacetylase and N-Sulfotransferase 4; *Cadps2*: calcium dependent secretion activator 2; *Arc*: activity regulated cytoskeleton associated protein; *Sgk1*: serum/glucocorticoid regulated kinase 1; $T_a$: annealing temperature; Bp: Base pairs.

# 8.5 Supplementary Table 4: Buffers and solutions

| | |
|---|---|
| Avidin–biotin complex solution | According to the manufacturer information from Elite ABC kit<br>96% v / v PBS<br>2% v / v reagent A.<br>2% v / v reagent B. |
| Blocking buffer for IHC/IF | 95% v / v PBS<br>5% v / v normal serum (species from the host species of the secondary antibody) |
| Citrate buffer | Distilled water<br>2.1 g / l $C_6H_8O_7$<br>pH=6.0 |
| DAB solution | According to the manufacturer information from Liquid DAB + Substrate Chromogen System<br>98% v / v DAB Substrate Buffer<br>2% v / v DAB chromogen |
| Formaldehyde fixative solution | Distilled water<br>37 g / l TRIS formaldehyde<br>4.6 g / l Sodium dihydrogen phosphate<br>8.0 g / l Disodium phosphate<br>pH=7.4 |
| Hydrogen peroxide buffer | 99.65% v / v PBS<br>0.35% v / v Hydrogen peroxide |
| PBS | Distilled water<br>80 g / l sodium chloride<br>2 g / l potassium chloride<br>16.8 g / l disodium hydrogen phosphate dihydrate<br>2.7 g / l potassium dihydrogen phosphate<br>pH=7.4 |
| Tris-EDTA buffer | Distilled water<br>1.21 g / l EDTA disodium salt dihydrate<br>0.37 g / l TRIS<br>pH=9.0 |

# 8.6 Supplementary Table 5: Differentially expressed genes in the gene array

**115 upregulated genes in the corpus callosum of the Cup-Recov mice**

| # | Gene Symbol | Control$_{Average}$ (log2) | Control$_{SD}$ | Cup-Recov$_{Average}$ (log2) | Cup-Recov$_{SD}$ | Fold Change (Cup-Recov/Control) |
|---|---|---|---|---|---|---|
| 1 | Prkcd | 9.35 | 1.59 | 11.68 | 1.98 | 5.01 |
| 2 | Ndst4 | 6.91 | 1.1 | 8.6 | 1.53 | 3.22 |
| 3 | Pln | 4.73 | 0.68 | 6.29 | 0.84 | 2.95 |
| 4 | Ntng1 | 10.92 | 0.69 | 12.39 | 0.9 | 2.76 |
| 5 | Slitrk6 | 6.93 | 0.79 | 8.29 | 1.07 | 2.57 |
| 6 | Tcf7l2 | 11.46 | 0.87 | 12.77 | 1.12 | 2.48 |
| 7 | Slc17a6 | 9.16 | 0.73 | 10.39 | 0.67 | 2.35 |
| 8 | Agt | 9.5 | 1.16 | 10.73 | 0.55 | 2.35 |
| 9 | Calb2 | 6.85 | 0.86 | 7.93 | 0.56 | 2.1 |
| 10 | Zic1 | 10.19 | 0.69 | 11.25 | 1.11 | 2.1 |
| 11 | Srgap1 | 10.06 | 0.49 | 11.09 | 0.42 | 2.03 |
| 12 | Egfem1 | 8.93 | 0.17 | 9.95 | 0.39 | 2.02 |
| 13 | Kcne1l | 6 | 0.36 | 7 | 0.35 | 2.01 |
| 14 | Shisa6 | 9.73 | 0.79 | 10.74 | 0.93 | 2.01 |
| 15 | Cbln1 | 8.3 | 0.54 | 9.3 | 0.53 | 1.99 |
| 16 | Klf5 | 9.15 | 0.2 | 10.14 | 0.26 | 1.98 |
| 17 | Epha6 | 11.44 | 0.68 | 12.41 | 0.31 | 1.96 |
| 18 | Ryr3 | 11.32 | 0.28 | 12.28 | 0.43 | 1.96 |
| 19 | Wfs1 | 10.44 | 0.7 | 11.39 | 0.14 | 1.94 |
| 20 | Anxa2 | 6.19 | 0.39 | 7.15 | 0.27 | 1.94 |
| 21 | Foxo1 | 10 | 0.2 | 10.93 | 0.46 | 1.91 |
| 22 | Prg4 | 5.83 | 0.37 | 6.76 | 1.42 | 1.91 |
| 23 | Lrrtm1 | 7.21 | 0.4 | 8.12 | 0.17 | 1.89 |
| 24 | Actn2 | 11.73 | 0.3 | 12.65 | 0.62 | 1.89 |
| 25 | Npsr1 | 7.61 | 0.6 | 8.52 | 0.5 | 1.88 |
| 26 | Isl1 | 7.82 | 0.35 | 8.72 | 0.24 | 1.87 |
| 27 | Synpo2 | 7.77 | 0.6 | 8.68 | 0.77 | 1.87 |
| 28 | Rab37 | 6.59 | 0.64 | 7.48 | 0.82 | 1.85 |
| 29 | Zfp735 | 3.88 | 0.36 | 4.75 | 0.29 | 1.83 |
| 30 | Cabp7 | 8.6 | 0.69 | 9.47 | 0.73 | 1.83 |
| 31 | Olfr1090 | 4.25 | 0.12 | 5.11 | 0.25 | 1.82 |
| 32 | Pbx3 | 10.08 | 0.58 | 10.95 | 0.33 | 1.82 |
| 33 | Dlx5 | 8.44 | 0.2 | 9.3 | 0.26 | 1.81 |
| 34 | Bmp4 | 6.08 | 0.47 | 6.94 | 0.42 | 1.81 |
| 35 | Necab2 | 10.78 | 0.14 | 11.62 | 0.52 | 1.79 |
| 36 | Unc13c | 11.87 | 0.63 | 12.69 | 0.33 | 1.76 |
| 37 | Prrg4 | 7.56 | 0.42 | 8.37 | 0.35 | 1.76 |
| 38 | Nrep | 10.3 | 0.26 | 11.11 | 0.2 | 1.75 |

| | | | | | | |
|---|---|---|---|---|---|---|
| 39 | Tox | 13.48 | 0.06 | 14.28 | 0.41 | 1.74 |
| 40 | Olfr195 | 4.4 | 0.6 | 5.2 | 0.24 | 1.74 |
| 41 | Shox2 | 4.9 | 0.42 | 5.69 | 1.4 | 1.73 |
| 42 | Wdr83os | 13.18 | 0.29 | 13.96 | 0.42 | 1.72 |
| 43 | Tshz2 | 12.34 | 0.74 | 13.12 | 0.56 | 1.71 |
| 44 | Etv1 | 12.95 | 0.11 | 13.71 | 0.57 | 1.7 |
| 45 | Six3 | 8.82 | 0.75 | 9.59 | 0.31 | 1.7 |
| 46 | Pcbd1 | 6.69 | 0.36 | 7.46 | 0.21 | 1.7 |
| 47 | Timp3 | 8.54 | 0.5 | 9.29 | 0.33 | 1.68 |
| 48 | Fmod | 5.86 | 0.38 | 6.61 | 1.02 | 1.68 |
| 49 | S100a11 | 9.72 | 0.15 | 10.47 | 0.5 | 1.68 |
| 50 | Ndnf | 6.93 | 0.19 | 7.67 | 0.09 | 1.67 |
| 51 | Rbms3 | 11.53 | 0.41 | 12.27 | 0.2 | 1.67 |
| 52 | Slc24a3 | 12.01 | 0.56 | 12.76 | 0.28 | 1.67 |
| 53 | Ccdc170 | 6.22 | 0.29 | 6.96 | 0.51 | 1.67 |
| 54 | Htr1d | 8.56 | 0.08 | 9.3 | 0.74 | 1.67 |
| 55 | St8sia2 | 6.6 | 0.29 | 7.34 | 0.29 | 1.66 |
| 56 | Lhfpl3 | 11.36 | 0.55 | 12.09 | 0.33 | 1.66 |
| 57 | Rgs10 | 11.1 | 0.58 | 11.83 | 0.15 | 1.65 |
| 58 | Cd55 | 7.22 | 0.36 | 7.93 | 0.05 | 1.64 |
| 59 | Lfng | 9 | 0.3 | 9.71 | 0.39 | 1.64 |
| 60 | Plppr1 | 10.69 | 0.36 | 11.4 | 0.53 | 1.64 |
| 61 | Zic2 | 7.15 | 0.4 | 7.87 | 0.33 | 1.64 |
| 62 | Rnf122 | 8.82 | 0.46 | 9.52 | 0.17 | 1.63 |
| 63 | Ascl1 | 9.43 | 0.21 | 10.13 | 0.51 | 1.62 |
| 64 | Ndst3 | 10.15 | 0.3 | 10.84 | 0.56 | 1.61 |
| 65 | Eya1 | 10.65 | 0.25 | 11.34 | 0.17 | 1.61 |
| 66 | Cd68 | 10.95 | 0.15 | 11.64 | 0.08 | 1.61 |
| 67 | F830001A07Rik | 11.63 | 0.38 | 12.32 | 0.16 | 1.61 |
| 68 | Myb | 6.52 | 0.41 | 7.21 | 0.14 | 1.61 |
| 69 | Gpr161 | 7.69 | 0.49 | 8.37 | 0.7 | 1.61 |
| 70 | Slc14a2 | 6.27 | 0.14 | 6.95 | 0.09 | 1.6 |
| 71 | Vmn2r89 | 5.99 | 0.26 | 6.66 | 0.23 | 1.6 |
| 72 | Gipc2 | 7.08 | 0.43 | 7.76 | 0.44 | 1.6 |
| 73 | Gli3 | 10.45 | 0.19 | 11.11 | 0.1 | 1.58 |
| 74 | BC026585 | 6.5 | 0.41 | 7.16 | 0.16 | 1.58 |
| 75 | Tek | 7.78 | 0.12 | 8.43 | 0.28 | 1.57 |
| 76 | Gad1 | 12.08 | 0.16 | 12.73 | 0.24 | 1.57 |
| 77 | Gpr12 | 10.37 | 0.23 | 11.03 | 0.23 | 1.57 |
| 78 | Nipal2 | 10 | 0.27 | 10.65 | 0.2 | 1.57 |
| 79 | Jag1 | 7.53 | 0.13 | 8.18 | 0.34 | 1.57 |
| 80 | Esp15 | 4.63 | 0.15 | 5.29 | 0.86 | 1.57 |
| 81 | Tacr1 | 8.73 | 0.48 | 9.38 | 0.44 | 1.57 |
| 82 | Cachd1 | 8.11 | 0.29 | 8.75 | 0.3 | 1.56 |
| 83 | Nlrp1c-ps | 5.41 | 0.17 | 6.05 | 0.1 | 1.56 |
| 84 | Dapp1 | 9.31 | 0.24 | 9.96 | 0.22 | 1.56 |

| | | | | | | |
|---|---|---|---|---|---|---|
| 85 | Tgif1 | 6.42 | 0.11 | 7.05 | 0.46 | 1.56 |
| 86 | Dynlrb2 | 7.08 | 0.22 | 7.72 | 0.48 | 1.55 |
| 87 | Pou3f4 | 9.68 | 0.29 | 10.31 | 0.62 | 1.55 |
| 88 | Gpr83 | 12.54 | 0.16 | 13.16 | 0.34 | 1.54 |
| 89 | Pltp | 12.86 | 0.49 | 13.48 | 0.27 | 1.54 |
| 90 | Gm2573 | 11.29 | 0.21 | 11.91 | 0.24 | 1.54 |
| 91 | Gdpd2 | 7.44 | 0.31 | 8.07 | 0.41 | 1.54 |
| 92 | Stk32a | 9.83 | 0.13 | 10.44 | 0.47 | 1.54 |
| 93 | Dpysl3 | 8.18 | 0.29 | 8.79 | 0.27 | 1.53 |
| 94 | Eps8 | 9.25 | 0.45 | 9.86 | 0.31 | 1.53 |
| 95 | Skint1 | 4.32 | 0.33 | 4.94 | 0.25 | 1.53 |
| 96 | Cdhr3 | 8.5 | 0.41 | 9.11 | 0.74 | 1.53 |
| 97 | Arhgap6 | 9.85 | 0.26 | 10.46 | 0.18 | 1.52 |
| 98 | Acta2 | 8.52 | 0.21 | 9.12 | 0.25 | 1.52 |
| 99 | Adcy8 | 9.99 | 0.1 | 10.6 | 0.3 | 1.52 |
| 100 | Ccdc115 | 8.98 | 0.61 | 9.58 | 0.4 | 1.52 |
| 101 | Lrrc9 | 8.57 | 0.35 | 9.18 | 0.08 | 1.52 |
| 102 | Nts | 6.36 | 0.54 | 6.97 | 0.35 | 1.52 |
| 103 | B130024G19Rik | 6.52 | 0.61 | 7.13 | 0.37 | 1.52 |
| 104 | Ano2 | 9.85 | 0.53 | 10.45 | 0.57 | 1.52 |
| 105 | Angpt1 | 8.08 | 0.29 | 8.67 | 0.33 | 1.51 |
| 106 | Sncg | 6.75 | 0.52 | 7.34 | 0.25 | 1.51 |
| 107 | Lpp | 9.56 | 0.34 | 10.16 | 0.34 | 1.51 |
| 108 | Gm8267 | 4.05 | 0.35 | 4.64 | 0.2 | 1.51 |
| 109 | Cyp2j9 | 12.02 | 0.34 | 12.62 | 0.24 | 1.51 |
| 110 | Eaf2 | 5.34 | 0.41 | 5.93 | 0.39 | 1.51 |
| 111 | Creg1 | 12.06 | 0.32 | 12.66 | 0.14 | 1.51 |
| 112 | Teddm3 | 8.04 | 0.38 | 8.64 | 0.58 | 1.51 |
| 113 | Ass1; Gm5424 | 10.05 | 0.21 | 10.64 | 0.2 | 1.5 |
| 114 | Whrn | 11.17 | 0.42 | 11.75 | 0.32 | 1.5 |
| 115 | Dlx6 | 8.56 | 0.15 | 9.14 | 0.4 | 1.5 |

**103 downregulated genes in the corpus callosum of the Cup-Recov mice**

| # | Gene Symbol | $Control_{Average}$ (log2) | $Control_{SD}$ | $Cup\text{-}Recov_{Average}$ (log2) | $Cup\text{-}Recov_{SD}$ | Fold Change(Cup-Recov/Control) |
|---|---|---|---|---|---|---|
| 1 | Lcn2 | 6.22 | 0.86 | 4.76 | 1.04 | -2.75 |
| 2 | Gm10591 | 11.28 | 0.69 | 9.88 | 2.05 | -2.64 |
| 3 | Gm13304 | 11.14 | 0.71 | 9.79 | 1.97 | -2.55 |
| 4 | Gm13304; Gm21541; Ccl21b | 11.24 | 0.78 | 9.88 | 2.22 | -2.55 |
| 5 | Gm1987; Ccl21a | 11.4 | 0.64 | 10.08 | 1.67 | -2.5 |
| 6 | Gm13304 | 10.89 | 0.71 | 9.57 | 1.66 | -2.49 |
| 7 | Ccl21b; Gm13304 | 10.89 | 0.71 | 9.57 | 1.66 | -2.49 |
| 8 | Sgk1 | 13.83 | 0.34 | 12.52 | 0.42 | -2.48 |
| 9 | Gm13304 | 11.01 | 0.72 | 9.81 | 1.61 | -2.3 |

| | | | | | | |
|---|---|---|---|---|---|---|
| 10 | Ccl21c; Gm21541 | 11.01 | 0.72 | 9.81 | 1.61 | -2.3 |
| 11 | Vmn1r90; Nlrp5-ps; Vmn1r181 | 8.89 | 0.37 | 7.7 | 0.37 | -2.29 |
| 12 | Rxfp2 | 6.86 | 0.27 | 5.76 | 0.2 | -2.13 |
| 13 | Gm10600 | 14.71 | 0.3 | 13.63 | 2.77 | -2.12 |
| 14 | Tmem196 | 11.57 | 0.24 | 10.58 | 0.22 | -1.99 |
| 15 | Ccl21a; Gm1987 | 10.74 | 0.5 | 9.76 | 0.9 | -1.97 |
| 16 | Fam205a2; Gm10600 | 13.88 | 0.28 | 12.91 | 1.37 | -1.95 |
| 17 | Cbln4 | 8.91 | 0.29 | 7.96 | 0.15 | -1.93 |
| 18 | Gm3893; 4933409K07Rik | 15.81 | 0.31 | 14.87 | 2.25 | -1.92 |
| 19 | Arc | 11.05 | 0.29 | 10.11 | 0.83 | -1.92 |
| 20 | Cadps2 | 11.8 | 0.4 | 10.87 | 0.24 | -1.91 |
| 21 | Arhgap15 | 7.68 | 0.44 | 6.74 | 0.07 | -1.91 |
| 22 | 4933409K07Rik | 12.2 | 0.37 | 11.3 | 0.63 | -1.87 |
| 23 | 4933409K07Rik | 12.2 | 0.37 | 11.3 | 0.63 | -1.87 |
| 24 | Prss23 | 9.26 | 0.12 | 8.37 | 0.13 | -1.86 |
| 25 | Ipcef1 | 11.19 | 0.21 | 10.32 | 0.37 | -1.84 |
| 26 | Gm13298; Fam205a2 | 11.46 | 0.3 | 10.58 | 0.55 | -1.84 |
| 27 | Myl4 | 11 | 0.24 | 10.13 | 0.53 | -1.83 |
| 28 | C4a | 6.97 | 0.42 | 6.12 | 0.25 | -1.81 |
| 29 | Ide | 13.71 | 0.2 | 12.86 | 0.67 | -1.8 |
| 30 | 3110035E14Rik | 14.87 | 0.24 | 14.04 | 0.2 | -1.78 |
| 31 | Skint8 | 6.73 | 0.48 | 5.9 | 0.24 | -1.77 |
| 32 | Apold1 | 8.2 | 0.26 | 7.39 | 0.29 | -1.76 |
| 33 | Ccl3 | 7.66 | 0.49 | 6.85 | 0.26 | -1.75 |
| 34 | Hcrtr1 | 5.11 | 0.37 | 4.3 | 0.42 | -1.74 |
| 35 | Gm13298; Fam205a4; Gm20938 | 11.86 | 0.33 | 11.06 | 0.51 | -1.74 |
| 36 | Car10 | 10.82 | 0.44 | 10.03 | 0.14 | -1.73 |
| 37 | Olah | 6 | 0.38 | 5.2 | 0.12 | -1.73 |
| 38 | Arhgap25 | 6.87 | 0.48 | 6.08 | 0.28 | -1.73 |
| 39 | Sdk2 | 9.15 | 0.52 | 8.36 | 0.57 | -1.73 |
| 40 | Gm3676 | 5.14 | 0.5 | 4.35 | 0.21 | -1.73 |
| 41 | Rprm | 10.19 | 0.12 | 9.41 | 0.34 | -1.72 |
| 42 | Nptx1 | 10.53 | 0.45 | 9.74 | 0.21 | -1.72 |
| 43 | H2-T23 | 8.59 | 0.4 | 7.8 | 0.3 | -1.72 |
| 44 | Vmn1r100 | 5.89 | 0.25 | 5.12 | 0.26 | -1.71 |
| 45 | Vmn1r148 | 5.89 | 0.25 | 5.12 | 0.26 | -1.71 |
| 46 | Ttc9b | 10.69 | 0.26 | 9.93 | 0.32 | -1.7 |
| 47 | Steap1 | 6.39 | 0.84 | 5.63 | 0.46 | -1.69 |
| 48 | Glra4 | 5.25 | 0.19 | 4.5 | 0.18 | -1.68 |

| | | | | | | |
|---|---|---|---|---|---|---|
| 49 | Btk | 6.65 | 0.31 | 5.91 | 0.41 | -1.67 |
| 50 | Vipr1 | 9.3 | 0.31 | 8.57 | 0.31 | -1.66 |
| 51 | Krt80 | 7.77 | 0.46 | 7.04 | 0.29 | -1.65 |
| 52 | Fam205a1 | 10.7 | 0.29 | 9.97 | 0.58 | -1.65 |
| 53 | Ccl9 | 7.78 | 0.18 | 7.08 | 0.19 | -1.63 |
| 54 | F630003A18Rik | 5.21 | 0.17 | 4.51 | 0.36 | -1.63 |
| 55 | Cabp1 | 13.15 | 0.22 | 12.45 | 0.19 | -1.62 |
| 56 | 4933409K07Rik | 12.23 | 0.43 | 11.53 | 0.78 | -1.62 |
| 57 | Rgs6 | 11.66 | 0.22 | 10.97 | 0.17 | -1.61 |
| 58 | Gm5468 | 6.3 | 0.62 | 5.61 | 0.25 | -1.61 |
| 59 | Tmem132d | 10.75 | 0.46 | 10.08 | 0.22 | -1.6 |
| 60 | Gm13298; Fam205a3; Gm21598 | 11.85 | 0.32 | 11.17 | 0.53 | -1.6 |
| 61 | Bpifa2 | 4.74 | 0.46 | 4.06 | 0.28 | -1.6 |
| 62 | Ccdc22 | 7.96 | 0.37 | 7.28 | 0.1 | -1.6 |
| 63 | Eif4ebp2 | 9.31 | 0.27 | 8.63 | 0.4 | -1.59 |
| 64 | Chrng | 4.6 | 0.37 | 3.92 | 0.22 | -1.59 |
| 65 | Jdp2 | 9.74 | 0.45 | 9.07 | 0.15 | -1.59 |
| 66 | Cybb | 6.97 | 0.49 | 6.3 | 0.15 | -1.58 |
| 67 | Mmp17 | 10.04 | 0.49 | 9.37 | 0.45 | -1.58 |
| 68 | Keg1 | 6.66 | 0.35 | 6.01 | 0.15 | -1.57 |
| 69 | Vmn2r122 | 6.2 | 0.41 | 5.56 | 0.16 | -1.57 |
| 70 | Slc26a8 | 8.31 | 0.16 | 7.66 | 0.13 | -1.56 |
| 71 | Frmd6 | 9.4 | 0.34 | 8.76 | 0.19 | -1.56 |
| 72 | Olfr780 | 4.89 | 0.41 | 4.24 | 0.25 | -1.56 |
| 73 | Il17ra | 8.62 | 0.34 | 7.99 | 0.25 | -1.55 |
| 74 | Pcdh7 | 14.66 | 0.26 | 14.03 | 0.42 | -1.55 |
| 75 | Ces3a | 5.89 | 0.27 | 5.26 | 0.27 | -1.55 |
| 76 | Rasl10a | 8.72 | 0.54 | 8.08 | 0.24 | -1.55 |
| 77 | Olfr885 | 5.89 | 0.46 | 5.25 | 0.18 | -1.55 |
| 78 | Serpinb8 | 8.22 | 0.56 | 7.6 | 0.36 | -1.54 |
| 79 | Sstr3 | 8.46 | 0.25 | 7.84 | 0.13 | -1.54 |
| 80 | Cldn2 | 5.74 | 0.42 | 5.12 | 0.3 | -1.54 |
| 81 | Gm12394 | 11.82 | 0.31 | 11.19 | 0.85 | -1.54 |
| 82 | Ntn5 | 7.12 | 0.41 | 6.49 | 0.21 | -1.54 |
| 83 | Lilrb4a | 8.03 | 0.8 | 7.41 | 0.64 | -1.54 |
| 84 | Pisd-ps3 | 13.72 | 0.52 | 13.1 | 0.79 | -1.54 |
| 85 | Per1 | 11.22 | 0.07 | 10.61 | 0.24 | -1.53 |
| 86 | Olfr1457 | 5.39 | 0.49 | 4.78 | 0.31 | -1.53 |
| 87 | Adcy1 | 13.29 | 0.42 | 12.68 | 0.19 | -1.53 |
| 88 | Il10ra | 7.78 | 0.32 | 7.17 | 0.22 | -1.53 |
| 89 | Kcnt2 | 12.06 | 0.37 | 11.46 | 0.12 | -1.52 |
| 90 | Vwa5b2 | 10.02 | 0.25 | 9.42 | 0.06 | -1.52 |
| 91 | Tmem252 | 7.21 | 0.28 | 6.61 | 0.36 | -1.52 |
| 92 | Tmem132a | 9.97 | 0.44 | 9.36 | 0.34 | -1.52 |

| | | | | | | |
|---|---|---|---|---|---|---|
| 93 | Il23r | 6.04 | 0.34 | 5.44 | 0.18 | -1.52 |
| 94 | Hgf | 7.05 | 0.53 | 6.45 | 0.26 | -1.52 |
| 95 | Chrm3 | 9.86 | 0.47 | 9.25 | 0.3 | -1.52 |
| 96 | 1700016D06Rik | 4.98 | 0.11 | 4.37 | 0.26 | -1.52 |
| 97 | Acer2 | 7.26 | 0.36 | 6.66 | 0.26 | -1.51 |
| 98 | Anp32e | 8.03 | 0.34 | 7.44 | 0.11 | -1.51 |
| 99 | Gm9745 | 5.79 | 0.12 | 5.19 | 0.21 | -1.51 |
| 100 | Hpcal4 | 12.11 | 0.36 | 11.51 | 0.38 | -1.51 |
| 101 | Mettl24 | 7.02 | 0.24 | 6.43 | 0.21 | -1.5 |
| 102 | Lypd6 | 11.28 | 0.3 | 10.69 | 0.31 | -1.5 |
| 103 | Tagap | 6.24 | 0.2 | 5.65 | 0.27 | -1.5 |

**148 upregulated genes in the cortex of the Cup-Recov mice**

| # | Gene Symbol | $Control_{Average}$ (log2) | $Control_{SD}$ | $Cup\text{-}Recov_{Average}$ (log2) | $Cup\text{-}Recov_{SD}$ | Fold Change(Cup-Recov/Control) |
|---|---|---|---|---|---|---|
| 1 | LOC102639117 | 5.92 | 0.19 | 7 | 0.53 | 2.13 |
| 2 | Gm17611 | 4.95 | 0.16 | 6.02 | 0.44 | 2.11 |
| 3 | Olfr919 | 5.6 | 0.53 | 6.63 | 0.26 | 2.04 |
| 4 | Smim3 | 6.29 | 0.17 | 7.31 | 0.63 | 2.03 |
| 5 | Olfr341 | 4.01 | 0.72 | 5.03 | 0.27 | 2.03 |
| 6 | Nxpe2 | 6.24 | 0.23 | 7.26 | 0.6 | 2.02 |
| 7 | Gm19607 | 5.37 | 0.31 | 6.36 | 0.14 | 1.99 |
| 8 | Mpeg1 | 7.39 | 0.22 | 8.35 | 0.37 | 1.95 |
| 9 | Sntb1 | 6.79 | 0.4 | 7.76 | 0.36 | 1.95 |
| 10 | Vmn1r70 | 5.4 | 0.16 | 6.37 | 0.42 | 1.95 |
| 11 | Skint11 | 6.15 | 0.48 | 7.08 | 0.54 | 1.9 |
| 12 | Ugt2b35 | 4.64 | 0.29 | 5.57 | 0.59 | 1.89 |
| 13 | Inhba | 8.63 | 0.57 | 9.52 | 0.31 | 1.85 |
| 14 | Olfr724 | 5.76 | 0.22 | 6.65 | 0.25 | 1.85 |
| 15 | Stat4 | 5.53 | 0.45 | 6.4 | 0.19 | 1.82 |
| 16 | Ankrd35 | 6.19 | 0.31 | 7.02 | 0.51 | 1.78 |
| 17 | Olfr391-ps | 4.53 | 0.48 | 5.36 | 0.61 | 1.78 |
| 18 | Olfr1346 | 4.05 | 0.56 | 4.87 | 0.54 | 1.77 |
| 19 | Gm21921 | 4.97 | 0.21 | 5.78 | 0.19 | 1.76 |
| 20 | Erp27 | 6.07 | 0.32 | 6.89 | 0.47 | 1.76 |
| 21 | Gpr18 | 5.28 | 0.2 | 6.09 | 0.41 | 1.76 |
| 22 | 4930563E22Rik | 5.38 | 0.13 | 6.19 | 0.13 | 1.75 |
| 23 | Ifna16 | 6.49 | 0.49 | 7.29 | 0.14 | 1.75 |
| 24 | Olfr557 | 4.78 | 0.28 | 5.58 | 0.25 | 1.74 |
| 25 | Trim55 | 5.61 | 0.39 | 6.41 | 0.54 | 1.74 |
| 26 | Kif27; Mir6369 | 5.87 | 0.25 | 6.66 | 0.39 | 1.73 |
| 27 | Obox8; Gm5585 | 4.28 | 0.31 | 5.07 | 0.42 | 1.73 |
| 28 | Lst1 | 5 | 0.33 | 5.79 | 0.24 | 1.73 |
| 29 | Vmn1r76 | 4.75 | 0.42 | 5.54 | 0.61 | 1.73 |

| | | | | | | |
|---|---|---|---|---|---|---|
| 30 | Psd4 | 5.99 | 0.39 | 6.77 | 0.37 | 1.72 |
| 31 | Sdr16c6 | 4 | 0.44 | 4.79 | 0.16 | 1.72 |
| 32 | Nnmt | 7.04 | 0.41 | 7.82 | 0.4 | 1.72 |
| 33 | Gm15850 | 5.58 | 0.35 | 6.35 | 0.28 | 1.71 |
| 34 | Olfr1317 | 4.53 | 0.2 | 5.3 | 0.41 | 1.7 |
| 35 | Fbxw27 | 4.86 | 0.48 | 5.61 | 0.15 | 1.69 |
| 36 | Gm21891 | 5.43 | 0.2 | 6.19 | 0.95 | 1.69 |
| 37 | Gm21828 | 5.43 | 0.2 | 6.19 | 0.95 | 1.69 |
| 38 | Gm21725 | 5.43 | 0.2 | 6.19 | 0.95 | 1.69 |
| 39 | Gm21904 | 5.43 | 0.2 | 6.19 | 0.95 | 1.69 |
| 40 | Gm21764 | 5.43 | 0.2 | 6.19 | 0.95 | 1.69 |
| 41 | Gm21852 | 5.43 | 0.2 | 6.19 | 0.95 | 1.69 |
| 42 | Olfr723 | 4.83 | 0.31 | 5.59 | 0.22 | 1.69 |
| 43 | Gm732 | 4.38 | 0.34 | 5.14 | 0.62 | 1.69 |
| 44 | Vmn2r104 | 4.32 | 0.38 | 5.06 | 0.6 | 1.68 |
| 45 | Vmn1r129 | 6.35 | 0.26 | 7.1 | 0.39 | 1.68 |
| 46 | Mid1 | 13.02 | 0.5 | 13.77 | 0.22 | 1.68 |
| 47 | Mid1 | 13.02 | 0.5 | 13.77 | 0.22 | 1.68 |
| 48 | Gm13088 | 5.03 | 0.18 | 5.77 | 0.44 | 1.68 |
| 49 | Psmb10 | 8.35 | 0.17 | 9.1 | 0.46 | 1.68 |
| 50 | Gm16442; Gm16451 | 4.56 | 0.52 | 5.3 | 0.53 | 1.68 |
| 51 | Gm10330; LOC100861601 | 7.72 | 0.56 | 8.47 | 0.28 | 1.68 |
| 52 | Serinc4 | 5.09 | 0.3 | 5.82 | 0.27 | 1.67 |
| 53 | Tex30 | 6.93 | 0.15 | 7.67 | 0.34 | 1.67 |
| 54 | Ms4a4a | 6.19 | 0.15 | 6.93 | 0.44 | 1.67 |
| 55 | Ddx19a | 7.1 | 0.68 | 7.83 | 0.37 | 1.66 |
| 56 | Gm5592 | 5.24 | 0.36 | 5.97 | 0.19 | 1.66 |
| 57 | Psg27 | 6.01 | 0.23 | 6.75 | 0.44 | 1.66 |
| 58 | Ovol1 | 4.01 | 0.24 | 4.73 | 0.4 | 1.65 |
| 59 | Mov10 | 7.06 | 0.21 | 7.78 | 0.35 | 1.65 |
| 60 | Nlrp1a | 3.79 | 0.12 | 4.51 | 0.6 | 1.65 |
| 61 | Gm436 | 6.47 | 0.06 | 7.19 | 0.54 | 1.65 |
| 62 | Gm5751 | 5.02 | 0.37 | 5.73 | 0.65 | 1.64 |
| 63 | BC067074 | 5.47 | 0.51 | 6.18 | 0.36 | 1.64 |
| 64 | Epha3 | 8.34 | 0.12 | 9.05 | 0.35 | 1.64 |
| 65 | Serpinb6e | 5.41 | 0.25 | 6.13 | 0.41 | 1.64 |
| 66 | Spag17 | 4.4 | 0.4 | 5.11 | 0.26 | 1.64 |
| 67 | Gm5615 | 4.24 | 0.17 | 4.94 | 0.36 | 1.63 |
| 68 | Ifna7 | 6.41 | 0.41 | 7.11 | 0.17 | 1.63 |
| 69 | Esp4 | 4.61 | 0.23 | 5.31 | 0.23 | 1.63 |
| 70 | Gm1070 | 5.26 | 0.53 | 5.96 | 0.39 | 1.62 |
| 71 | Olfr769 | 4.59 | 0.18 | 5.28 | 0.57 | 1.62 |
| 72 | Ear1 | 5.34 | 0.3 | 6.04 | 0.5 | 1.62 |
| 73 | Plag1 | 6.47 | 0.22 | 7.16 | 0.2 | 1.62 |

| | | | | | | |
|---|---|---|---|---|---|---|
| 74 | Rnd3 | 8.63 | 0.23 | 9.32 | 0.29 | 1.62 |
| 75 | Pim1 | 5.98 | 0.43 | 6.66 | 0.14 | 1.61 |
| 76 | Gpr183 | 4.96 | 0.1 | 5.65 | 0.32 | 1.61 |
| 77 | Klra16 | 4.91 | 0.11 | 5.59 | 0.24 | 1.61 |
| 78 | Pabpc4l | 4.18 | 0.15 | 4.87 | 0.53 | 1.61 |
| 79 | Lipi | 5.69 | 0.41 | 6.38 | 0.51 | 1.61 |
| 80 | Nlrp12 | 4.15 | 0.17 | 4.85 | 0.54 | 1.61 |
| 81 | Klf6 | 10.52 | 0.25 | 11.21 | 0.06 | 1.61 |
| 82 | Olfr1247 | 5.18 | 0.35 | 5.86 | 0.66 | 1.6 |
| 83 | Olfr239 | 7.46 | 0.47 | 8.14 | 0.21 | 1.6 |
| 84 | Olfr1044 | 5.67 | 0.29 | 6.34 | 0.42 | 1.6 |
| 85 | Slfn4 | 5.02 | 0.36 | 5.7 | 0.32 | 1.6 |
| 86 | 1110017D15Rik | 5.95 | 0.36 | 6.62 | 0.34 | 1.59 |
| 87 | 1700012A03Rik | 5.28 | 0.26 | 5.95 | 0.28 | 1.59 |
| 88 | Ivl | 5.22 | 0.29 | 5.9 | 0.23 | 1.59 |
| 89 | 4931400O07Rik | 6.51 | 0.26 | 7.18 | 0.33 | 1.59 |
| 90 | 9030612E09Rik | 5.37 | 0.33 | 6.04 | 0.55 | 1.59 |
| 91 | Syt10 | 11.63 | 0.41 | 12.29 | 0.24 | 1.58 |
| 92 | Olfr1162 | 4.24 | 0.2 | 4.9 | 0.26 | 1.58 |
| 93 | Esp34 | 4.14 | 0.39 | 4.8 | 0.2 | 1.58 |
| 94 | Gm21447 | 6.39 | 0.18 | 7.05 | 0.55 | 1.58 |
| 95 | Gm21657 | 6.39 | 0.18 | 7.05 | 0.55 | 1.58 |
| 96 | Gm3005; Gm2897 | 10.52 | 0.12 | 11.18 | 0.25 | 1.58 |
| 97 | Olfr1535 | 5.52 | 0.42 | 6.16 | 0.39 | 1.57 |
| 98 | Gm21739 | 5.17 | 0.21 | 5.82 | 0.43 | 1.57 |
| 99 | Gm21739 | 5.17 | 0.21 | 5.82 | 0.43 | 1.57 |
| 100 | Gm21739 | 5.17 | 0.21 | 5.82 | 0.43 | 1.57 |
| 101 | Gm21739 | 5.17 | 0.21 | 5.82 | 0.43 | 1.57 |
| 102 | Gm21739 | 5.17 | 0.21 | 5.82 | 0.43 | 1.57 |
| 103 | Gm21739 | 5.17 | 0.21 | 5.82 | 0.43 | 1.57 |
| 104 | Il1f6 | 6.29 | 0.19 | 6.93 | 0.36 | 1.57 |
| 105 | Mid1 | 12.5 | 0.59 | 13.15 | 0.27 | 1.57 |
| 106 | Gm3424 | 4.94 | 0.2 | 5.59 | 0.48 | 1.57 |
| 107 | Vmn2r116 | 4.18 | 0.38 | 4.82 | 0.3 | 1.56 |
| 108 | Gm13128 | 4.91 | 0.29 | 5.56 | 0.51 | 1.56 |
| 109 | Vmn2r77 | 5 | 0.44 | 5.64 | 0.28 | 1.56 |
| 110 | Gm21913 | 5.13 | 0.55 | 5.77 | 0.25 | 1.56 |
| 111 | Gm21776 | 5.13 | 0.55 | 5.77 | 0.25 | 1.56 |
| 112 | Cldn1 | 6.93 | 0.25 | 7.58 | 0.24 | 1.56 |
| 113 | Alg3 | 8.77 | 0.15 | 9.39 | 0.06 | 1.55 |
| 114 | Esyt3 | 5.74 | 0.42 | 6.37 | 0.19 | 1.55 |
| 115 | Samt2; 4930524N10Rik | 4.72 | 0.53 | 5.35 | 0.43 | 1.55 |

| | | | | | | |
|---|---|---|---|---|---|---|
| 116 | Rhox3c | 5.16 | 0.2 | 5.79 | 0.67 | 1.55 |
| 117 | Gm3752; Gm2897 | 10.15 | 0.13 | 10.78 | 0.36 | 1.55 |
| 118 | Faiml | 5.6 | 0.27 | 6.24 | 0.77 | 1.55 |
| 119 | Lrrc71 | 5.19 | 0.36 | 5.82 | 0.29 | 1.54 |
| 120 | Cdkn1a | 10.1 | 0.35 | 10.72 | 0.34 | 1.54 |
| 121 | Ccnf; Mir5134 | 4.88 | 0.24 | 5.5 | 0.34 | 1.54 |
| 122 | Saa3 | 5.94 | 0.07 | 6.56 | 0.26 | 1.54 |
| 123 | Tcp11 | 4.89 | 0.34 | 5.51 | 0.24 | 1.54 |
| 124 | Gm17019 | 5.15 | 0.38 | 5.76 | 0.3 | 1.53 |
| 125 | Bglap2 | 6.33 | 0.17 | 6.95 | 0.39 | 1.53 |
| 126 | 4933411G06Rik | 4.38 | 0.34 | 4.99 | 0.51 | 1.53 |
| 127 | Olfr543 | 3.45 | 0.13 | 4.06 | 0.15 | 1.52 |
| 128 | Ipp | 6.97 | 0.34 | 7.58 | 0.25 | 1.52 |
| 129 | Dsc2 | 4.58 | 0.27 | 5.18 | 0.39 | 1.52 |
| 130 | Gm21866 | 4.99 | 0.21 | 5.6 | 0.62 | 1.52 |
| 131 | Efhc2 | 6.84 | 0.23 | 7.45 | 0.19 | 1.52 |
| 132 | Slco1b2 | 4.78 | 0.26 | 5.38 | 0.29 | 1.52 |
| 133 | Olfr763 | 6.02 | 0.43 | 6.62 | 0.26 | 1.52 |
| 134 | CK137956 | 4.93 | 0.42 | 5.52 | 0.06 | 1.51 |
| 135 | Gm5891; Gm10662 | 5.24 | 0.33 | 5.83 | 0.17 | 1.51 |
| 136 | Gm10662; Gm5891 | 5.24 | 0.33 | 5.83 | 0.17 | 1.51 |
| 137 | Crocc | 6.79 | 0.26 | 7.38 | 0.41 | 1.51 |
| 138 | Muc3 | 6.05 | 0.42 | 6.65 | 0.4 | 1.51 |
| 139 | 4930447F04Rik | 4.87 | 0.27 | 5.47 | 0.21 | 1.51 |
| 140 | Krt20 | 6.03 | 0.18 | 6.62 | 1.08 | 1.51 |
| 141 | Atp10b | 5.43 | 0.36 | 6.02 | 0.11 | 1.5 |
| 142 | Chchd5 | 6.49 | 0.29 | 7.07 | 0.27 | 1.5 |
| 143 | Mul1 | 7.6 | 0.32 | 8.19 | 0.22 | 1.5 |
| 144 | Mpzl2 | 6.02 | 0.17 | 6.61 | 0.33 | 1.5 |
| 145 | Hemgn | 5.96 | 0.14 | 6.54 | 0.35 | 1.5 |
| 146 | Zw10 | 7.28 | 0.05 | 7.86 | 0.3 | 1.5 |
| 147 | Ly6d | 6.83 | 0.39 | 7.42 | 0.31 | 1.5 |
| 148 | Tlr11 | 4.75 | 0.47 | 5.33 | 0.22 | 1.5 |

**112 downregulated genes in the cortex of the Cup-Recov mice**

| # | Gene Symbol | $Control_{Average}$ (log2) | $Control_{SD}$ | $Cup\text{-}Recov_{Average}$ (log2) | $Cup\text{-}Recov_{SD}$ | Fold Change(Cup-Recov/Control) |
|---|---|---|---|---|---|---|
| 1 | Gm11096 | 7.38 | 2.56 | 4.85 | 0.63 | -5.79 |
| 2 | Kif4 | 6.34 | 0.22 | 5.32 | 0.6 | -2.03 |
| 3 | Gm3893; 4933409K07Rik | 15.87 | 0.37 | 14.9 | 2.01 | -1.95 |
| 4 | Gm11077 | 5.56 | 0.16 | 4.6 | 0.5 | -1.94 |
| 5 | Sec14l5 | 8.47 | 0.6 | 7.51 | 0.54 | -1.93 |
| 6 | Gm11559 | 5.4 | 0.59 | 4.45 | 0.3 | -1.93 |

| | | | | | | |
|---|---|---|---|---|---|---|
| 7 | Hapln2 | 7.69 | 0.22 | 6.75 | 0.26 | -1.92 |
| 8 | Mptx2 | 7.12 | 0.62 | 6.2 | 0.14 | -1.9 |
| 9 | Zfp202 | 6.31 | 0.42 | 5.41 | 0.43 | -1.87 |
| 10 | Gm21719 | 5.83 | 0.5 | 4.93 | 0.31 | -1.87 |
| 11 | Ifi44 | 7.39 | 0.12 | 6.53 | 0.26 | -1.82 |
| 12 | Pah | 5.81 | 0.2 | 4.97 | 0.37 | -1.78 |
| 13 | Mog | 10.55 | 0.17 | 9.72 | 0.46 | -1.78 |
| 14 | Gm13298; Fam205a2 | 11.93 | 0.47 | 11.11 | 0.74 | -1.77 |
| 15 | 1700013H16Rik | 7.11 | 0.2 | 6.28 | 0.23 | -1.77 |
| 16 | Gm13298; Fam205a4; Gm20938 | 12.32 | 0.48 | 11.5 | 0.7 | -1.76 |
| 17 | Vmn1r4 | 5.68 | 0.44 | 4.86 | 0.36 | -1.76 |
| 18 | Gm12394 | 11.96 | 0.3 | 11.15 | 1.02 | -1.75 |
| 19 | Traf2 | 6.97 | 0.16 | 6.17 | 0.19 | -1.75 |
| 20 | Arhgef33 | 6.56 | 0.06 | 5.75 | 0.24 | -1.75 |
| 21 | Myrf | 10.46 | 0.26 | 9.66 | 0.19 | -1.73 |
| 22 | Adamts1 | 6.97 | 0.12 | 6.19 | 0.33 | -1.73 |
| 23 | Dppa1 | 5.24 | 0.36 | 4.45 | 0.23 | -1.73 |
| 24 | Olfr533 | 5.62 | 0.36 | 4.83 | 0.41 | -1.73 |
| 25 | Fpr-rs6 | 5.53 | 0.32 | 4.75 | 0.21 | -1.72 |
| 26 | H1foo | 5.03 | 0.19 | 4.24 | 0.3 | -1.72 |
| 27 | Olfr1386 | 5.16 | 0.26 | 4.39 | 0.43 | -1.71 |
| 28 | Olfr224; Olfr329-ps | 5.05 | 0.34 | 4.3 | 0.45 | -1.69 |
| 29 | Fam205a1 | 11.05 | 0.36 | 10.3 | 0.74 | -1.68 |
| 30 | Gm5927 | 7.96 | 0.28 | 7.21 | 0.26 | -1.68 |
| 31 | Vmn2r102 | 5.17 | 0.28 | 4.42 | 0.42 | -1.68 |
| 32 | Scnn1a | 7.96 | 0.09 | 7.21 | 0.37 | -1.68 |
| 33 | Nat9 | 6.87 | 0.26 | 6.13 | 0.1 | -1.68 |
| 34 | Kcnq4 | 7.63 | 0.28 | 6.88 | 0.42 | -1.68 |
| 35 | Vmn1r103 | 5.34 | 0.11 | 4.59 | 0.55 | -1.68 |
| 36 | Prkd2 | 7.38 | 0.66 | 6.64 | 0.36 | -1.67 |
| 37 | Rnf17 | 5.86 | 0.34 | 5.12 | 0.45 | -1.66 |
| 38 | Gm13298; Fam205a3; Gm21598 | 12.17 | 0.44 | 11.44 | 0.7 | -1.65 |
| 39 | Mobp | 13.08 | 0.27 | 12.36 | 0.53 | -1.65 |
| 40 | Urb1 | 8.51 | 0.23 | 7.79 | 0.36 | -1.65 |
| 41 | Lmcd1 | 7.47 | 0.47 | 6.75 | 0.22 | -1.65 |
| 42 | Olfr1484 | 6.06 | 0.23 | 5.35 | 0.27 | -1.64 |
| 43 | Vmn2r9 | 5.96 | 0.11 | 5.25 | 0.3 | -1.64 |
| 44 | Pcdhb6 | 8.52 | 0.23 | 7.81 | 0.15 | -1.64 |
| 45 | Ybey | 6.19 | 0.13 | 5.48 | 0.2 | -1.63 |
| 46 | Gm3763 | 4.79 | 0.3 | 4.09 | 0.28 | -1.63 |
| 47 | Cyp2j12 | 7.29 | 0.17 | 6.59 | 0.67 | -1.62 |
| 48 | Gm5483 | 5.75 | 0.34 | 5.05 | 0.64 | -1.62 |

| | | | | | | |
|---|---|---|---|---|---|---|
| 49 | Tmem252 | 7.22 | 0.11 | 6.53 | 0.21 | -1.61 |
| 50 | Ccdc79 | 7.5 | 0.1 | 6.81 | 0.36 | -1.61 |
| 51 | Nlrp5 | 5.76 | 0.27 | 5.09 | 0.45 | -1.6 |
| 52 | Gata2 | 7.15 | 0.41 | 6.47 | 0.22 | -1.6 |
| 53 | 4930481A15Rik | 7.37 | 0.12 | 6.7 | 0.21 | -1.6 |
| 54 | 1700009J07Rik | 7.05 | 0.24 | 6.37 | 0.22 | -1.6 |
| 55 | Slc26a11 | 7.08 | 0.41 | 6.41 | 0.28 | -1.59 |
| 56 | Zfp217 | 5.77 | 0.47 | 5.1 | 0.69 | -1.59 |
| 57 | 2410131K14Rik | 6.51 | 0.19 | 5.85 | 0.21 | -1.59 |
| 58 | Olfr1436 | 5.12 | 0.5 | 4.46 | 0.39 | -1.58 |
| 59 | Dkk2 | 6.23 | 0.56 | 5.57 | 0.23 | -1.58 |
| 60 | Vmn1r12 | 5.08 | 0.32 | 4.41 | 0.12 | -1.58 |
| 61 | 4933409K07Rik | 12.27 | 0.39 | 11.62 | 0.65 | -1.57 |
| 62 | 4933409K07Rik | 12.27 | 0.39 | 11.62 | 0.65 | -1.57 |
| 63 | Etnk2 | 9.43 | 0.35 | 8.78 | 0.22 | -1.57 |
| 64 | Olfr603 | 4.54 | 0.31 | 3.89 | 0.21 | -1.57 |
| 65 | Pcdhb9 | 10.04 | 0.25 | 9.39 | 0.25 | -1.57 |
| 66 | Ssfa2 | 9.29 | 0.21 | 8.64 | 0.23 | -1.56 |
| 67 | Il12a | 7.15 | 0.14 | 6.51 | 0.38 | -1.56 |
| 68 | Gm5709 | 4.85 | 0.59 | 4.2 | 0.17 | -1.56 |
| 69 | Hsfy2 | 5.36 | 0.24 | 4.72 | 0.09 | -1.56 |
| 70 | Ltbr | 8.46 | 0.45 | 7.82 | 0.19 | -1.56 |
| 71 | Casc5 | 4.72 | 0.28 | 4.08 | 0.07 | -1.56 |
| 72 | Ppef2 | 5.18 | 0.23 | 4.54 | 0.35 | -1.56 |
| 73 | Asb4 | 6.09 | 0.36 | 5.44 | 0.55 | -1.56 |
| 74 | Rxfp3 | 5.76 | 0.15 | 5.12 | 0.39 | -1.55 |
| 75 | Clec4a2 | 5.84 | 0.57 | 5.2 | 0.35 | -1.55 |
| 76 | Agxt | 4.76 | 0.27 | 4.13 | 0.14 | -1.55 |
| 77 | Foxred2 | 7.43 | 0.11 | 6.8 | 0.45 | -1.55 |
| 78 | Tnfsf18 | 5.03 | 0.28 | 4.4 | 0.22 | -1.55 |
| 79 | Khdc3 | 5.39 | 0.21 | 4.75 | 0.36 | -1.55 |
| 80 | Sel1l2 | 6.26 | 0.55 | 5.63 | 0.43 | -1.55 |
| 81 | Klf11 | 7.26 | 0.16 | 6.63 | 0.41 | -1.55 |
| 82 | 4933409K07Rik | 12.3 | 0.49 | 11.68 | 0.71 | -1.54 |
| 83 | BC061237 | 5.2 | 0.21 | 4.57 | 0.06 | -1.54 |
| 84 | Col1a1 | 7.89 | 0.38 | 7.26 | 0.1 | -1.54 |
| 85 | Olfr1245 | 6.06 | 0.31 | 5.44 | 0.15 | -1.54 |
| 86 | Olfr194 | 5.25 | 0.62 | 4.63 | 0.28 | -1.54 |
| 87 | Gm5861 | 5.56 | 0.39 | 4.94 | 0.27 | -1.54 |
| 88 | Arl5c | 5.2 | 0.37 | 4.58 | 0.28 | -1.54 |
| 89 | Erbb3 | 5.67 | 0.26 | 5.05 | 0.59 | -1.53 |
| 90 | Peo1 | 5.93 | 0.41 | 5.32 | 0.31 | -1.53 |
| 91 | Ak8 | 8.56 | 0.14 | 7.95 | 0.27 | -1.53 |

| | | | | | | |
|---|---|---|---|---|---|---|
| 92 | Klf10 | 9.16 | 0.3 | 8.55 | 0.49 | -1.53 |
| 93 | Gm13157 | 5.59 | 0.35 | 4.98 | 0.46 | -1.53 |
| 94 | Btc | 7.13 | 0.25 | 6.52 | 0.46 | -1.53 |
| 95 | Jmjd7; Pla2g4b; Gm28042 | 6.62 | 0.17 | 6.01 | 0.31 | -1.53 |
| 96 | D6Ertd527e | 8.44 | 0.4 | 7.83 | 0.49 | -1.53 |
| 97 | Fam205a2; Gm10600 | 13.87 | 0.4 | 13.26 | 1.39 | -1.52 |
| 98 | Mmp10 | 5.14 | 0.14 | 4.54 | 0.16 | -1.52 |
| 99 | Olfr843 | 5.01 | 0.33 | 4.4 | 0.11 | -1.52 |
| 100 | Iigp1 | 6.45 | 0.27 | 5.85 | 0.33 | -1.52 |
| 101 | Olig1 | 9.47 | 0.3 | 8.88 | 0.23 | -1.51 |
| 102 | Zfp189 | 8.14 | 0.46 | 7.55 | 0.32 | -1.51 |
| 103 | Fbxo48 | 5.58 | 0.33 | 4.99 | 0.33 | -1.51 |
| 104 | Ddx4 | 6.44 | 0.29 | 5.84 | 0.37 | -1.51 |
| 105 | Ddx51 | 8.03 | 0.45 | 7.43 | 0.35 | -1.51 |
| 106 | Crybb1 | 7.81 | 0.08 | 7.21 | 0.44 | -1.51 |
| 107 | Prl8a2 | 4.72 | 0.41 | 4.13 | 0.16 | -1.51 |
| 108 | 4932415M13Rik | 6.48 | 0.45 | 5.89 | 0.48 | -1.51 |
| 109 | Gpr37 | 10.49 | 0.27 | 9.9 | 0.15 | -1.5 |
| 110 | Etnppl | 11.03 | 0.3 | 10.44 | 0.33 | -1.5 |
| 111 | Als2 | 8.91 | 0.14 | 8.32 | 0.52 | -1.5 |
| 112 | Tmem266 | 7.29 | 0.39 | 6.7 | 0.25 | -1.5 |

# 9. List of Figures

# 10. List of Tables



# 11. References

Adams, K. L., & Gallo, V. (2018). The diversity and disparity of the glial scar. *Nat Neurosci, 21*(1), 9-15. doi:10.1038/s41593-017-0033-9

Allen, I. V., McQuaid, S., Mirakhur, M., & Nevin, G. (2001). Pathological abnormalities in the normal-appearing white matter in multiple sclerosis. *Neurol Sci, 22*(2), 141-144. doi:10.1007/s100720170012

Amende, I., Kale, A., McCue, S., Glazier, S., Morgan, J. P., & Hampton, T. G. (2005). Gait dynamics in mouse models of Parkinson's disease and Huntington's disease. *J Neuroeng Rehabil, 2*, 20. doi:10.1186/1743-0003-2-20

Anantharam, V., Kitazawa, M., Wagner, J., Kaul, S., & Kanthasamy, A. G. (2002). Caspase-3-dependent proteolytic cleavage of protein kinase Cdelta is essential for oxidative stress-mediated dopaminergic cell death after exposure to methylcyclopentadienyl manganese tricarbonyl. *J Neurosci, 22*(5), 1738-1751. Retrieved from http://www.ncbi.nlm.nih.gov/pubmed/11880503

Ashburner, M., Ball, C. A., Blake, J. A., Botstein, D., Butler, H., Cherry, J. M., . . . Sherlock, G. (2000). Gene ontology: tool for the unification of biology. The Gene Ontology Consortium. *Nat Genet, 25*(1), 25-29. doi:10.1038/75556

Barmack, N. H., Qian, Z., & Yoshimura, J. (2000). Regional and cellular distribution of protein kinase C in rat cerebellar Purkinje cells. *J Comp Neurol, 427*(2), 235-254. doi:10.1002/1096-9861(20001113)427:2<235::aid-cne6>3.0.co;2-6

Becker, B., Demirbas, M., Johann, S., Zendedel, A., Beyer, C., Clusmann, H., . . . Kipp, M. (2018). Effect of Intrastriatal 6-OHDA Lesions on Extrastriatal Brain Structures in the Mouse. *Mol Neurobiol, 55*(5), 4240-4252. doi:10.1007/s12035-017-0637-9

Benecke, R., & Conrad, B. (1980). Evaluation of motor deficits in patients suffering from Multiple Sclerosis *Progress in Multiple Sclerosis Research* (pp. 589-595): Springer.

Bergman, P., James, T., Kular, L., Ruhrmann, S., Kramarova, T., Kvist, A., . . . Jagodic, M. (2013). Next-generation sequencing identifies microRNAs that associate with pathogenic autoimmune neuroinflammation in rats. *J Immunol, 190*(8), 4066-4075. doi:10.4049/jimmunol.1200728

Bey, E. A., Xu, B., Bhattacharjee, A., Oldfield, C. M., Zhao, X., Li, Q., . . . Cathcart, M. K. (2004). Protein kinase C delta is required for p47phox phosphorylation and translocation in activated human monocytes. *J Immunol, 173*(9), 5730-5738. doi:10.4049/jimmunol.173.9.5730

Beynon, S. B., & Walker, F. R. (2012). Microglial activation in the injured and healthy brain: what are we really talking about? Practical and theoretical issues associated with the measurement of changes in microglial morphology. *Neuroscience, 225*, 162-171. doi:10.1016/j.neuroscience.2012.07.029

Bonzano, L., Tacchino, A., Roccatagliata, L., Abbruzzese, G., Mancardi, G. L., & Bove, M. (2008). Callosal contributions to simultaneous bimanual finger movements. *J Neurosci, 28*(12), 3227-3233. doi:10.1523/JNEUROSCI.4076-07.2008

Bramow, S., Frischer, J. M., Lassmann, H., Koch-Henriksen, N., Lucchinetti, C. F., Sorensen, P. S., & Laursen, H. (2010). Demyelination versus remyelination in progressive multiple sclerosis. *Brain, 133*(10), 2983-2998. doi:10.1093/brain/awq250

Brooks, S. P., & Dunnett, S. B. (2009). Tests to assess motor phenotype in mice: a user's guide. *Nat Rev Neurosci, 10*(7), 519-529. doi:10.1038/nrn2652

Cai, H., Haubensak, W., Anthony, T. E., & Anderson, D. J. (2014). Central amygdala PKC-delta(+) neurons mediate the influence of multiple anorexigenic signals. *Nat Neurosci, 17*(9), 1240-1248. doi:10.1038/nn.3767

Carpenter, A. C., & Alexander, J. S. (2008). Endothelial PKC delta activation attenuates neutrophil transendothelial migration. *Inflamm Res, 57*(5), 216-229. doi:10.1007/s00011-007-7031-4

Chard, D. T., Griffin, C. M., McLean, M. A., Kapeller, P., Kapoor, R., Thompson, A. J., & Miller, D. H. (2002). Brain metabolite changes in cortical grey and normal-appearing white matter in clinically early relapsing-remitting multiple sclerosis. *Brain, 125*(Pt 10), 2342-2352. doi:10.1093/brain/awf240

Chen, X. H., Johnson, V. E., Uryu, K., Trojanowski, J. Q., & Smith, D. H. (2009). A lack of amyloid beta plaques despite persistent accumulation of amyloid beta in axons of long-term survivors of traumatic brain injury. *Brain Pathol, 19*(2), 214-223. doi:10.1111/j.1750-3639.2008.00176.x

Chrzanowski, U., Bhattarai, S., Scheld, M., Clarner, T., Fallier-Becker, P., Beyer, C., . . . Kipp, M. (2019). Oligodendrocyte degeneration and concomitant microglia activation directs peripheral immune cells into the forebrain. *Neurochem Int, 126*, 139-153. doi:10.1016/j.neuint.2019.03.005

Chrzanowski, U., Schmitz, C., Horn-Bochtler, A., Nack, A., & Kipp, M. (2019). Evaluation strategy to determine reliable demyelination in the cuprizone model. *Metab Brain Dis, 34*(2), 681-685. doi:10.1007/s11011-018-0375-3

Clarner, T., Diederichs, F., Berger, K., Denecke, B., Gan, L., van der Valk, P., . . . Kipp, M. (2012). Myelin debris regulates inflammatory responses in an experimental demyelination animal model and multiple sclerosis lesions. *Glia, 60*(10), 1468-1480. doi:10.1002/glia.22367

Constantinescu, C. S., Farooqi, N., O'Brien, K., & Gran, B. (2011). Experimental autoimmune encephalomyelitis (EAE) as a model for multiple sclerosis (MS). *Br J Pharmacol, 164*(4), 1079-1106. doi:10.1111/j.1476-5381.2011.01302.x

Correale, J., Gaitan, M. I., Ysrraelit, M. C., & Fiol, M. P. (2017). Progressive multiple sclerosis: from pathogenic mechanisms to treatment. *Brain, 140*(3), 527-546. doi:10.1093/brain/aww258

Crews, F. T., & Vetreno, R. P. (2016). Mechanisms of neuroimmune gene induction in alcoholism. *Psychopharmacology (Berl), 233*(9), 1543-1557. doi:10.1007/s00213-015-3906-1

Dang, D. K., Shin, E. J., Kim, D. J., Tran, H. Q., Jeong, J. H., Jang, C. G., . . . Kim, H. C. (2018). PKCdelta-dependent p47phox activation mediates methamphetamine-induced dopaminergic neurotoxicity. *Free Radic Biol Med, 115*, 318-337. doi:10.1016/j.freeradbiomed.2017.12.018

de Carvalho, F. P., Benfato, I. D., Moretto, T. L., Barthichoto, M., & de Oliveira, C. A. (2016). Voluntary running decreases nonexercise activity in lean and diet-induced obese mice. *Physiol Behav, 165*, 249-256. doi:10.1016/j.physbeh.2016.08.003

Dekker, I., Eijlers, A. J. C., Popescu, V., Balk, L. J., Vrenken, H., Wattjes, M. P., . . . Schoonheim, M. M. (2019). Predicting clinical progression in multiple sclerosis after 6 and 12 years. *Eur J Neurol, 26*(6), 893-902. doi:10.1111/ene.13904

Dendrou, C. A., Fugger, L., & Friese, M. A. (2015). Immunopathology of multiple sclerosis. *Nat Rev Immunol, 15*(9), 545-558. doi:10.1038/nri3871

Dorman, C. W., Krug, H. E., Frizelle, S. P., Funkenbusch, S., & Mahowald, M. L. (2014). A comparison of DigiGait and TreadScan imaging systems: assessment of pain using gait analysis in murine monoarthritis. *J Pain Res, 7*, 25-35. doi:10.2147/JPR.S52195

Drai, D., Kafkafi, N., Benjamini, Y., Elmer, G., & Golani, I. (2001). Rats and mice share common ethologically relevant parameters of exploratory behavior. *Behav Brain Res, 125*(1-2), 133-140. doi:10.1016/s0166-4328(01)00290-x

Dunham, N. W., & Miya, T. S. (1957). A note on a simple apparatus for detecting neurological deficit in rats and mice. *J Am Pharm Assoc Am Pharm Assoc, 46*(3), 208-209. doi:10.1002/jps.3030460322

Emerich, D. F., Dean III, R. L., & Sanberg, P. R. (1999). *Central nervous system diseases: innovative animal models from lab to clinic*: Springer Science & Business Media.

Evangelou, N., Esiri, M. M., Smith, S., Palace, J., & Matthews, P. M. (2000). Quantitative pathological evidence for axonal loss in normal appearing white matter in multiple sclerosis. *Ann Neurol, 47*(3), 391-395. Retrieved from http://www.ncbi.nlm.nih.gov/pubmed/10716264

Evangelou, N., Konz, D., Esiri, M. M., Smith, S., Palace, J., & Matthews, P. M. (2000). Regional axonal loss in the corpus callosum correlates with cerebral white matter lesion volume and distribution in multiple sclerosis. *Brain, 123 ( Pt 9)*, 1845-1849. doi:10.1093/brain/123.9.1845

Evangelou, N., Konz, D., Esiri, M. M., Smith, S., Palace, J., & Matthews, P. M. (2001). Size-selective neuronal changes in the anterior optic pathways suggest a differential susceptibility to injury in multiple sclerosis. *Brain, 124*(Pt 9), 1813-1820. doi:10.1093/brain/124.9.1813

Faissner, S., Plemel, J. R., Gold, R., & Yong, V. W. (2019). Progressive multiple sclerosis: from pathophysiology to therapeutic strategies. *Nat Rev Drug Discov, 18*(12), 905-922. doi:10.1038/s41573-019-0035-2

Feys, P., Lamers, I., Francis, G., Benedict, R., Phillips, G., LaRocca, N., . . . Multiple Sclerosis Outcome Assessments, C. (2017). The Nine-Hole Peg Test as a manual dexterity performance measure for multiple sclerosis. *Mult Scler, 23*(5), 711-720. doi:10.1177/1352458517690824

Filippi, M., Preziosa, P., Copetti, M., Riccitelli, G., Horsfield, M. A., Martinelli, V., . . . Rocca, M. A. (2013). Gray matter damage predicts the accumulation of disability 13 years later in MS. *Neurology, 81*(20), 1759-1767. doi:10.1212/01.wnl.0000435551.90824.d0

Fischbach, F., Nedelcu, J., Leopold, P., Zhan, J., Clarner, T., Nellessen, L., . . . Kipp, M. (2019). Cuprizone-induced graded oligodendrocyte vulnerability is regulated by the transcription factor DNA damage-inducible transcript 3. *Glia, 67*(2), 263-276. doi:10.1002/glia.23538

Flachenecker, P. (2015). Clinical implications of neuroplasticity - the role of rehabilitation in multiple sclerosis. *Front Neurol, 6*, 36. doi:10.3389/fneur.2015.00036

Franco-Pons, N., Torrente, M., Colomina, M. T., & Vilella, E. (2007). Behavioral deficits in the cuprizone-induced murine model of demyelination/remyelination. *Toxicol Lett, 169*(3), 205-213. doi:10.1016/j.toxlet.2007.01.010

Frischer, J. M., Weigand, S. D., Guo, Y., Kale, N., Parisi, J. E., Pirko, I., . . . Lucchinetti, C. F. (2015). Clinical and pathological insights into the dynamic nature of the white matter multiple sclerosis plaque. *Ann Neurol, 78*(5), 710-721. doi:10.1002/ana.24497

Gentile, A. M., Green, S., Nieburgs, A., Schmelzer, W., & Stein, D. G. (1978). Disruption and recovery of locomotor and manipulatory behavior following cortical lesions in rats. *Behav Biol, 22*(4), 417-455. doi:10.1016/s0091-6773(78)92547-6

Goldberg, J., Clarner, T., Beyer, C., & Kipp, M. (2015). Anatomical Distribution of Cuprizone-Induced Lesions in C57BL6 Mice. *J Mol Neurosci, 57*(2), 166-175. doi:10.1007/s12031-015-0595-5

Gordon, R., Singh, N., Lawana, V., Ghosh, A., Harischandra, D. S., Jin, H., . . . Kanthasamy, A. (2016). Protein kinase Cdelta upregulation in microglia drives neuroinflammatory responses and dopaminergic neurodegeneration in experimental models of Parkinson's disease. *Neurobiol Dis, 93*, 96-114. doi:10.1016/j.nbd.2016.04.008

Grillner, S., & Wallen, P. (1985). Central pattern generators for locomotion, with special reference to vertebrates. *Annu Rev Neurosci, 8*, 233-261. doi:10.1146/annurev.ne.08.030185.001313

Grillner, S., Wallen, P., Saitoh, K., Kozlov, A., & Robertson, B. (2008). Neural bases of goal-directed locomotion in vertebrates--an overview. *Brain Res Rev, 57*(1), 2-12. doi:10.1016/j.brainresrev.2007.06.027

Grosse-Veldmann, R., Becker, B., Amor, S., van der Valk, P., Beyer, C., & Kipp, M. (2016). Lesion Expansion in Experimental Demyelination Animal Models and Multiple Sclerosis Lesions. *Mol Neurobiol, 53*(7), 4905-4917. doi:10.1007/s12035-015-9420-y

Gudi, V., Gingele, S., Skripuletz, T., & Stangel, M. (2014). Glial response during cuprizone-induced de- and remyelination in the CNS: lessons learned. *Front Cell Neurosci, 8*, 73. doi:10.3389/fncel.2014.00073

Hall, C. S. (1934). Emotional behavior in the rat. I. Defecation and urination as measures of individual differences in emotionality. *Journal of Comparative psychology, 18*(3), 385.

Hamers, F. P., Lankhorst, A. J., van Laar, T. J., Veldhuis, W. B., & Gispen, W. H. (2001). Automated quantitative gait analysis during overground locomotion in the rat: its application to spinal cord contusion and transection injuries. *J Neurotrauma, 18*(2), 187-201. doi:10.1089/08977150150502613

Hampton, D. W., Serio, A., Pryce, G., Al-Izki, S., Franklin, R. J., Giovannoni, G., . . . Chandran, S. (2013). Neurodegeneration progresses despite complete elimination of clinical relapses in a mouse model of multiple sclerosis. *Acta Neuropathol Commun, 1*, 84. doi:10.1186/2051-5960-1-84

Hampton, T. G., Stasko, M. R., Kale, A., Amende, I., & Costa, A. C. (2004). Gait dynamics in trisomic mice: quantitative neurological traits of Down syndrome. *Physiol Behav, 82*(2-3), 381-389. doi:10.1016/j.physbeh.2004.04.006

Han, M. H., Lundgren, D. H., Jaiswal, S., Chao, M., Graham, K. L., Garris, C. S., . . . Steinman, L. (2012). Janus-like opposing roles of CD47 in autoimmune brain inflammation in humans and mice. *J Exp Med, 209*(7), 1325-1334. doi:10.1084/jem.20101974

Hanrott, K., Murray, T. K., Orfali, Z., Ward, M., Finlay, C., O'Neill, M. J., & Wonnacott, S. (2008). Differential activation of PKC delta in the substantia nigra of rats following striatal or nigral 6-hydroxydopamine lesions. *Eur J Neurosci, 27*(5), 1086-1096. doi:10.1111/j.1460-9568.2008.06097.x

Heesen, C., Bohm, J., Reich, C., Kasper, J., Goebel, M., & Gold, S. M. (2008). Patient perception of bodily functions in multiple sclerosis: gait and visual function are the most valuable. *Mult Scler, 14*(7), 988-991. doi:10.1177/1352458508088916

Hibbits, N., Pannu, R., Wu, T. J., & Armstrong, R. C. (2009). Cuprizone demyelination of the corpus callosum in mice correlates with altered social interaction and impaired bilateral sensorimotor coordination. *ASN Neuro, 1*(3). doi:10.1042/AN20090032

Hicks, J. A., Hatzidis, A., Arruda, N. L., Gelineau, R. R., De Pina, I. M., Adams, K. W., & Seggio, J. A. (2016). Voluntary wheel-running attenuates insulin and weight gain and affects anxiety-like behaviors in C57BL6/J mice exposed to a high-fat diet. *Behav Brain Res, 310*, 1-10. doi:10.1016/j.bbr.2016.04.051

Hoflich, K. M., Beyer, C., Clarner, T., Schmitz, C., Nyamoya, S., Kipp, M., & Hochstrasser, T. (2016). Acute axonal damage in three different murine models of multiple sclerosis: A comparative approach. *Brain Res, 1650*, 125-133. doi:10.1016/j.brainres.2016.08.048

Howell, O. W., Reeves, C. A., Nicholas, R., Carassiti, D., Radotra, B., Gentleman, S. M., . . . Reynolds, R. (2011). Meningeal inflammation is widespread and linked to cortical pathology in multiple sclerosis. *Brain, 134*(Pt 9), 2755-2771. doi:10.1093/brain/awr182

Inglese, M., van Waesberghe, J. H., Rovaris, M., Beckmann, K., Barkhof, F., Hahn, D., . . . Filippi, M. (2003). The effect of interferon beta-1b on quantities derived from MT MRI in secondary progressive MS. *Neurology, 60*(5), 853-860. doi:10.1212/01.wnl.0000049929.27032.29

Irani, B. G., Donato, J., Jr., Olson, D. P., Lowell, B. B., Sacktor, T. C., Reyland, M. E., . . . Clegg, D. J. (2010). Distribution and neurochemical characterization of protein kinase C-theta and -delta in the rodent hypothalamus. *Neuroscience, 170*(4), 1065-1079. doi:10.1016/j.neuroscience.2010.07.064

Irizarry, R. A., Bolstad, B. M., Collin, F., Cope, L. M., Hobbs, B., & Speed, T. P. (2003). Summaries of Affymetrix GeneChip probe level data. *Nucleic Acids Res, 31*(4), e15.

Irvine, K. A., & Blakemore, W. F. (2008). Remyelination protects axons from demyelination-associated axon degeneration. *Brain, 131*(Pt 6), 1464-1477. doi:10.1093/brain/awn080

Johnson, V. E., Stewart, W., & Smith, D. H. (2010). Traumatic brain injury and amyloid-beta pathology: a link to Alzheimer's disease? *Nat Rev Neurosci, 11*(5), 361-370. doi:10.1038/nrn2808

Kale, A., Amende, I., Meyer, G. P., Crabbe, J. C., & Hampton, T. G. (2004). Ethanol's effects on gait dynamics in mice investigated by ventral plane videography. *Alcohol Clin Exp Res, 28*(12), 1839-1848. doi:10.1097/01.alc.0000148103.09378.81

Kappos, L., Bar-Or, A., Cree, B. A. C., Fox, R. J., Giovannoni, G., Gold, R., . . . Investigators, E. C. (2018). Siponimod versus placebo in secondary progressive multiple sclerosis (EXPAND): a double-blind, randomised, phase 3 study. *Lancet, 391*(10127), 1263-1273. doi:10.1016/S0140-6736(18)30475-6

Kaul, S., Kanthasamy, A., Kitazawa, M., Anantharam, V., & Kanthasamy, A. G. (2003). Caspase-3 dependent proteolytic activation of protein kinase C delta mediates and regulates 1-methyl-4-phenylpyridinium (MPP+)-induced apoptotic cell death in dopaminergic cells: relevance to oxidative stress in dopaminergic degeneration. *Eur J Neurosci, 18*(6), 1387-1401. doi:10.1046/j.1460-9568.2003.02864.x

Kennerley, S. W., Diedrichsen, J., Hazeltine, E., Semjen, A., & Ivry, R. B. (2002). Callosotomy patients exhibit temporal uncoupling during continuous bimanual movements. *Nat Neurosci, 5*(4), 376-381. doi:10.1038/nn822

Kerschensteiner, M., Bareyre, F. M., Buddeberg, B. S., Merkler, D., Stadelmann, C., Brück, W., . . . Schwab, M. E. (2004). Remodeling of axonal connections contributes to recovery in an animal model of multiple sclerosis. *J Exp Med, 200*(8), 1027-1038. doi:10.1084/jem.20040452

Kipp, M. (2020). Does Siponimod Exert Direct Effects in the Central Nervous System? *Cells, 9*(8). doi:10.3390/cells9081771

Kipp, M., & Amor, S. (2012). FTY720 on the way from the base camp to the summit of the mountain: relevance for remyelination. *Mult Scler, 18*(3), 258-263. doi:10.1177/1352458512438723

Kipp, M., Clarner, T., Dang, J., Copray, S., & Beyer, C. (2009). The cuprizone animal model: new insights into an old story. *Acta Neuropathol, 118*(6), 723-736. doi:10.1007/s00401-009-0591-3

Kipp, M., Gingele, S., Pott, F., Clarner, T., van der Valk, P., Denecke, B., . . . Beyer, C. (2011). BLBP-expression in astrocytes during experimental demyelination and in human multiple sclerosis lesions. *Brain Behav Immun, 25*(8), 1554-1568. doi:10.1016/j.bbi.2011.05.003

Kipp, M., Norkute, A., Johann, S., Lorenz, L., Braun, A., Hieble, A., . . . Beyer, C. (2008). Brain-region-specific astroglial responses in vitro after LPS exposure. *J Mol Neurosci, 35*(2), 235-243. doi:10.1007/s12031-008-9057-7

Kipp, M., Nyamoya, S., Hochstrasser, T., & Amor, S. (2017). Multiple sclerosis animal models: a clinical and histopathological perspective. *Brain Pathol, 27*(2), 123-137. doi:10.1111/bpa.12454

Kipp, M., van der Valk, P., & Amor, S. (2012). Pathology of multiple sclerosis. *CNS Neurol Disord Drug Targets, 11*(5), 506-517. doi:10.2174/187152712801661248

Kirov, II, Patil, V., Babb, J. S., Rusinek, H., Herbert, J., & Gonen, O. (2009). MR spectroscopy indicates diffuse multiple sclerosis activity during remission. *J Neurol Neurosurg Psychiatry, 80*(12), 1330-1336. doi:10.1136/jnnp.2009.176263

Klapdor, K., Dulfer, B. G., Hammann, A., & Van der Staay, F. J. (1997). A low-cost method to analyse footprint patterns. *J Neurosci Methods, 75*(1), 49-54. doi:10.1016/s0165-0270(97)00042-3

Koo, E. H., Sisodia, S. S., Archer, D. R., Martin, L. J., Weidemann, A., Beyreuther, K., . . . Price, D. L. (1990). Precursor of amyloid protein in Alzheimer disease undergoes fast anterograde axonal transport. *Proc Natl Acad Sci U S A, 87*(4), 1561-1565.

Krauspe, B. M., Dreher, W., Beyer, C., Baumgartner, W., Denecke, B., Janssen, K., . . . Kipp, M. (2015). Short-term cuprizone feeding verifies N-acetylaspartate quantification as a marker of neurodegeneration. *J Mol Neurosci, 55*(3), 733-748. doi:10.1007/s12031-014-0412-6

Kurtzke, J. F., & Berlin, L. (1954). The effects of isoniazid on patients with multiple sclerosis; preliminary report. *Am Rev Tuberc, 70*(4), 577-592. doi:10.1164/art.1954.70.4.577

Kutzelnigg, A., Lucchinetti, C. F., Stadelmann, C., Bruck, W., Rauschka, H., Bergmann, M., . . . Lassmann, H. (2005). Cortical demyelination and diffuse white matter injury in multiple sclerosis. *Brain, 128*(Pt 11), 2705-2712. doi:10.1093/brain/awh641

Lein, E. S., Hawrylycz, M. J., Ao, N., Ayres, M., Bensinger, A., Bernard, A., . . . Jones, A. R. (2007). Genome-wide atlas of gene expression in the adult mouse brain. *Nature, 445*(7124), 168-176. doi:10.1038/nature05453

Liebetanz, D., & Merkler, D. (2006). Effects of commissural de- and remyelination on motor skill behaviour in the cuprizone mouse model of multiple sclerosis. *Exp Neurol, 202*(1), 217-224. doi:10.1016/j.expneurol.2006.05.032

Loevner, L. A., Grossman, R. I., Cohen, J. A., Lexa, F. J., Kessler, D., & Kolson, D. L. (1995). Microscopic disease in normal-appearing white matter on conventional MR images in patients with multiple sclerosis: assessment with magnetization-transfer measurements. *Radiology, 196*(2), 511-515. doi:10.1148/radiology.196.2.7617869

Lubetzki, C., Zalc, B., Williams, A., Stadelmann, C., & Stankoff, B. (2020). Remyelination in multiple sclerosis: from basic science to clinical translation. *Lancet Neurol, 19*(8), 678-688. doi:10.1016/S1474-4422(20)30140-X

Mahurkar, S., Moldovan, M., Suppiah, V., & O'Doherty, C. (2013). Identification of shared genes and pathways: a comparative study of multiple sclerosis susceptibility, severity and response to interferon beta treatment. *PLoS One, 8*(2), e57655. doi:10.1371/journal.pone.0057655

Makinodan, M., Yamauchi, T., Tatsumi, K., Okuda, H., Takeda, T., Kiuchi, K., . . . Kishimoto, T. (2009). Demyelination in the juvenile period, but not in adulthood, leads to long-lasting cognitive impairment and deficient social interaction in mice. *Prog Neuropsychopharmacol Biol Psychiatry, 33*(6), 978-985. doi:10.1016/j.pnpbp.2009.05.006

Manrique-Hoyos, N., Jurgens, T., Gronborg, M., Kreutzfeldt, M., Schedensack, M., Kuhlmann, T., . . . Merkler, D. (2012). Late motor decline after accomplished remyelination: impact for progressive multiple sclerosis. *Ann Neurol, 71*(2), 227-244. doi:10.1002/ana.22681

McIntosh-Michaelis, S. A., Roberts, M. H., Wilkinson, S. M., Diamond, I. D., McLellan, D. L., Martin, J. P., & Spackman, A. J. (1991). The prevalence of cognitive impairment in a community survey of multiple sclerosis. *Br J Clin Psychol, 30*(4), 333-348. doi:10.1111/j.2044-8260.1991.tb00954.x

Mecklenbräuker, I., Kalled, S. L., Leitges, M., Mackay, F., & Tarakhovsky, A. (2004). Regulation of B-cell survival by BAFF-dependent PKCdelta-mediated nuclear signalling. *Nature, 431*(7007), 456-461. doi:10.1038/nature02955

Mi, H., Muruganujan, A., Ebert, D., Huang, X., & Thomas, P. D. (2019). PANTHER version 14: more genomes, a new PANTHER GO-slim and improvements in enrichment analysis tools. *Nucleic Acids Res, 47*(D1), D419-D426. doi:10.1093/nar/gky1038

Moll, N. M., Rietsch, A. M., Thomas, S., Ransohoff, A. J., Lee, J. C., Fox, R., . . . Fisher, E. (2011). Multiple sclerosis normal-appearing white matter: pathology-imaging correlations. *Ann Neurol, 70*(5), 764-773. doi:10.1002/ana.22521

Montalban, X., Hauser, S. L., Kappos, L., Arnold, D. L., Bar-Or, A., Comi, G., . . . Investigators, O. C. (2017). Ocrelizumab versus Placebo in Primary Progressive Multiple Sclerosis. *N Engl J Med, 376*(3), 209-220. doi:10.1056/NEJMoa1606468

Morell, P., Barrett, C. V., Mason, J. L., Toews, A. D., Hostettler, J. D., Knapp, G. W., & Matsushima, G. K. (1998). Gene expression in brain during cuprizone-induced demyelination and remyelination. *Mol Cell Neurosci, 12*(4-5), 220-227. doi:10.1006/mcne.1998.0715

Morrison, H., Young, K., Qureshi, M., Rowe, R. K., & Lifshitz, J. (2017). Quantitative microglia analyses reveal diverse morphologic responses in the rat cortex after diffuse brain injury. *Sci Rep, 7*(1), 13211. doi:10.1038/s41598-017-13581-z

Morrison, H. W., & Filosa, J. A. (2013). A quantitative spatiotemporal analysis of microglia morphology during ischemic stroke and reperfusion. *J Neuroinflammation, 10*, 4. doi:10.1186/1742-2094-10-4

Motl, R. W., Cohen, J. A., Benedict, R., Phillips, G., LaRocca, N., Hudson, L. D., . . . Multiple Sclerosis Outcome Assessments, C. (2017). Validity of the timed 25-foot walk as an ambulatory performance outcome measure for multiple sclerosis. *Mult Scler, 23*(5), 704-710. doi:10.1177/1352458517690823

Musella, A., Gentile, A., Rizzo, F. R., De Vito, F., Fresegna, D., Bullitta, S., . . . Mandolesi, G. (2018). Interplay Between Age and Neuroinflammation in Multiple Sclerosis: Effects on Motor and Cognitive Functions. *Front Aging Neurosci, 10*, 238. doi:10.3389/fnagi.2018.00238

Nack, A., Brendel, M., Nedelcu, J., Daerr, M., Nyamoya, S., Beyer, C., . . . Kipp, M. (2019). Expression of Translocator Protein and [18F]-GE180 Ligand Uptake in Multiple Sclerosis Animal Models. *Cells, 8*(2). doi:10.3390/cells8020094

Nakatsuji, Y., Okuno, T., Moriya, M., Sugimoto, T., Kinoshita, M., Takamatsu, H., . . . Kumanogoh, A. (2012). Elevation of Sema4A implicates Th cell skewing and the efficacy of IFN-beta therapy in multiple sclerosis. *J Immunol, 188*(10), 4858-4865. doi:10.4049/jimmunol.1102023

Nutma, E., Willison, H., Martino, G., & Amor, S. (2019). Neuroimmunology - the past, present and future. *Clin Exp Immunol, 197*(3), 278-293. doi:10.1111/cei.13279

Nyamoya, S., Leopold, P., Becker, B., Beyer, C., Hustadt, F., Schmitz, C., . . . Kipp, M. (2019). G-Protein-Coupled Receptor Gpr17 Expression in Two Multiple Sclerosis Remyelination Models. *Mol Neurobiol, 56*(2), 1109-1123. doi:10.1007/s12035-018-1146-1

Olitsky, P. K., & Yager, R. H. (1949). Experimental disseminated encephalomyelitis in white mice. *J Exp Med, 90*(3), 213-224. doi:10.1084/jem.90.3.213

Popescu, B. F., Pirko, I., & Lucchinetti, C. F. (2013). Pathology of multiple sclerosis: where do we stand? *Continuum (Minneap Minn), 19*(4 Multiple Sclerosis), 901-921. doi:10.1212/01.con.0000433291.23091.65

Richert, N. D., Ostuni, J. L., Bash, C. N., Duyn, J. H., McFarland, H. F., & Frank, J. A. (1998). Serial whole-brain magnetization transfer imaging in patients with relapsing-remitting multiple sclerosis at baseline and during treatment with interferon beta-1b. *AJNR Am J Neuroradiol, 19*(9), 1705-1713. Retrieved from http://www.ncbi.nlm.nih.gov/pubmed/9802494

Rohr, S. O., Greiner, T., Joost, S., Amor, S., Valk, P. V., Schmitz, C., & Kipp, M. (2020). Aquaporin-4 Expression during Toxic and Autoimmune Demyelination. *Cells, 9*(10). doi:10.3390/cells9102187

Rossignol, S., Dubuc, R., & Gossard, J. P. (2006). Dynamic sensorimotor interactions in locomotion. *Physiol Rev, 86*(1), 89-154. doi:10.1152/physrev.00028.2005

Sahoo, P. K., Smith, D. S., Perrone-Bizzozero, N., & Twiss, J. L. (2018). Axonal mRNA transport and translation at a glance. *J Cell Sci, 131*(8). doi:10.1242/jcs.196808

Schalomon, P. M., & Wahlsten, D. (2002). Wheel running behavior is impaired by both surgical section and genetic absence of the mouse corpus callosum. *Brain Res Bull, 57*(1), 27-33. doi:10.1016/s0361-9230(01)00633-5

Schnell, S. A., Staines, W. A., & Wessendorf, M. W. (1999). Reduction of lipofuscin-like autofluorescence in fluorescently labeled tissue. *J Histochem Cytochem, 47*(6), 719-730. doi:10.1177/002215549904700601

Sherriff, F. E., Bridges, L. R., Gentleman, S. M., Sivaloganathan, S., & Wilson, S. (1994). Markers of axonal injury in post mortem human brain. *Acta Neuropathol, 88*(5), 433-439.

Sherwin, C. M. (1998). Voluntary wheel running: a review and novel interpretation. *Anim Behav, 56*(1), 11-27. doi:10.1006/anbe.1998.0836

Shin, E. J., Jeong, J. H., Sharma, G., Sharma, N., Kim, D. J., Pham, D. T., . . . Kim, H. C. (2019). Protein kinase Cdelta mediates methamphetamine-induced dopaminergic neurotoxicity in mice via activation of microsomal epoxide hydrolase. *Food Chem Toxicol, 133*, 110761. doi:10.1016/j.fct.2019.110761

Silva, G. A., Pradella, F., Moraes, A., Farias, A., dos Santos, L. M., & de Oliveira, A. L. (2014). Impact of pregabalin treatment on synaptic plasticity and glial reactivity during the course of experimental autoimmune encephalomyelitis. *Brain Behav, 4*(6), 925-935. doi:10.1002/brb3.276

Slowik, A., Schmidt, T., Beyer, C., Amor, S., Clarner, T., & Kipp, M. (2015). The sphingosine 1-phosphate receptor agonist FTY720 is neuroprotective after cuprizone-induced CNS demyelination. *Br J Pharmacol, 172*(1), 80-92. doi:10.1111/bph.12938

Smith, K. J., Blakemore, W. F., & McDonald, W. I. (1979). Central remyelination restores secure conduction. *Nature, 280*(5721), 395-396. doi:10.1038/280395a0

Smith, K. J., Blakemore, W. F., & McDonald, W. I. (1981). The restoration of conduction by central remyelination. *Brain, 104*(2), 383-404. doi:10.1093/brain/104.2.383

Spach, K. M., Pedersen, L. B., Nashold, F. E., Kayo, T., Yandell, B. S., Prolla, T. A., & Hayes, C. E. (2004). Gene expression analysis suggests that 1,25-dihydroxyvitamin D3 reverses experimental autoimmune encephalomyelitis by stimulating inflammatory cell apoptosis. *Physiol Genomics, 18*(2), 141-151. doi:10.1152/physiolgenomics.00003.2004

Stone, J. R., Singleton, R. H., & Povlishock, J. T. (2000). Antibodies to the C-terminus of the beta-amyloid precursor protein (APP): a site specific marker for the detection of traumatic axonal injury. *Brain Res, 871*(2), 288-302.

Stromnes, I. M., & Goverman, J. M. (2006). Active induction of experimental allergic encephalomyelitis. *Nat Protoc, 1*(4), 1810-1819. doi:10.1038/nprot.2006.285

The Gene Ontology, C. (2019). The Gene Ontology Resource: 20 years and still GOing strong. *Nucleic Acids Res, 47*(D1), D330-D338. doi:10.1093/nar/gky1055

Thompson, A. J., Banwell, B. L., Barkhof, F., Carroll, W. M., Coetzee, T., Comi, G., . . . Cohen, J. A. (2018). Diagnosis of multiple sclerosis: 2017 revisions of the McDonald criteria. *Lancet Neurol, 17*(2), 162-173. doi:10.1016/S1474-4422(17)30470-2

Tomassini, V., Matthews, P. M., Thompson, A. J., Fuglø, D., Geurts, J. J., Johansen-Berg, H., . . . Palace, J. (2012). Neuroplasticity and functional recovery in multiple sclerosis. *Nat Rev Neurol, 8*(11), 635-646. doi:10.1038/nrneurol.2012.179

Tran, H. Q., Shin, E. J., Hoai Nguyen, B. C., Phan, D. H., Kang, M. J., Jang, C. G., . . . Kim, H. C. (2019). 5-HT1A receptor agonist 8-OH-DPAT induces serotonergic behaviors in mice via interaction between PKCdelta and p47phox. *Food Chem Toxicol, 123*, 125-141. doi:10.1016/j.fct.2018.10.049

Trepanier, M. O., Hildebrand, K. D., Nyamoya, S. D., Amor, S., Bazinet, R. P., & Kipp, M. (2018). Phosphatidylcholine 36:1 concentration decreases along with demyelination in the cuprizone animal model and in post-mortem multiple sclerosis brain tissue. *J Neurochem, 145*(6), 504-515. doi:10.1111/jnc.14335

van der Valk, P., & De Groot, C. J. (2000). Staging of multiple sclerosis (MS) lesions: pathology of the time frame of MS. *Neuropathol Appl Neurobiol, 26*(1), 2-10. doi:10.1046/j.1365-2990.2000.00217.x

van Horssen, J., Singh, S., van der Pol, S., Kipp, M., Lim, J. L., Peferoen, L., . . . Amor, S. (2012). Clusters of activated microglia in normal-appearing white matter show signs of innate immune activation. *J Neuroinflammation, 9*, 156. doi:10.1186/1742-2094-9-156

Wahlsten, D., Crabbe, J. C., & Dudek, B. C. (2001). Behavioural testing of standard inbred and 5HT(1B) knockout mice: implications of absent corpus callosum. *Behav Brain Res, 125*(1-2), 23-32. doi:10.1016/s0166-4328(01)00283-2

Wattjes, M. P., Harzheim, M., Lutterbey, G. G., Klotz, L., Schild, H. H., & Träber, F. (2007). Axonal damage but no increased glial cell activity in the normal-appearing white matter of patients with clinically isolated syndromes suggestive of multiple sclerosis using high-field magnetic resonance spectroscopy. *AJNR Am J Neuroradiol, 28*(8), 1517-1522. doi:10.3174/ajnr.A0594

Wendeln, A. C., Degenhardt, K., Kaurani, L., Gertig, M., Ulas, T., Jain, G., . . . Neher, J. J. (2018). Innate immune memory in the brain shapes neurological disease hallmarks. *Nature, 556*(7701), 332-338. doi:10.1038/s41586-018-0023-4

Xu, H., Yang, H. J., McConomy, B., Browning, R., & Li, X. M. (2010). Behavioral and neurobiological changes in C57BL/6 mouse exposed to cuprizone: effects of antipsychotics. *Front Behav Neurosci, 4*, 8. doi:10.3389/fnbeh.2010.00008

Xu, H., Yang, H. J., Zhang, Y., Clough, R., Browning, R., & Li, X. M. (2009). Behavioral and neurobiological changes in C57BL/6 mice exposed to cuprizone. *Behav Neurosci, 123*(2), 418-429. doi:10.1037/a0014477

York, E. M., LeDue, J. M., Bernier, L. P., & MacVicar, B. A. (2018). 3DMorph Automatic Analysis of Microglial Morphology in Three Dimensions from Ex Vivo and In Vivo Imaging. *eNeuro, 5*(6). doi:10.1523/ENEURO.0266-18.2018

Yu, K., Ahrens, S., Zhang, X., Schiff, H., Ramakrishnan, C., Fenno, L., . . . Li, B. (2017). The central amygdala controls learning in the lateral amygdala. *Nat Neurosci, 20*(12), 1680-1685. doi:10.1038/s41593-017-0009-9

Zeis, T., Graumann, U., Reynolds, R., & Schaeren-Wiemers, N. (2008). Normal-appearing white matter in multiple sclerosis is in a subtle balance between inflammation and neuroprotection. *Brain, 131*(Pt 1), 288-303. doi:10.1093/brain/awm291

Zhan, J., Mann, T., Joost, S., Behrangi, N., Frank, M., & Kipp, M. (2020). The Cuprizone Model: Dos and Do Nots. *Cells, 9*(4). doi:10.3390/cells9040843

Zhan, J., Yakimov, V., Ruhling, S., Fischbach, F., Nikolova, E., Joost, S., . . . Kipp, M. (2019). High Speed Ventral Plane Videography as a Convenient Tool to Quantify Motor Deficits during Pre-Clinical Experimental Autoimmune Encephalomyelitis. *Cells, 8*(11). doi:10.3390/cells8111439

Zhang, D., Anantharam, V., Kanthasamy, A., & Kanthasamy, A. G. (2007). Neuroprotective effect of protein kinase C delta inhibitor rottlerin in cell culture and animal models of Parkinson's disease. *J Pharmacol Exp Ther, 322*(3), 913-922. doi:10.1124/jpet.107.124669

Zhang, Y., Chen, K., Sloan, S. A., Bennett, M. L., Scholze, A. R., O'Keeffe, S., . . . Wu, J. Q. (2014). An RNA-sequencing transcriptome and splicing database of glia, neurons, and vascular cells of the cerebral cortex. *J Neurosci, 34*(36), 11929-11947. doi:10.1523/JNEUROSCI.1860-14.2014

Zivadinov, R., Sepcic, J., Nasuelli, D., De Masi, R., Bragadin, L. M., Tommasi, M. A., . . . Zorzon, M. (2001). A longitudinal study of brain atrophy and cognitive disturbances in the early phase of relapsing-remitting multiple sclerosis. *J Neurol Neurosurg Psychiatry, 70*(6), 773-780. doi:10.1136/jnnp.70.6.773